The Chemistry of Solvated Ions studied by FT-ICR Mass Spectrometry

Balaj Ovidiu-Petru

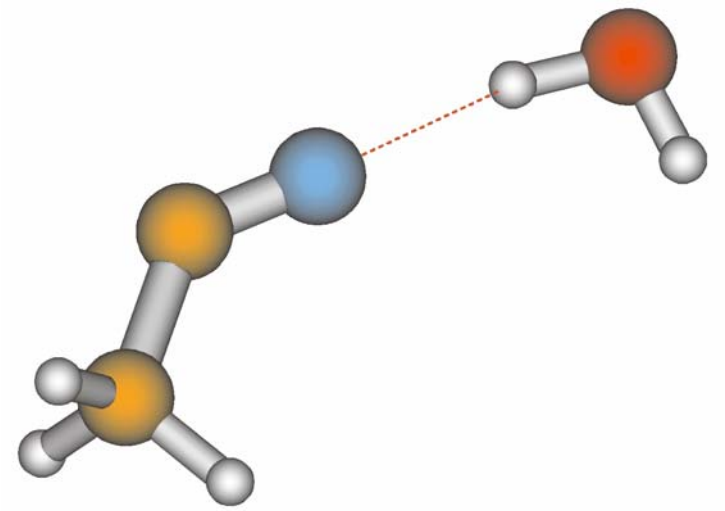

Dissertation

Technische Universität München

Technische Universität München
Fakultät für Chemie
- Lehrstuhl II für Physikalische Chemie -

The Chemistry of Solvated Ions studied by FT-ICR Mass Spectrometry

Balaj Ovidiu-Petru

Vollständiger Abdruck der von der Fakultät für Chemie der Technischen Universität München zur Erlangung des akademischen Grades eines

Doktors der Naturwissenschaften

genehmigten Dissertation.

Vorsitzender: Univ.-Prof. Dr. St. J. Glaser

Prüfer der Dissertation:

1. Univ.-Prof. V. E. Bondybey, Ph.D. (Univ. of California, Berkeley, USA)
2. Univ.-Prof. Dr. W. Domcke
3. Univ.-Prof. Dr. E. Nolte

Die Dissertation wurde am 21.12.2004 bei der Technischen Universität München eingereicht und durch die Fakultät für Chemie am 15.02.2005 angenommen.

Pentru mama si tata.

The most beautiful thing we can experience is the mysterious. It is the source of all true art and all science. He to whom this emotion is a stranger, who can no longer pause to wonder and stand rapt in awe, is as good as dead: his eyes are closed.

ALBERT EINSTEIN

Contents

1. Introduction 9

2. Experimental Methods 17

2.1. Fourier Transform Ion Cyclotron Resonance Mass Spectrometry (FT-ICR MS) 17

2.1.1. General 17

2.1.2. The FT-ICR Mass Spectrometer in Garching 20

2.1.3. The Laser Vaporization Molecular Beam Ion Source 24

2.2. References 27

3. Free Electrons, the Simplest Radicals of them All: Chemistry of Aqueous Electrons as studied by Mass Spectrometry 29

3.1. Introduction 29

3.2. Generation of Hydrated Electrons $(H_2O)_n^-$ 31

3.3. Cluster Stability and Fragmentation 32

3.4. Reactions of Solvated Electrons 35

3.4.1. Collisional activation 36

3.4.2. Ligand exchange 36

3.4.3. Core exchange 40

3.4.4. Rearrangement of covalent bonds 45

3.5. Conclusions 49

3.6. References 51

4. Reaction of Hydrated Electrons $(H_2O)_n^-$ with Carbon Dioxide and Molecular Oxygen: Hydration of the CO_2^- and O_2^- Anion 55

4.1. Introduction 55

4.2. Experimental Section 57

4.3. Results and Discussion 58

4.3.1. Reactions of $(H_2O)_n^-$ clusters with Carbon Dioxide 58

4.3.2. Reactions of $(H_2O)_n^-$ clusters with O_2 61
4.3.3. Ionic core exchange reactions 64
4.3.3. Quantum Chemical Computations of Hydrated CO_2^- and O_2^- Anions 64
4.3.5. Mechanism of the $(H_2O)_n^-$ Cluster Reaction with O_2 and CO_2 71
4.4. Conclusions 76
4.5. References 78

5. The Hydrated Electron Nanodroplets in reaction with Acetonitrile 83
5.1. Introduction 83
5.2. Experimental Section 84
5.3. Results and Discussion 85
5.3.1. Addition of a Hydrogen Atom to Acetonitrile 85
5.3.2. Base Catalyzed Hydrogen/Deuterium Exchange between Water and d3-Acetonitrile 88
5.3.2.1. Uptake of CD_3CN by $OH^-(H_2O)_n$ 91
5.3.2.2. H/D-exchange in $OH^-(CD_3CN)(H_2O)_2$ 93
5.3.2.3. Evidence of the OH^- role in the H/D exchange Reactions of $(H_2O)_n^-$ with CD_3CDO 96
5.3.2.4 Density functional calculations of $OH^-(CH_3CN)(H_2O)_m$, m = 0 – 3. 97
5.4. Conclusions 104
5.5. References 106

6. Reactions of Hydrated Electrons with Hydrogen Chloride: Formation of Atomic Hydrogen 109
6.1. Introduction 109
6.2. Experimental Details 111
6.3. Results and Discussion 112
6.3.1. Reaction with the first HCl molecule, and switch in the ionic cluster core 113
6.3.2 Subsequent reactions of $Cl(H_2O)_n$ with HCl 117
6.3.3 Solubility of HCl in Aqueous Clusters 122

6.4. Conclusions 124
6.5. References 125

7. Reactions of hydrated aluminum ions with methanol and formic acid. 129
7.1. Introduction 129
7.2 Experimental and computational details 131
7.2.1 Experimental procedure 131
7.2.2 Theoretical Methods 132
7.3 Results and Discussion 132
7.3.1 Reactions of $Al^+(H_2O)_n$ with methanol (CH_3OH) 132
7.3.2 Reactions of $Al^+(H_2O)_n$ with formic acid 136
7.3.3 Theoretical results 141
7.4 Conclusions 145
7.5 References 146

8. Development of a temperature controlled FT-ICR "infinity" cell 151
8.1 Introduction 151
8.2 Construction details of the Garching "infinity" cooled cell 152
8.3 The characteristics, performance and parameters of the cooled-cell. 155
8.4 References 159

9. Summary 161

Appendix
A. Publications 165
B. List of Presentations at Scientific Workshops and Conferences 169

Acknowledgements 173

1. Introduction

Most of the chemical reactions involve the presence of one or more reacting components dissolved in a suitable medium for the reaction to take place. The presence of the solvent can influence the chemical properties of the reactants or modify the reaction mechanisms, therefore changing the course of the reaction itself. The most important and abundant solvent on Earth is water. The ability to form hydrogen bonds with other water molecules and hydrogen bonded networks, its polar nature makes water an ideal solvent for ions and polar species. Most processes essential for terrestrial life proceed in aqueous environment. Life, as we know it today, would be unthinkable without it.

The last years saw a considerable increase in studies of solvated ions in the gas phase.[1-23] Viewed as ideal model systems used to understand the chemistry of solvation, they were intensely studied both by experimental and theoretical means. Spectroscopic studies of bulk aqueous solutions are hindered due to the various mechanism of line broadening leading to broad, almost featureless, spectral lines with little information to be obtained. In small clusters the effects are reduced so that information about solvated ion structures can be obtained.[1-5] Collision induced dissociation studies and black-body infrared dissociation experiments are used to extract binding energies, and computational studies of finite clusters yield additional structural information.

The Fourier transform ion-cyclotron resonance mass spectrometry (FT-ICR MS) technique has the advantage of very high resolution so that the elemental composition of reactants and products can be determined, any impurity effect being eliminated. Not negligible is the fact that the FT-ICR mass spectrometry has the unique ability of selecting any desired elemental composition, corresponding to a specific solvated ion, thus giving the possibility to study its particular chemistry. Clusters exposed to the room temperature

background infrared radiation in the ICR cell fragment, gradually loosing solvent, water, molecules one by one. This way it is easy to study the influence of solvation upon chemical reactions.

Electrons are present in all chemical reactions, no matter when or where they are taking place. In redox reactions an electron is transferred from one atom or molecule to another, from solute to the solvent, from a catalyst surface to a reactant, or from a reactant to a catalyst surface. Even in mono-molecular reactions and isomerizations, electrons are transferred from one bond to another; an electron undergoes a transition from one molecular orbital to another. During chemical reactions charges move, separate and recombine, always involving the movement of electrons. An electron can therefore be viewed as the simplest, most elementary, prototypic chemical reactant.

The aqueous electron, its existence in solution, and its solvation are therefore topics of a particular interest. Solvated electrons have, in fact, been first observed already in the very early days of chemistry, almost two hundred years ago. It took, however, almost a century of research, among others by Weyl,[24] before this early observation by Humphrey Davy of a deep blue color appearing when liquefied NH_3 came in contact with sodium or potassium were correctly interpreted, as being due to electrons solvated by the ammonia.[25]

In recent decades, it was demonstrated that besides bulk solutions, electrons solvated in small, finite clusters[26-27] can also be prepared in experiments with cold, supersonic beams. Such hydrated, charged clusters can be manipulated by electric or magnetic fields, and eventually stored and investigated in electromagnetic traps.[28] By letting the hydrated clusters interact with various gaseous reagents, one or several molecules can be dissolved in the cluster and their reactions studied in great detail.[28-47]

The chapter two of this thesis presents in detail the experimental methods used, including the basic principles of FT-ICR and the description of our instrument.

The reactions of hydrated electron clusters are the main topic of this thesis. The laser vaporization source used in our experiments can produce hydrated electron clusters up to almost 100 water molecules. Experiments showed that these exhibit a multifaceted chemistry depending of the reagent used. Chapter 3 describes their behavior and properties in the presence of a variety of organic and inorganic reagents, the study of the observed reaction mechanisms resulted in a loose classification of several reaction types.

In chapter 4, the reactions of aqueous electrons with molecular oxygen and carbon dioxide are described. These molecules are important components of the atmosphere, and also electrons are extremely ubiquitous, being formed by radioactive processes, cosmic and vacuum UV radiation, as well as by electric discharges and lightening. In view of the abundance and frequent occurrence of these species, and their importance for atmospheric chemistry, the reactions of aqueous electrons with oxygen and carbon dioxide, and the properties and chemistry of the solvated anions investigated in chapter 4 may be of more than just academic interest.

The reaction of the hydrated electron clusters with acetonitrile was observed by ESR spectroscopy in solution more than 25 years ago. At that time, the product was not identified.[2] The use of fully deuterated acetonitrile as reactant resulted in a interesting H/D exchange occurring only at a certain cluster size and composition. To elucidate this peculiar behavior of the cluster additional experiments were made, supplemented with DFT calculations by Chi-Kit Siu. The results are presented in the chapter 5.

The behavior of aqueous electrons in the presence of HCl is the subject of chapter 6. The reaction is accompanied by loss of a atomic hydrogen, followed by a intake of hydrogen chlorine into the clusters. The fragmentation pattern of the reaction products reveal that at certain points an HCl molecule will be lost instead of water until the clusters equilibrate with the medium.

The chemistry of hydrated aluminium clusters $Al^+(H_2O)_n$, $n \leq 60$, in the reaction with methanol and formic acid is the subject of chapter 7. The observed trend of the reaction rate, which increases with the acidity of the reactant, from pure water over CH_3OH, HCOOH to HCl provides strong support for the previously proposed proton transfer mechanism of the reaction.[48] Theoretical computations performed by our collaborators in Southampton confirm the feasibility of the proposed reaction pathways.

A temperature controlled ICR cell would increase the range of experiments and allow a move from a qualitative to quantitative description of the molecular clusters. The "infinity cell" cooled by liquid nitrogen can reach a minimum temperature of 135K. The design and the detailed testing results are presented in the chapter 8.

References

[1] J. M. Weber, J. A. Kelley, S. B. Nielsen, P. Ayotte, M. A.Johnson, *Science* **2000**, *287*, 2461.

[2] Y. Cao, J.-H. Choi, B.-M. Haas, M. Okumura, *J. Phys. Chem.* **1994**, *98*, 12177.

[3] J.-H. Choi, K. T. Kuwata, B.-M. Haas, Y. Cao, M. S. Johnson, M. Okumura, *J. Chem. Phys.* **1994**, *100*, 7153.

[4] C. E. H. Dessent, J. Kim, M. A. Johnson, *Account. Chem. Res.* **1998**, *31*, 527.

[5] J. M. Lisy, *Int. Rev. Phys. Chem.* **1997**, *16*, 267.

[6] M. Beyer, A.Lammers, E. V. Savchenko, G. Niedner-Schatteburg, V. E. Bondybey *Phys. Chem. Chem. Phys.* **1999**, *1*, 2213.

[7] M. T. Rodgers, P. B. Armentrout, *Mass Spectrom. Rev.* **2000**, *19*, 215.

[8] A. Ricca, C. W. Bauschlicher, *J. Phys. Chem.* **1995**, *99*, 9003.

[9] N. Agmon, *J. Phys. Chem. A* **1998**, *102*, 192.

[10] M. Beyer, E. V. Savchenko, G. Niedner-Schatteburg, V. E. Bondybey, *J. Chem. Phys.* **1999**, *110*, 11950.

[11] M. A. Duncan, *Annu. Rev. Phys. Chem.* **1997**, *48*, 69.

[12] G. Niedner-Schatteburg, V. E. Bondybey, *Chem. Rev.* **2000**, *100*, 4059.

[13] C. Dedonder-Lardeux, G. Gregoire, C. Jouvet, S. Martenchard, D. Solgadi, *Chem. Rev.* **2000**, *100*, 4023.

[14] L.A. Posey, M.J. Deluca, P.J. Campagnola, M.A. Johnson, *J. Phys. Chem.* **1989,** *93*, 1178.

[15] C. E. Dykstra, J. M. Lisy, *J. Mol. Struc.-Theochem.* **2000**, *500*, 375.

[16] P. Kebarle, *Int. J. Mass Spectrom.* **2000**, *200*, 313.

[17] H. Watanabe, S. Iwata, *J. Phys. Chem.* **1996**, *100*, 3377.

[18] S.T. Arnold, R.A. Morris, A.A. Viggiano, M.A. Johnson, *J. Phys. Chem.* **1996,** *100*, 2900.

[19] I. Yourshaw, Y. X. Zhao, D. M. Neumark, *J. Chem. Phys.* **1996**, *105*, 351.

[20] B. S. Freiser, *J. Mass Spectrometry* **1996**, *31*, 703.

[21] D. Feller, E. D. Glendening, W. A. de Jong, *J. Chem. Phys.* **1999**, *110*, 1475.

[22] Q. Zhong, A. W. Castleman, *Chem. Rev.* **2000**, *100*, 4039.

[23] R. G. Keesee , A. W. Castleman, *J. Phys. Chem. Ref. Data* **1986**, *15*, 1011.

[24] W. Weyl, *Poggendorff's Annalen der Physik und Chemie* **1864**, *121*, 601-612.

[25] C. A. Kraus, *J. Am. Chem. Soc.* **1908**, *30*, 1323.

[26] H. Haberland, C. Ludewigt, H. G. Schindler and D. R. Worsnop, *J. Chem. Phys.* **1984**, *81*, 3742-3744.

[27] H. Haberland, H. Langosch, H. G. Schindler and D. R. Worsnop, *J. Phys. Chem.* **1984**, *88*, 3903-3904.

[28] H. Haberland, H. G. Schindler and D. R. Worsnop, *Ber. Bunsen-Ges. Phys. Chem.* **1984**, *88*, 270-272.

[29] V. E. Bondybey and M. K. Beyer, *Int. Rev. Phys. Chem.* **2002**, *21*, 277-306.

[30] T. Schindler, C. Berg, G. Niedner-Schatteburg and V. E. Bondybey, *Chem. Phys.* **1995**, *201*, 491-496.

[31] T. Schindler, C. Berg, G. Niedner-Schatteburg and V. E. Bondybey, *J. Phys. Chem.* **1995**, *99*, 12434-12443.

[32] T. Schindler, C. Berg, G. Niedner-Schatteburg and V. E. Bondybey, *Chem. Phys. Lett.* **1994**, *229*, 57-64.

[33] C. Berg, U. Achatz, M. Beyer, S. Joos, G. Albert, T. Schindler, G. Niedner-Schatteburg and V. E. Bondybey, *Int. J. Mass Spectrom.* **1997**, *167/168***,** 723-734.

[34] V. E. Bondybey, M. Beyer, U. Achatz, S. Joos and G. Niedner-Schatteburg, *Isr. J. Chem.* **1999**, *39*, 213-219.

[35] C. Berg, M. Beyer, U. Achatz, S. Joos, G. Niedner-Schatteburg and V. E. Bondybey, *Chem. Phys.* ***1998***, *239*, 379-392.

[36] M. Beyer, U. Achatz, C. Berg, S. Joos, G. Niedner-Schatteburg and V. E. Bondybey, *J. Phys. Chem. A* **1999**, *103*, 671-678.

[37] U. Achatz, S. Joos, C. Berg, T. Schindler, M. Beyer, G. Albert, G. Niedner-Schatteburg and V. E. Bondybey, *J. Am. Chem. Soc.* **1998**, *120*, 1876-1882.

[38] U. Achatz, B. S. Fox, M. K. Beyer and V. E. Bondybey, *J. Am. Chem. Soc.* **2001**, *123*, 6151-6156.

[39] B. S. Fox, M. K. Beyer, U. Achatz, S. Joos, G. Niedner-Schatteburg and V. E. Bondybey, *J. Phys. Chem. A* **2000**, *104*, 1147-1151.

[40] B. S. Fox, M. K. Beyer and V. E. Bondybey, *J. Am. Chem. Soc.* **2002**, *124*, 13613-13623.

[41] B. S. Fox, O. P. Balaj, L. Balteanu, M. K. Beyer and V. E. Bondybey, *Chem. Eur. J.* **2002**, *8*, 5534-5540.

[42] B. S. Fox, O. P. Balaj, I. Balteanu, M. K. Beyer and V. E. Bondybey, *J. Am. Chem. Soc.* **2002**, *124*, 172-173.

[43] O. P. Balaj, E. P. F. Lee, I. Balteanu, B. S. Fox, M. K. Beyer, J. M. Dyke and V. E. Bondybey, *Int. J. Mass Spectrom.* **2002**, *220*, 331-341.

[44] O. P. Balaj, I. Balteanu, B. S. Fox-Beyer, M. K. Beyer and V. E. Bondybey, *Angew. Chem. Int. Edit.* **2003**, *42*, 5516-5518.

[45] O. P. Balaj, C.-K. Siu, I. Balteanu, B. S. Fox-Beyer, M. K. Beyer and V. E. Bondybey, *J. Phys. Chem. A* **2004**, *108*, 7506-7512.

[46] O. P. Balaj, C.-K. Siu, I. Balteanu, M. K. Beyer and V. E. Bondybey, *Chem. Eur. J.* **2004**, *10*, 4822-4830.

[47] O. P. Balaj, C.-K. Siu, I. Balteanu, M. K. Beyer and V. E. Bondybey, *Int. J. Mass Spectrom.* **2004**, *238*, 65-74.

[48] M. Beyer, C. Berg, W. Görlitzer, T. Schindler, U. Achatz, G. Albert, G. Niedner-Schatteburg, V.E. Bondybey, *J. Am. Chem. Soc.* **1996**, *118*, 7386.

2. Eperimental Methods

2.1 Fourier Transform Ion Cyclotron Resonance Mass Spectrometry (FT-ICR MS)

2.1.1. General

The technique of ICR-MS was first published[1,2] in the mid-1950's where it was demonstrated for measurement of very small mass differences at very high precision. The technique remained a largely academic tool until the application of FT methods by Alan Marshall and Melvin Comisarow[3,4] in the early 1970.

An ion moving through a spatially uniform magnetic field will be influenced by the Lorenz force:

$$\vec{F} = m\frac{d\vec{v}}{dt} = q\vec{\mathbf{v}} \times \vec{B} \tag{1}$$

in which q, $\vec{v}$ are ionic charge, ion velocity and $\vec{B}$ is the magnetic field vector defined as $\vec{B} = -\vec{k}B_0$ (z-axis being defined as the direction opposite to $\vec{B}$). Given the angular acceleration $\left|d\vec{v}/dt\right| = v^2/r$ and the angular velocity $\omega = v/r$ in the plane perpendicular to $\vec{B}$, one can write down the "cyclotron" equation:

$$\nu_c = \frac{qB_0}{2\pi m} \tag{2}$$

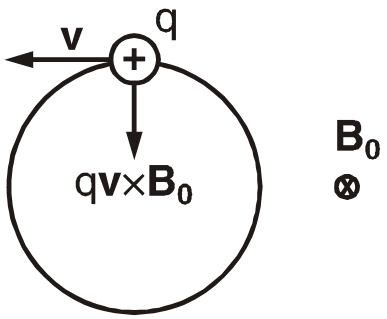

Figure 1. A particle with the charge q and velocity v perpendicular to the magnetic filed B_0 will move on a circular trajectory due to the Lorenz force acting upon it. This circular motion represents the ion cyclotron motion.

It is easy then, measuring the cyclotron frequency ν_c of an ion of charge q in a magnetic field B_0, to determine its mass. Interesting about equation (2) is that the ions having the same mass per charge ratio, m/q, will have the same ICR frequency independent of their velocity. This is especially useful because the translational energy does not impact the precise determination of m/q.

The cyclotron frequencies can be measured very precisely,[5] giving ICR-MS the possibility to determine masses with an accuracy of $\Delta m/m=10^{-6}$ or better.[6] Accordingly, the composition of ions with the same nominal mass can be determined by their mass defect. For example, N_2^+ with a mass of 28.0056 amu and CO^+ with a mass of 27.9944 amu are represented by two separate peaks.[6]

The trapping makes use of an electrostatic potential lower than 5V, applying the storage procedure of a Penning trap. There is a variety of analysis cell configurations whose most popular geometries are shown in the Figure 2. Ion cyclotron motion is not by itself useful. A broadband high frequency signal, containing all the frequencies in the desired mass range, converts the incoherent ion cyclotron orbital motion to a coherent and therefore detectable motion. The result is the formation of coherent ion packages as shown in the Figure 3. The now coherent ion packages move on a circular trajectory inducing

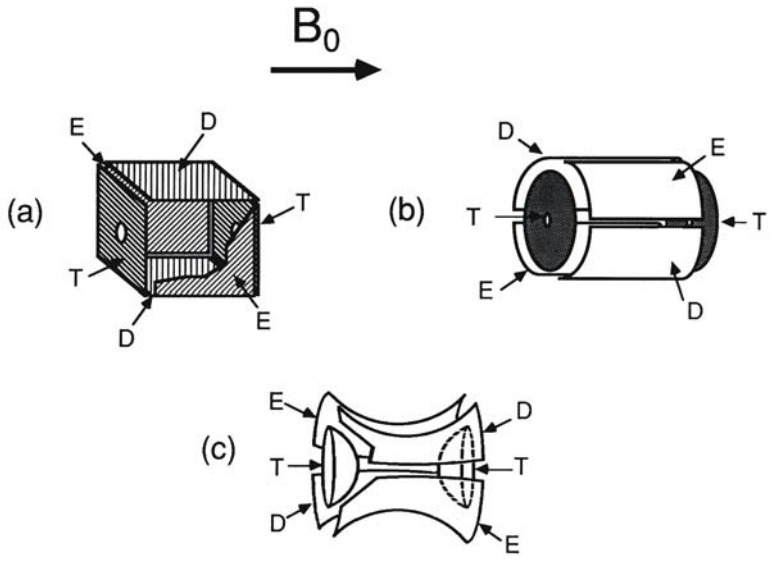

Figure 2. ICR cell[6] configurations: (a) cubic cell, (b) cylindric cell and (c) hyperbolic cell. The excitation electrodes are indicated by letter E, detection by D, trapping by T.

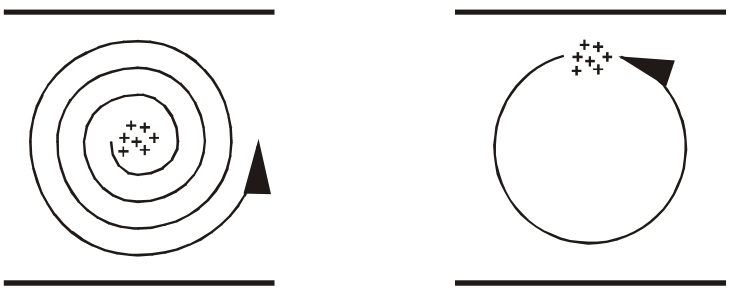

Figure 3. The incoherent ion cyclotron motion is converted, by excitation, into detectable coherent motion.[6]

a small electric potential between the detection plates which oscillates with the cyclotron frequency. This signal is amplified, recorded with an analog-digital converter and stored as the digitized transient. Fourier transformation of the transient yields a frequency spectrum, which is converted to a mass spectrum by applying Equation 2, as is shown schematically in Figure 4.

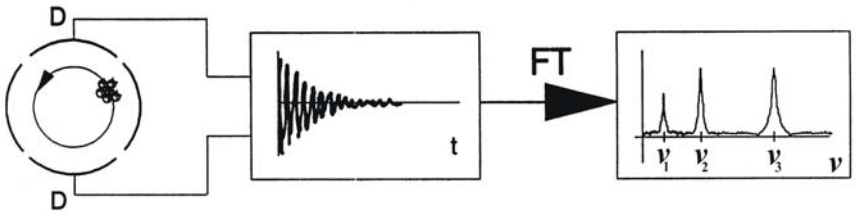

Figure 4. A coherent ion package induces a differential current between two opposed detection plates. Ion-neutral collisions and Coulomb repulsion among the ions lead to an exponential damping of the time-domain ICR signal. Fourier transformation applied to the transient will generate a frequency spectrum which is coverted to a mass spectrum using the cyclotron equation.

The ion motion inside the cell does not consist of only pure cyclotron motion. The quadrupol potential needed to trap the ions introduces additional oscillations of the ions: magnetron motion and trapping oscillations.[6,7] However, the cyclotron frequency is much higher, compared with the magnetron and trapping frequencies. Due to the fact that the magnetron and cyclotron motions are coupled, internal or external mass calibration is needed.

2.1.2 The FT-ICR Mass Spectrometer in Garching

The experiments were performed on a modified FT-ICR mass spectrometer Bruker/Spectroscopin CMS47X,[8] equipped with a superconducting 4.7 T magnet an APEX III data station and a cylindrical 60 x 60 mm "infinity" cell.[9] A schematic of the instrument can be seen in Figure 5. The mass spectrometer was modified by adding an additional chamber which houses the molecular ion source. The additional pumping stage allows the operation of the molecular beam expansion source while maintaining a pressure below 1 x 10^{-10} mbar in the ICR cell region. The ions produced by the source are confined by a cylindrical mesh, injected through a 0.4 mm skimmer and transferred, along the magnetic field axis, by a

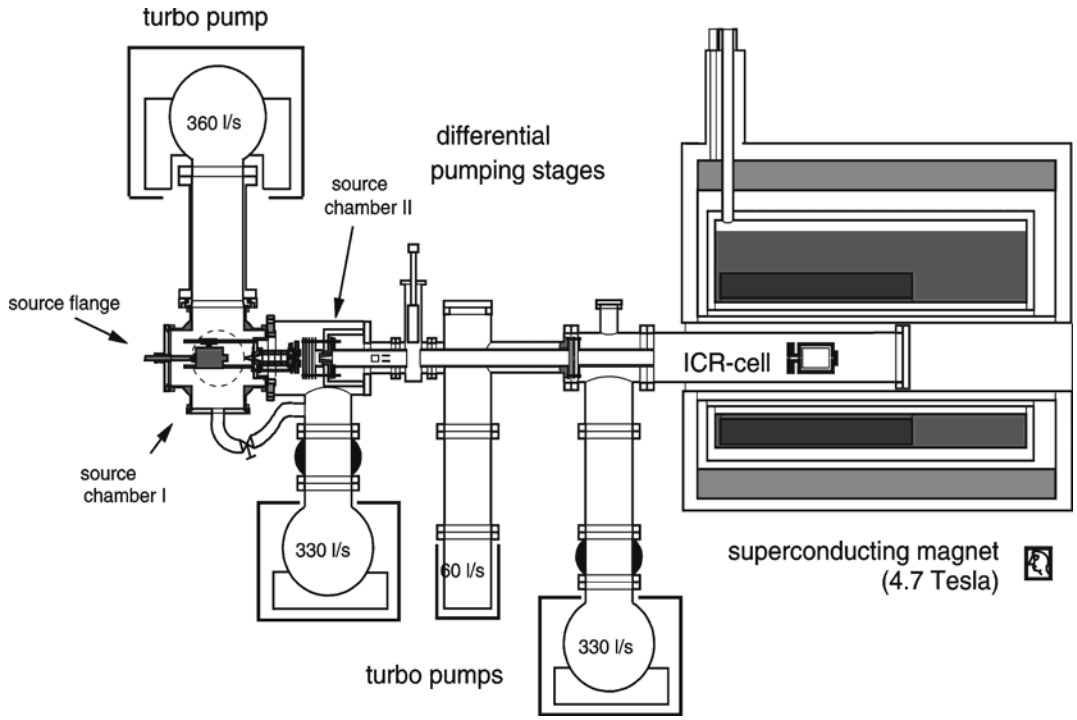

Figure 5. Side view of the FT-ICR mass spectrometer in Garching. The ions generated by the external ion source are transferred by a system of electrostatic lenses through four differential pumping stages and stored into the ICR-cell.

system of einzel lenses, into the high vacuum region of the magnet. To get the ions across the inhomogeneous stray filed of the magnet, the ions are accelerated to 3 keV kinetic energy and then stepwise decelerated and trapped within the cell. A small potential gradient applied perpendicular to the velocity of the ions will convert some of the translational energy into cyclotron movement, enhances the trapping efficiency and help decrease the cell trapping potentials. This method is called the Caravatti trapping scheme.[10]

Due to the high magnetic field, the turbomolecular pumps are shielded with soft iron. The rotary pumps are not shielded. We are using Pfeiffer turbo pumps with the following puming speeds: 360 l/s coupled with a 8 m^3/s Alcatel rotary pump for the source chamber I, 330 l/s and 16 m^3/s Pfeiffer for the second pumping stage, 60 l/s, 330 l/s and 8 m^3/s Alcatel rotary pump for the ultra high vacuum region. This setup will generate, without gas load, typical pressures of 5 x 10^{-6} mbar in the source chamber, 3 x 10^{-7} mbar in the source chamber II and below 1 x 10^{-10} mbar in the ultra high vacuum region. Different reaction gases can be

introduced into the UHV region using two Balzers UHD040 needle valves. One of them is corrosion proved and it is used for corrosive gases. A rotary pump attached to the UHV needle valves inlet is needed for cleaning purposes.

The pressure is monitored by Penning ionization gauges type Balzers IKR 020 in UHV region, source chamber one and two. In the UHV the ion gauge is situated as far as possible from central bore of the magnet so that the interaction with the molecular ion beam is minimal. The ion gauge is thus placed directly on top of the turbomolecular pump at a distance of about 80 centimeters from the ICR cell. Thus the real pressure in the cell is different from the ion gauge reading and it is obtained by correcting the reactant pressure with the sensitivity of the ion gauge R_x and the empirical geometry factor G:

$$p_x^{cell} = \frac{G \cdot p_x^{ion\ gauge}}{R_x} \tag{3}$$

The geometry factor G is a constant with the experimentally determined value of 3.7±1.0, being independent of the reactant gas and pressure range.[11] The ion gauge sensitivity R_x depends of the reactant gas and pressure range and its values can be found in a couple of tables.[12,13]

The aluminum experiments were done using a Bruker ASPECT3000 minicomputer for experiment and data processing. The processor has limited multitasking capabilities. It is equipped with 768 kB RAM and a 400 MB hard disk. Data are stored in 24 bit words. Two ADC analog-digital converters are integrated for transient recording. A fast ADC with 20 MHz sampling rate and 9 bit resolution is used for broad band detection, a slow ADC with 50 kHz sampling rate and 12 bit resolution is used for high resolution heterodyne[14] detection. The lowest detectable mass, i.e. the highest detectable frequency, is limited by the sampling rate of the fast ADC to 11.5 amu. Transients up to 128 kWords can be recorded. An FFT fast

fourier transform processor undertakes the computationally demanding fourier transformation of the transient. It is fast enough to allow for an online display of a nonlinearized mass spectrum for transients up to 32 kWords, which is very useful for signal optimization purposes.

The I89 FT-ICR operating system allows software control of the experiment by automation routines, which are programmed in a very limited, non-standard programming language. Up to ten different pulses can be applied for a variety of purposes, like ion excitation, gating of the ion trap, or triggering of external hardware, such as lasers or pulsed valves. Puls lengths may be integer multiples of 1 µs, delays between pulses are integer multiples of 10 µs.

Mass spectra are transferred with the Bruker software package NMRLINK[15] to a PC, which is linked to the local UNIX workstation cluster, transformed to ASCII format with the program BRUKER,[16] and displayed with the public domain graphics package XMGR.[17] In addition, the mass-intensity information can be transfered from the ASPECT to the PC via an RS232 serial port, and further processed under UNIX, to enable e.g. fits of reaction kinetics. A set of programs including LLCRUNCH,[18] LLCORR,[19] C2N,[20] NNORM,[19] and FIT,[20] have been developed for these purposes.

Two years ago, a new Bruker APEX III data station connected to a WindowsNT Pentium III computer lead to a considerable improvement in the set-up capacities and range of experiments. The APEX III console uses channel related real time events and analog RF signals generated by a central Signal Generation Unit, comunicating through a high speed link. The high speed link transfers all FTMS relevant real time events in 50 ns time slots (e.g. pulses, shapes, phase jumps, frequency jumps). Each RF channel is controlled by a separate high speed link. The console drives up to 64 programmable TTL pulses organized as two 32-bit words. The pulses are distributed to external devices and can have dedicated functions as deflection, quench or to control external devices as the piezo-driver or the laser pulses. The

pulses are triggered by experimental automatic subroutines read and executed by a dedicated software, *XMass*. The desired pulse length and real time succession is programmed using a special programming language.

2.1.3. The Laser Vaporization Molecular Beam Ion Source

In all the experiments described here, the water solvated electrons and water solvated aluminum ions were produced using the laser vaporization source[21-23] illustrated in Figure 6. Focused pulses of 532 nm green radiation, generated by a Continuum Surelite II Nd:YAG laser, are used to vaporize small amount of material of a rotating metal target disk. A pulse length of 5 nanoseconds and pulse energies of 2-20 ms are used. The plasma is expanding into 10^{-4} mbar vacuum. The hydrated clusters are obtained by seeding the carrier gas with water. The carrier gas pulses are generated by a homebuilt piezo-electric valve with a 50 μs opening

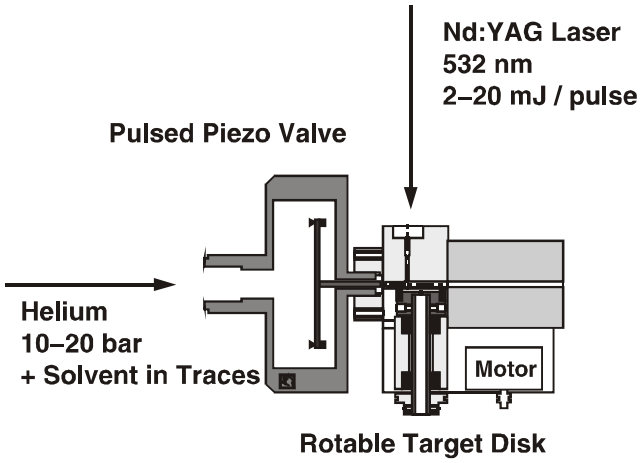

Figure 6. The leaser vaporization molecular beam ion source. An Nd:YAG laser vaporizes material from a rotating target disc. Entrained by a precisely times gas pulse, generated by a piezo valve, the plasma is confined into a expansion channel and expands into vacuum. The clusters are formed in the supersonic expansion following the collisional cooling of the plasma. By adding traces of water in the carrier gas, the hydrated clusters are generated.

entrained by a precisely timed carrier gas pulse and is cooled by supersonic expansion into time. Voltages up to 1kV can be applied by the piezo driver. Backing pressures of 10 to 20 mbar of carrier gas are used. By varying the experimental conditions, as the laser power, the source voltage or the delay between the firing of the laser flash lamps, the piezo valve opening and the laser q-switch, distributions of ions hydrated up to 100 water molecules can be produced.

In a typical experiment, the real time pulse sequence, shown in Figure 7, starts with the quench pulse P1. The pulse makes sure that the cell is empty at the beginning of the experiment. The laser vaporization cycle consists of firing of the laser lamps, opening of the piezo valve and laser q-switch trigger. The delay between the laser and gas pulse is critical in the amount and composition of the ions. The ions travel to the cell and are trapped. The pulse P2 lowers the trapping potential on the upper trapping plate allowing the ions

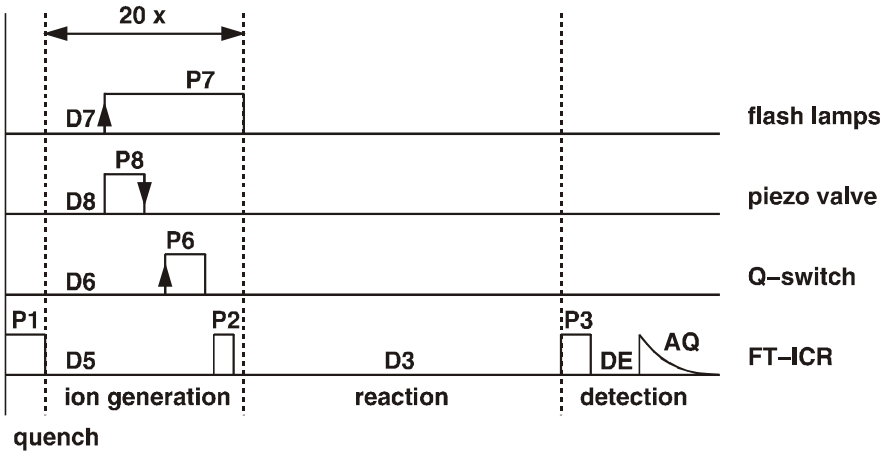

Figure 7. Pulse sequence of a typical ICR-experiment with the laser vaporization source. The quench pulse P1 cleans the cell from ions. Twenty ion generation cycles fill the cell. The piezo valve is triggered with the falling edge of the pulse, which allows 1 μs accuracy. After a reaction delay, the ions in the cell are accelerated by the broad-band pulse P3, and the transient is recorded during AQ. A delay, DE, ensures that the transient is not affected by the pulse P3.

to enter the cell. Twenty cycles insure that the cell contains enough ions for a good signal. The ions can be allowed to react for a variable time delay, mass selected and detected. The ion distribution can be shifted by varying D5, which insures the time of flight delay change, and the cell opening time P2.

2.2 References

[1] J.A Hipple, H. Sommer, H.A. Thomas, *Physical Reviews* **1949,** *76*, 1877-1878.

[2] H. Sommer, H.A. Thomas, J.A. Hipple, *Physical Reviews* **1951,** *82(5)*, 697-702.

[3] M.B. Comisarow, A.G. Marshall, *Physics Letters* **1974,** *25*, 282-283.

[4] M.B. Comisarow, A.G. Marshall, *Physics Letters* **1974,** *26*, 489-490.

[5] D. J. Wineland, *Science* **1984**, *226*, 395.

[6] A. G. Marshall, P. B. Grosshans, *Anal. Chem.* **1991**, *63*, 215A.

[7] A. G. Marshall, C. L. Hendrickson, G. S. Jackson, *Mass Spectrom. Reviews* **1998**, *17*, 1.

[8] C. Berg, T. Schindler, G. Niedner-Schatteburg, V.E. Bondybey, *J. Chem. Phys.* **1995,** *102*, 4870.

[9] P. Caravatti, M. Allemann, *Org. Mass Spectrom.* **1991**, *26*, 514.

[10] P. Caravatti, USA Patent Nr. 4 924 089, May 8, 1990.

[11] T. Schindler, *Diplomarbeit*. Physik Department, Technische Universität München, Garching, 1992.

[12] R.L. Summers, NASA Technical Note TN D-5285, 1969.

[13] J.E. Bartmess, R.M. Georgiadis, *Vacuum* **1969**, *33*, 149.

[14] P. Horowitz, W. Hill, *The Art of Electronics*; Cambridge University Press: Cambridge, 1989.

[15] Bruker Spectrospin, Nancy, 1992.

[16] Lammers, A. Garching, 1994.

[17] P. J. Turner, Beaverton 1994, A. Thoma, G. Schallmoser, A. Lammers, Garching, 1995, A. Lammers, Garching, 1996.

[18] M. Beyer, Garching, 1996.

[19] T. Schindler, Garching 1994, M. Beyer, Garching, 1996.

[20] T. Schindler, Garching, 1994.

[21] V. E. Bondybey, J. H. English, *J. Chem. Phys.* **1981**, *74*, 6978.

[22] V. E. Bondybey, *Science* **1985**, *227*, 4683.

[23] T. G. Dietz, M. A. Duncan, D. E. Powers, R. E. Smalley, *J. Chem. Phys.* **1981**, *74*, 6511.

3. Free Electrons, the Simplest Radicals of them All: Chemistry of Aqueous Electrons as studied by Mass Spectrometry

3.1. Introduction

Atoms are bound together in molecules by electrostatic forces. A molecular bond forms, when the attractive forces between the atomic nuclei and the shared electrons prevail over the repulsive forces between the positively charged nuclei. All chemical reactions therefore involve a rearrangement of electrons, and in this sense, the electron itself can be considered the simplest chemical reactant. Production of an electron typically requires an appreciable amount of energy, and free electrons in the gas phase therefore occur only in environments where large amounts of energy are available, such as flames, discharges, or plasmas. On the other hand, producing an electron in the condensed phase, where it is intimately solvated by surrounding molecules is surprisingly easy. A first clear, relevant observation of this fact in fact dates back to the early days of modern chemistry, and to the beginning of the 19th century.

Already around 1810 Humphry Davy noted that an intense blue color appeared when alkali metals were exposed to ammonia. Subsequent studies, among others by Weyl,[1] established that the blue solutions behaved like electrolytes, with high electric conductivity and magnetic susceptibility, and became bronze coloured and metallic in appearance at higher concentrations. Almost exactly a century after Davy's discovery, Kraus suggested that the metals are ionized in the ammonia solutions, resulting in a metal cation, and a free electron.[2] This process which requires some 5-6 eV in the gas phase proceeds in the ammonia solution

spontaneously and exothermically, with the energy required for the ionization being more than compensated by the combined solvation energies of the metal cation and of the electron.

A molecule of water, undoubtedly the most important solvent, has an even higher dipole moment (1.854 D) than ammonia (1.471 D), is capable of stronger hydrogen bonding, and might therefore be expected to be even more effective in promoting the metal ionization. In spite of that, more than an additional half century has elapsed before similar solvated electrons could be generated and observed in water.[3-5] A solvated electron is highly reactive, and can be destroyed by a variety of reactions with impurities, or with the solvent itself.[6] In ammonia, the reaction with the solvent resulting in amide formation and the development of hydrogen is hindered and quite slow. Water, however, even when quite pure, is partially ionized, $H_2O \rightarrow H^+ + OH^-$, so that free electrons can efficiently recombine with the protons, greatly facilitating the solvent reduction and formation of hydrogen atoms, which in turn recombine to form molecular hydrogen.

The problem thus does not lie in the difficulty of generating the hydrated electrons, but in the efficient processes leading to their destruction. They can, in fact, be produced by a wide variety of methods, including direct injection of energetic electrons into the solvent,[3-5] photoionization of water itself,[7,8] or of a suitable precursor[9,10] by UV radiation, and they also form, albeit transiently by the interaction of water with alkali metal surfaces.[11] Although they are easily produced by pulsed radiolysis of aqueous solutions and other methods, they have only very short, pH dependent lifetimes of less than 1 ms.[9] The appreciable volume increase which accompanies the injection of electrons into liquid water, motivated the development of the so called “cavity” model of solvated electrons.[12] This simple treatment of such a hydrated electron as a particle in a three-dimensional box leads to an s-type ground state, with an excited triply degenerate p-type excited state. It is the fully allowed s-p excitation in this model which gives the hydrated electrons their blue color, and the strong broad absorption in the red, with a maximum around 720 nm.[8,13,14]

Unlike in bulk liquid, water autoionization does not occur in finite clusters, and therefore no protons, or H_3O^+ ions, limiting the free electron lifetimes should be present. Haberland and coworkers have demonstrated, that gas phase hydrated electrons, that is small negatively charged water clusters $(H_2O)_n^-$ can be produced,[5-17] and since then these species have been quite extensively studied, both experimentally[18-23] and theoretically.[24-34] A more extensive account of these works is given in a previous publication.[21] Most of these studies concentrated upon the physical properties of the water clusters, upon the question of their formation,[35-37] stability,[21,38] and electronic and geometric structure.[18-20] The clusters or "nandodroplets" thus provide a suitable medium, free of interference by impurities, where the lifetime of the free electrons is not limited by the presence of protons. This then permits convenient studies of the chemistry of these interesting reactants, as already exemplified by a series of investigations both in our laboratory[23,39,40] and earlier by Johnson, Viggiano and coworkers.[41,42] These studies of hydrated electron reactions and chemistry form the subject of the present review.

3.2. Generation of Hydrated Electrons $(H_2O)_n^-$

As noted above, hydrated electrons $(H_2O)_n^-$ can be generated by a variety of methods. The studies by Haberland and coworkers have employed electrons produced by UV photons.[15-17] One can also first produce neutral water clusters in a supersonic expansion, and subsequently attach low energy electrons.[35-37] The versatile laser vaporization source developed in our laboratory can be used as a very efficient, clean source of hydrated electrons.[21,23] This source which combines supersonic expansion with pulsed laser vaporization of a solid metal sample can generate metal cations and cationic clusters, as well as electrons, anions and anionic clusters. When one employs a metal sample with negative electron affinity, such as magnesium or zinc, the metal anions and anion clusters can

effectively be eliminated.[23] When a small amount of water vapor is then introduced into the high pressure carrier gas, usually helium, pure hydrated electron clusters are produced.

These are then extracted from the beam, and guided along the magnetic field axis, through several stages of differential pumping from the source chamber into the high vacuum region of the ICR cell. The specific distribution of the clusters depends on the exact source conditions, the stagnation pressure of the carrier gas, on the water vapor partial pressure, and in particular on the relative timing between the opening of the pulsed valve controlling the gas expansion and the vaporization laser pulse. Typically, $(H_2O)_n^-$ clusters ranging in size from n = 15 to about 100 can be produced. At the high end, the distribution is limited by the rapid fragmentation and short lifetime of the large clusters due to absorption of the black body ambient infrared radiation. Clusters with $n < 13$, on the other hand, have very short lifetimes due to a rapid electron detachment process. These can be generated and studied on the shorter timescale of a molecular beam experiment, but do not survive sufficiently long to be detected in the ICR cell, which requires a lifetime of at least 100 ms due to the detection process.

3.3. Cluster Stability and Fragmentation

Before discussing the $(H_2O)_n^-$ cluster reactions and collisional fragmentation, it is necessary to note, that even in the total absence of collisions they gradually disappear from the ICR trap, due mainly to the absorption of black body infrared radiation. The clusters are held together by hydrogen bonds between the water molecules, and are not stable at room temperature. In the ICR trap they can survive, because their temperature upon leaving the supersonic expansion is quite low, initially surely below 50 K. The water molecules are, however, in particular when hydrogen bonded, excellent infrared absorbers, and are continuously exposed to the black body radiation of the room temperature apparatus walls. Absorption of the infrared photons steadily supplies energy, and leads to gradual evaporation

of the water ligands.[21,43-50] The cluster temperature is thus controlled by the competition between evaporative cooling and radiative heating. This process will only come to a halt when the clusters reach the ambient temperature of around 300 K, when they are in thermal equilibrium with the environment. The hydrated ions thus eventually reach some minimum size, at which the available thermal energy content is no longer sufficient to break the bonds and cause unimolecular decomposition.[45] They become stable at room temperature on the time scale of the ICR experiment – usually in the range of many seconds. Thus, for instance for hydrated protons, the final, effectively stable product of fragmentation is $H^+(H_2O)_4$, perhaps better formulated as hydrated hydroxonium, $(H_3O^+)(H_2O)_3$, which then survives in the absence of collisions for seconds or even minutes.[46]

Unlike the compact, effectively point-like proton, the diffuse charge of the electrons binds much more tenuously to the water ligands. In the case of the hydrated electron clusters, there are therefore two competing processes which contribute to the loss of a cluster of a given size. The cluster can either "evaporate" a water ligand, or it can detach the electron, and both processes are actually experimentally observed.[21]

A detailed study in our laboratory has shown,[21] that for clusters above about n = 30 the latter process is negligible, and ligand loss is the dominant process. Figure 1 shows the rate constants of the two processes together with their branching ratio. For $16 < n < 32$, one observes a wild fluctuation in the relative importance of the two process, with some species almost exclusively fragmenting with the loss of ligand, while for other sizes detachment of the electron making a significant contribution to the overall cluster decay. The electron detachment is the only process detectable for $n < 17$, and this is reflected in the drastic drop in intensity in the initial mass spectra below n = 17, with the smallest cluster observed only in traces being n = 13. The interpretation lies in the fact that, experimentally the larger clusters lose a ligand rather than the electron as an effect of entropy.[21,22] In essence, while most of the internal energy of the cluster would have to be concentrated in the vibrational modes localized

around the solvated electron to enable it to exit the cluster, any of the n water ligands can evaporate, making the latter process statistically more probable.

It may be noted, that the smaller clusters below n = 13 can be detected in experiments where the time scale is shorter than the > 100 ms for ICR studies. For instance, in molecular

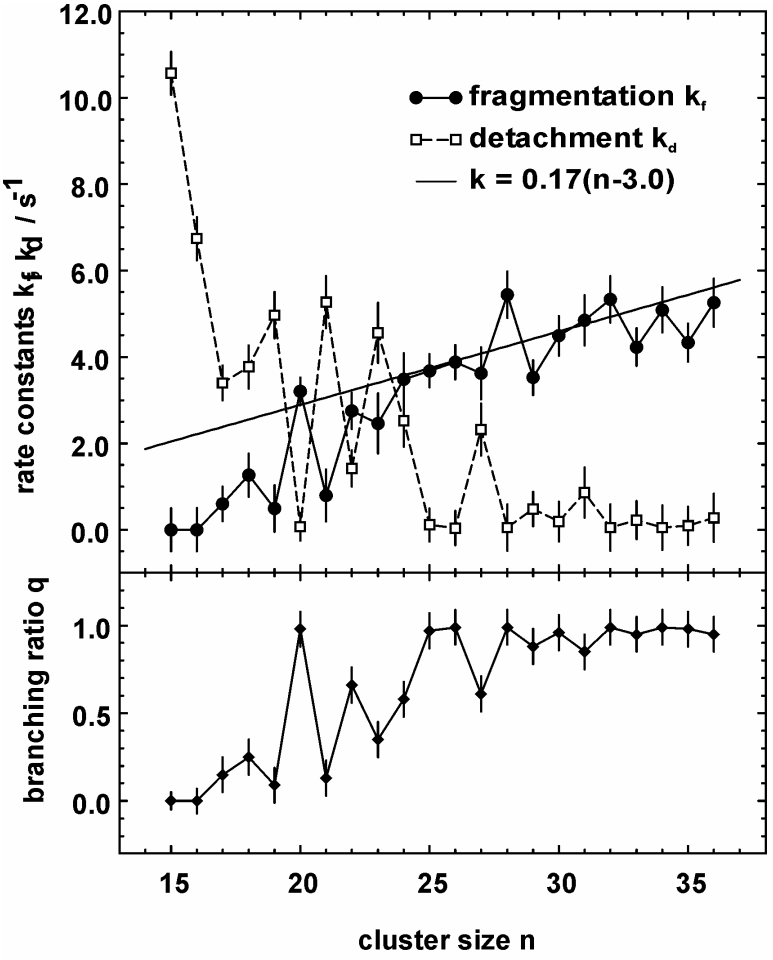

Figure 1. Fragmentation k_f and detachment k_d rate constants and branching ratio q of the black-body radiation induced decay of size selected hydrated electron clusters $(H_2O)_n^-$ as a function of cluster size. The branching ratio increases from 0 to 1, but pronounced odd-even oscillations are observed around n = 20. While the larger clusters exclusively fragment, the electron detachment becomes more important with decreasing cluster size, and is the only process detectable for clusters containing less than 17 water molecules. The solid line shows the expected rate constant based on the linear dependence of the fragmentation rate constants on the cluster size.[45,46] Reprinted with permission from ref.[21]

beams, clusters with n ≥ 6 are routinely observed, as well as the dipole bound anion of the water dimer. Recently, also the previously "missing" n = 3-5 clusters were observed.[51]

3.4. Reactions of Solvated Electrons

As noted above, the solvated electron clusters provide an interesting medium for studying reactions of aqueous electrons. These simple reactants exhibit a very multifaceted chemistry with a surprising variety of their chemical reactions, which can be crudely classified into at least the following four categories:

(a) Collisional activation. Nonreactive, nonpolar species, with low or negative electron affinity, for example rare gases like He or Ar, or stable molecules like carbon monoxide or ethylene, do not react at all with the solvated electron. The only process observed is a collision-induced increase of the fragmentation rate of the cluster.

(b) Ligand exchange. Polar molecules, which similar to water capable of forming strong hydrogen bonds and hydrogen bonded networks, such as methanol or other alcohols, react with the clusters by ligand exchange, replacing gradually part or even all of the aqueous shell by the reactant molecules.

(c) Core exchange. Species characterized by appreciable electron affinity can simply attach the electron, forming a negative ion, and replacing thus the ionic core of the cluster.

(d) Rearrangement of covalent bonds. Finally, a true chemical reaction, that is a process where existing covalent bonds are broken or new ones are formed may occur.

Below we will give a brief review of the previous studies, and give some examples of the various types of processes.

3.4.1. Collisional activation (a)

In view of reactivity studies with a collision gas introduced into the ICR cell, collisional fragmentation will obviously only be significant, if its rate becomes comparable to the rate of the radiative process, that is when the time between collisions between the clusters and the reactant gas are short compared the rate of energy absorption from the black body radiation. Typically, the studies in our laboratory are carried out at pressures of the order of 10^{-8} mbar, under conditions when only about one collision per second takes place. Under these circumstances, the effects of collisional fragmentation are small for clusters containing more than 10 water molecules, which is always the case for hydrated electrons. Collisional activation will thus lead to a small increase in the dissociation rate constants, which will usually still be dominated by black-body radiation.

As an example, no reactions of the hydrated electrons with CO, toluene and C_2H_4 were observed, and even when the pressure was increased appreciably above what we typically use in the reactivity studies, the collisions resulted in only a marginal acceleration of the fragmentation process. Similar apparent unreactivity was reported for N_2 and CH_3F colliding with $(H_2O)_n^-$ by Johnson and coworkers.[42]

3.4.2. Ligand exchange (b)

While one or more water ligands can be ejected when a water cluster undergoes a binary collision with a gas phase molecule or an atom, it is also possible for the collision partner to be trapped and inserted into the solvation shell.

$$(H_2O)_n^- + M \rightarrow M(H_2O)_{n-p}^- + p\ H_2O \qquad (1)$$

The simplest ligand exchange would obviously be replacing one water ligand by another water molecule, but since such a process leaves the mass unchanged, it cannot be seen in the mass spectrum. Obviously, one might study this process in an isotopic experiment, for instance by allowing the $(H_2O)_n^-$ clusters to collide with heavy water, D_2O. Such an experiment could in fact yield some interesting information about the rate of isotopic scrambling. In bulk water, as noted above, H^+ ions are present with about 1 molecule in 10^9 being spontaneously ionized, and proton transfer and isotopic scrambling are extremely rapid,

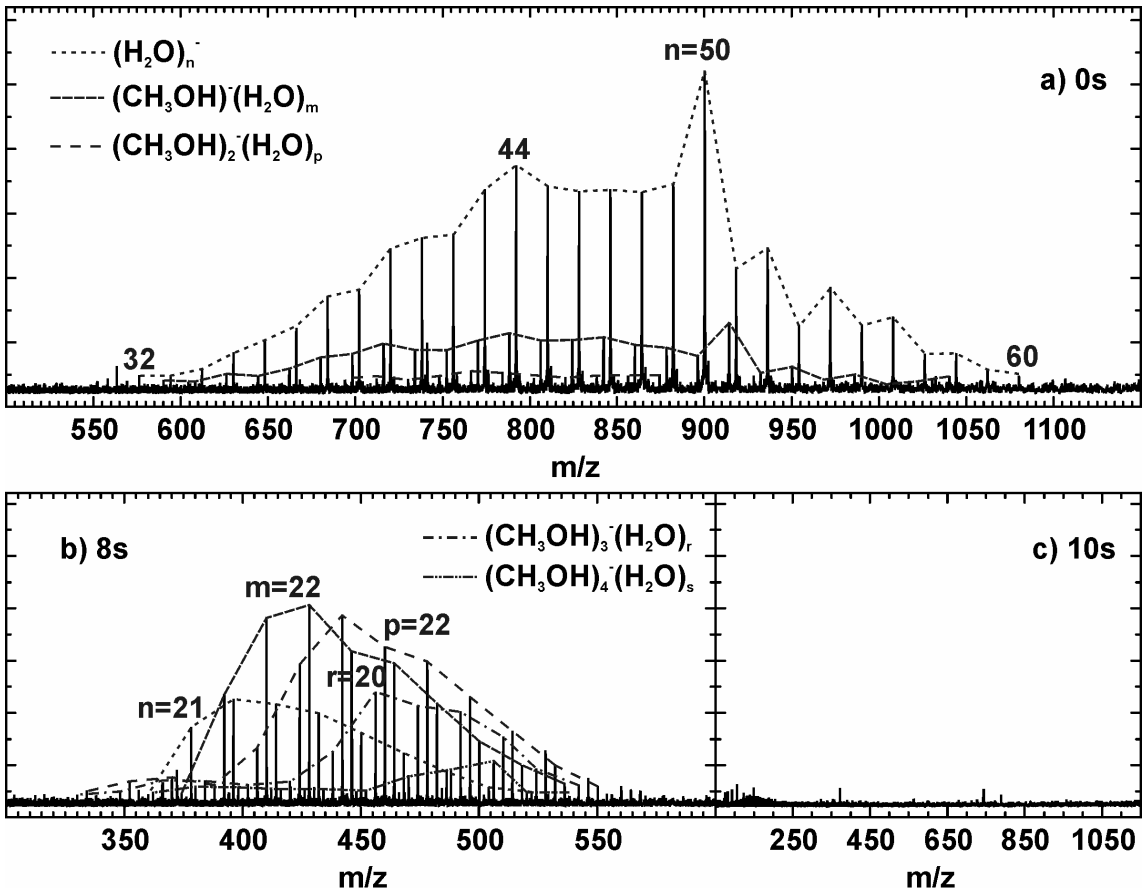

Figure 2. Mass spectra of the reaction of $(H_2O)_n^-$ with methanol after a) 0 s, b) 8 s and c) 10s. Already at 0 seconds product peaks containing a molecule of methanol can be observed. After 8 s the clusters containing one, $(CH_3OH)(H_2O)_n^-$, n = 18-27, or two methanol molecules $(CH_3OH)_2(H_2O)_n^-$, n = 18-28, are most intense. After additional 2 s all signal disappears due to the electron detachment.

so that in a mixture of H_2O and D_2O very rapidly a statistical concentration of HDO will be formed. In a finite $(H_2O)_n^-$ cluster, on the other hand, neither H^+ nor OH^- ions are present, and it would be of some interest to establish the probability of an exchange of hydrogen for deuterium in collisions with D_2O.

The water clusters are held together by a network of hydrogen bonds, and the above process will be particularly prevalent with species which also contain polar XH bonds, and which are thus capable of strong hydrogen bonding, for instance ammonia or alcohols. The ligand exchange of a solvated electron cluster distribution (n = 35-60) with methanol, that is reaction (1) where M = CH_3OH, was examined. The ligand exchange proceeds with high collisional efficiency, and already at a nominal time t = 0, one can observe product peaks containing a molecule of methanol, indicating that nearly 20% of the $(H_2O)_n^-$ clusters have already reacted, as evidenced in Figure 2, resulting in a solvated electron, where besides the water molecules, there is also one methanol ligands. Obviously, such reaction can proceed further and additional water ligands – perhaps in some cases ultimately all – can be replaced by the reaction partner, and this is confirmed by the further course of the reaction with methanol. After a further 1 s reaction, the clusters with one molecule of methanol have in fact intensities higher than the unreacted water clusters, and also clusters with 2-4 methanol ligands, that is $(H_2O)_n(CH_3OH)_m^-$ with m = 2, 3, and 4 species are present. Simultaneously, the overall distribution shifts progressively towards lower values of n. After 6 s reaction one finds that the m = 0, that is pure hydrated electron clusters are basically gone, most prominent are species with m = 3 (n = 19-28), m = 2 (n = 19-28) and m = 1 (n = 20-27) are most prominent, and clusters with up to m = 6, that is six methanol molecules are observable. Beyond this point, the clusters continue to lose ligands, but interestingly, the pure hydrated clusters make a comeback. Apperently, in the fragmentation process the clusters lose methanol faster than the water ligands. After 8 s one again sees pure hydrated electrons, m = 0 (n = 20-27), clusters with one or two methanols, m = 1 (n = 18-27) and m = 2

(n = 18-28) are now most abundant, and the overall signal intensity decreases. After additional 2 s all signal disappears, and only noise is detectable, as can be seen in Figure 2.

Methanol is, similar to water in that it can form relatively strong hydrogen bonds. It is, however, less polar (μ = 1.7 D), the bonds are weaker, as also evidenced by its much higher vapor pressure, and lower boiling point of 64.6 ^{o}C. Unlike water, it also has only one polar OH bond, and can therefore not so easily form extended hydrogen bonded networks. The exchange according to equation (1) is probably slightly endothermic, but can occur in ambient temperature gas phase collisions. In our experiment, where essentially only methanol molecules are present in the gas phase, their collisions with the hydrated electron clusters can gradually exchange several water ligands for methanol. These will, however, most likely remain near the cluster surface, and as the fragmentation becomes dominant, will eventually also preferentially "evaporate" from the cluster. When in the course of the cluster fragmentation process the number of water ligands drops below about 25-30, the electron detachment process will starts to compete with ligand loss, and before it can drop below twenty or so, all clusters will be lost. The fact that the mixed clusters seem to disappear around the comparable value of n = 20-25, that is with a comparable number of water ligands as the pure hydrated electrons, indicates that the methanol does not provide any additional stabilization of the electron, which is probably mainly stabilized by the water ligands.

Characteristic of a ligand exchange where molecules in the solvation shell are replaced is that multiple exchanges can take place, with the probability of the process taking place on a given collision being dependent on a number of factors. The most important factor undoubtedly is the enthalpy change associated with the reaction (1). The second crucial factor is the ratio m/n, i.e. the number of new ligands m vs. the number of water molecules n in the cluster. With increasing m/n, the probability for loss of a previously exchanged ligand instead of water decreases. This is evidenced by the gradual slowing and phasing out of the methanol exchange.

3.4.3. Core exchange (c)

In the experiments discussed in the previous sections, the molecules of the reaction partner are simply traded for the water ligands of the hydrated electron. A conceptually different process involves reactions with species which bind the electron, producing a negatively charged ion. This results in the change of the ionic core of the cluster. Since the clusters contain only one solvated electron – and one ionic core - in reactions of this type one and only one of the neutral reactant molecules is taken up by the cluster.

A simple example is the reaction with oxygen.[40-42] Molecular oxygen has a $^3\Pi_g$ ground state, with a $\sigma_g^2\pi_u^4\pi_g^2$ electronic configuration, and can accommodate two additional electrons in its highest occupied degenerate antibonding π_g orbital. Accordingly, it has an appreciable electron affinity of about 2 eV. Upon collision with an $(H_2O)_n^-$ cluster, the molecular oxygen attaches the electron, forming a ground state $^2\Pi_g$ O_2^- anion. In the aqueous cluster, the water molecules will form hydrogen bonds to the negatively charged anion, which will be much more strongly hydrated than the very diffuse free electron. The electron will consequently be further stabilized in the cluster by the presence of the molecular oxygen, and this stabilization is clearly evidenced in the mass spectrometric experiment. As discussed above, when the $(H_2O)_n^-$ clusters gradually fragment and lose the solvent, the stabilization of the electron is reduced, so that eventually it is detached, with the ions completely disappearing from the ICR trap. While for pure hydrated electrons, this process is completed around n = 15, in the presence of a molecule of oxygen, the fragmentation proceeds further, with the total number of the anions in the trap remaining basically constant.[40] The final products of the fragmentation are the $O_2^-(H_2O)_n$, n = 2 and n = 3 species, which remain in the trap even after several minutes. The $O_2^-(H_2O)_2$ cluster neither detaches the electron, nor further fragments to n = 1, and is stable under the conditions of our experiment. As already noted, the electron in

these clusters is tightly bound to O_2. Since the electron is intimately involved in the course of the reaction and binding the oxygen molecule, we have never observed a second O_2 to be taken up by the cluster, regardless of its size. Note that it was recently shown by infrared spectroscopy, that the first "solvation shell" of $O_2^-(H_2O)_n$ is completed with n = 4.[52,53]

Equally interesting, albeit somewhat different, is the case of carbon dioxide.[40-42] The linear nonpolar CO_2 owes its high stability to a closed shell structure, with a completely filled 2p π_g highest occupied molecular orbital. However, it possesses an empty, low lying antibonding orbital, also derived from the 2p electrons, which strongly favors a bent structure. Placing an additional electron in this orbital to produce the bent CO_2^- anion, which is isoelectronic with NO_2, requires a considerable energy, since unlike that of molecular oxygen, the electron affinity of ground state CO_2 is negative. On the other hand, the bent, strongly polar CO_2^- anion can form very strong hydrogen bonds to water molecules so that the reaction (2), which is strongly endothermic for n=0, becomes exothermic already with n = 1.

$$(H_2O)_n^- + CO_2 \rightarrow CO_2^-(H_2O)_n \qquad (2)$$

This was first demonstrated by the experimental observation of the mass spectrum of the $CO_2^-(H_2O)$ anion.[54] These early results were confirmed more recently by photoelectron spectroscopy[55] as well as by ab initio calculations.[56] The carbon dioxide anion forms a cyclic planer C_{2v} $CO_2^-(H_2O)$ anion where the two strong O…H hydrogen bonds stabilize the structure, and more than compensate for the negative electron affinity of CO_2. The electron is then further stabilized by additional water ligands.[40] In contrast with pure water solvated electrons, which are lost when the number of ligands drops below about n = 15, in the presence of carbon dioxide one finds again that the fragmentation proceeds further, until the final product cluster $CO_2^-(H_2O)_2$ is formed. Similar to the oxygen containing clusters, these then do not seem to fragment further to form the n = 1 cluster. The stabilization of the

electron is, however, in this case apparently less efficient, and as the clusters are further activated by black body radiation and collisions with the CO_2 reactant gas, they slowly detach the electron, so that the intensity gradually decreases, and after about 1 minute all the ions disappear from the trap.

The detailed descripton, experimental setup and result discussion, of the hydrated electron reaction with oxygen and carbon dioxide are the subject of Chapter 4.

In another experiment a 1:1 mixture of CO_2 and C_2H_4 induced the formation of $CO_2^-(H_2O)_n$ as the only product. The only contribution of ethylene is in the increase of the-collision induced fragmentation, while a coupling of the CO_2^- radical anion with the carbene was not observed.

Acetone behaves similar to CO_2. After 1 s about 50% of the initial hydrated electron clusters have reacted to $(CH_3COCH_3)^-(H_2O)_n$, at an acetone pressure which is twice as high as the CO_2 pressure in the comparable experiment. For comparison, the clusters need 2 s in the case of CO_2 to achieve a 50% conversion into products. This suggests that acetone, like CO_2, reacts with collision rate with the cluster. After 7 s reaction delay, the clusters have been completely transformed into products. The $(CH_3COCH_3)^-(H_2O)_n$ ions fragment, after 28 seconds, to the final product, $(CH_3COCH_3)^-(H_2O)_4$. Due to the presence of a very small amount of methanol in the UHV, $(CH_3COCH_3)^-(CH_3OH)(H_2O)_{3,4}$ peaks are also present at this stage of the reaction. This suggests that a minimum of four solvents molecules, regardless of the type of solvent, is needed to stabilize the $CH_3COCH_3^-$ anion. $(CH_3COCH_3)^-(H_2O)_4$, as well as $(CH_3COCH_3)^-(CH_3OH)(H_2O)_3$, undergo a slow electron detachment.

Acetaldehyde behaves almost identical to acetone. The hydrated electron cluster efficiently take in only one acetaldehyde molecule and solvated $CH_3CHO^-(H_2O)_m$ anions are formed. After a single molecule of the reactant has entered the cluster, no further uptake of acetaldehyde is observed in the early stage of the reaction. Conversion of 50% of the initial distribution is reached fast, in less than 1 s. After 7 seconds the initial $(H_2O)_n^-$ clusters are

again barely visible. The $CH_3CHO^-(H_2O)_m$ clusters then fragment, losing one by one the water molecules down to $CH_3CHO^-(H_2O)_3$. When the clusters are very small an endothermic ligand exchange takes place leading to the formation of $(CH_3CHO)_2^-(H_2O)_2$. We repeated the experiments using perdeuterated acetaldehyde, CD_3CDO. Similarly to the acetaldehyde, the $CD_3CDO^-(H_2O)_m$ clusters are formed, followed by fragmentation down to $CD_3CDO^-(H_2O)_3$. The intake of a second CD_3CDO molecule leads to $(CD_3CDO)_2^-(H_2O)_2$ formation. No H/D exchange is observed, even after long reaction delays. For both, acetaldehyde and perdeuterated acetaldehyde, after long reaction delays of 50 s, the signal has disappeared due to black-body radiation and collision-induced electron detachment.

Benzonitrile is one of the molecules which react with the electron inducing a ionic core exchange. The peaks corresponding to an uptake of one benzonitrile molecule $(C_6H_5CN)^-(H_2O)_m$ into the clusters are already visible at 0 s reaction delay. Once the free electron is not anymore available, the clusters start to exchange ligands. Thus two seconds later the clusters have exchanged several water molecules for a second benzonitrile. From the offset of the cluster distributions one can approximate the number of water molecules exchanged for one benzonitrile to be 5 or 6. The clusters continue to fragment and exchange ligand molecules until, after 15 s reaction delay, five progressions of product peaks are visible, each containing 1-5 benzonitrile molecules. Clearly, the most intense peak distribution is $(C_6H_5CN)^-(H_2O)_n$, n = 4-12, with an intensity maximum at m/z = 265 and corresponding to m = 9 water molecules. After 20 seconds the clusters have completely exhanged or lost all the water molecules, and one can clearly identify $(C_6H_5CN)_m^-$, m = 2-7. At the same time two other distributions can be seen. The first one as intense as the products, with the peaks at m/z = 266, 369, 472, 575, 678 and the other about one fifth with peaks at m/z = 429, 532, 636. Both contain benzonitrile, but are shifted by 60 amu and 120 amu, respectively, to higher masses. We are not able to rationalize these products in terms of reaction with benzonitrile alone. The most probable explanation is that, at long reaction

delays, due to the very high number of collisions, a minor, unidentified impurity in the benzonitrile solution, is taken in by the clusters. However, after additional 10 seconds, the impurity is lost from the clusters, and the products seen after 30 seconds are $(C_6H_5CN)_{2,3,4}^-$. After a total of 40 s reaction delay, the clusters have detached the electron and the signal is lost.

Another example for ionic core exchange are the reactions with NO reported in the literature by Johnson, Viggiano and coworkers.[41,42] These differ slightly from the O_2 and CO_2 reactions. Again, in the first reaction step, $NO^-(H_2O)_n$ is formed, where NO^- undoubtedly form the ionic core. $NO^-(H_2O)_n$, however, undergo at least to additional steps of ligand exchange, which is, however, conceptually different from the case b). NO does not participate in the hydrogen bonded network, but rather forms strong bonds to NO^-. The $(NO)_3^-$ unit thus might be seen as the "real" ionic core of the cluster.

A different case of chemical reaction is observed with hydrogen chlorine. We have reported previously that the strong HCl acid can dissolve in large hydrated ions, that is in clusters with at least 10-12 water ligands, and, like in bulk water, an ionization into an H^+ proton and a halide anion occurs. In bulk solutions, the lifetime of free electrons is essentially limited by the presence of the H^+ ions, with which they can recombine. Similarly, in the finite cluster the electron apparently immediately recombines with the HCl proton, yielding a hydrogen atom. The neutral hydrogen atom is held far too weakly by the water solvent, and evaporates from the cluster leaving behind a Cl^-_{aq}. Following the described mechanism, a switch in the ionic core of the cluster takes place according to the equation:

$$e^-(H_2O)_n + HCl \rightarrow Cl^-(H_2O)_{n-k} + k\,H_2O + H \qquad (3)$$

The HCl attaches the electron and dissociates. The proton which is again released, originates in this case at least formally from the HCl collision partner, rather than from one of the water molecules of the original water cluster, with the Cl^- becoming the new ionic core.

The cluster mass should thus be increased by the mass of chlorine, that is depending on the isotope, by 35 or 37 AMU. Actually, however, the dissociation energy of HCl, 4.43 eV, is more than balanced by the large electron affinity of the Cl atom (3.6127 eV), and the increased hydration energy of the chlorine anion, Cl^- which is considerably larger than that of a free electron. Consequently, the reaction (3) is exothermic, and the switch in the ionic core and reduction of the proton to generate atomic hydrogen is accompanied by the evaporation of two molecules of water.

At this point however, the clusters have enough water molecules so they can ionically solvate and stabilize additional HCl molecules. Since the free electron is not available anymore to recombine with a proton, no other neutral hydrogen atom lives the cluster. The process is a simple ligand exchange with the clusters giving away water for hydrogen chlorine. After 9 seconds reaction delay, up to 6 HCl molecules are in the clusters. The ligand exchange process proceeds concurrently with the blackbody radiation induced fragmentation the clusters being fast saturated by HCl. In the further course of reaction, they just lose ligands, either due to the above mentioned black body radiation, or to collisions. In either case, in the course of such a fragmentation, one can expect that at each stage, the weakest bound remaining ligand is most likely to be lost. Finally, after 40 seconds reaction delay, the only patterns present are due to $Cl^-(HCl)_{2,3,4}$. The most intense peaks correspond to the C_{3v} $Cl^-(HCl)_3$. This then only very reluctantly further fragments losing HCl, to form the m = 2, C_{2v} $Cl^-(HCl)_2$ cluster. The details of this reaction can be found in chapter 6.

3.4.4. Rearrangement of covalent bonds (d)

One usually understands under chemical reaction a process, where chemical bonds between atoms are broken or formed, and strictly speaking, none of the processes discussed above really falls into this category. There are, however, numerous reactions where

interaction with the hydrated electron does indeed result in a breakage of a real, covalent chemical bond, or formation of a new one, or both. Such reactions are very often initiated by a change in the nature of the ionic core of the $(H_2O)_n^-$ cluster. Very simple examples are the reactions with Br_2 and CH_3Br studied by Johnson and coworkers,[42] which result in formation of $Br^-(H_2O)_n$. In these cases, the electron affinity of the Br atom of 3.36 eV is the driving force of the reaction, which in itself is sufficient for the bond cleavage in Br_2 and CH_3Br.[42]

Repeating the experiments with N_2O under ICR conditions, the results are similar to the flow reactor study.[41] We also observe two different products, formation of $O^-(H_2O)_n$ and

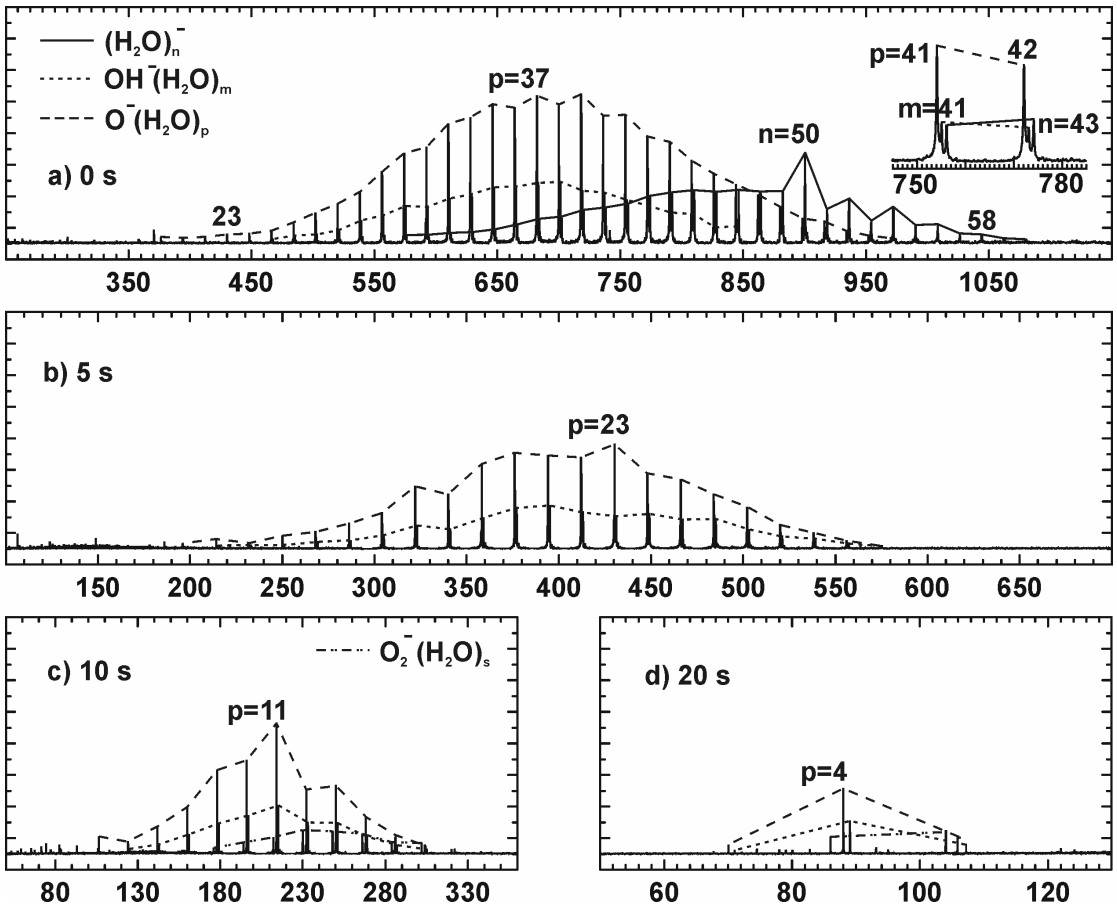

Figure 3. Mass spectra of the reaction of $(H_2O)_n^-$ with N_2O after a) 0s, b) 5s, c) 10 s and d) 20 s. Already at 0 seconds two different product distributions are visible. Shifted lower by one AMU are the $OH^-(H_2O)_m$, while a shift of two AMU to the left corresponds to the $O^-(H_2O)_p$ products. After 5 seconds the initial hydrated electron clusters have completely reacted. The clusters fragment due to the black-body radiation to $OH^-(H_2O)_3$ and $O^-(H_2O)_3$. Species $O_2^-(H_2O)_s$ are present due to minor impurities of O_2, after long reaction delays.

$OH^-(H_2O)_n$, with a branching ratio of approximately 3:1. Figure 3 shows the temporal evolution of the mass spectra with reaction time. The branching ratio can best be seen in the primary product, which exhibits almost exactly three times the intensity for $O^-(H_2O)_{41}$, compared with $OH^-(H_2O)_{41}$. Initially, $O^-(H_2O)_n$ is formed by abstraction of the oxygen atom from N_2O, which will immediately recombine with the electron. In this initially hot cluster, isomerization of $O^-(H_2O)_n$ to $OH^-(OH)(H_2O)_{n-1}$ is energetically feasible, and an OH radical can be lost. $OH^-(OH)$ core switching competes with H_2O evaporation, and this competition would be responsible for the observed branching ratio.

Another, more complex involves the reaction of hydrated electrons with acetonitrile,[23] chapter 5 being dedicated to this subject. Shortly, a*b initio* studies have shown that the nitrile carbon atom of CH_3CN may attach an additional hydrogen atom to form a relatively stable CH_3CHN radical[59]. The CH binding energy is, however, not sufficient to make a reaction such as, for instance, $CH_3CN + H_2O \rightarrow CH_3CHN + OH$, accessible. This situation, however, changes appreciably in the presence of an electron:

$$(H_2O)_n^- + CH_3CN \rightarrow OH^-(H_2O)_{n-m-1} + CH_3CHN + m\ H_2O \qquad (4)$$

The reaction (4) is assisted in the first place by the appreciable, 1.8277 eV electron affinity of the hydroxyl group. Furthermore, it is also promoted by the solvation energy of the relatively compact OH^- anion, which is considerably higher than that of the diffuse free electron. Accordingly, reaction (4) proceeds in the ICR cell spontaneously, and probably with close to the collision rate, as evidenced by the presence of a considerable concentration of the reaction product already at nominally t = 0 s. In the presence of gaseous acetonitrile in the cell, the aqueous electron clusters lose a hydrogen atom, and are thus converted into hydrated hydroxyl anions. Using deuterated acetonitrile instead reveals that the methyl group is not

involved in the reaction, and one of the aqueous protons is lost from the cluster. Like the reactions listed in the previous section, this reaction is also accompanied by a change in the ionic core of the cluster. Obviously, it again requires the presence of a free electron, and each cluster can therefore react only once. The product clusters containing the hydroxyl anion, $OH^-(H_2O)_n$, are, similar to clusters containing molecular oxygen, stable with respect to electron detachment due to the high electron affinity of the OH radical.

In our previous study we have shown that the hydrated hydroxyl anions, prepared directly in the ionic source, when left alone in the ICR cell gradually fragment, leaving $OH^-(H_2O)_3$ as a final product. This anion eventually reaches thermal equilibrium with the ambient temperature apparatus walls, and is effectively stable under our experimental conditions both with respect to electron detachment and with respect to further fragmentation. In the presence of gas phase acetonitrile in the cell, however, the small $OH^-(H_2O)_n$ clusters below about n = 10 can take up one additional CH_3CN molecule, undoubtedly due to its high basicity. These then further fragment losing either H_2O or CD_3CN molecules, yielding eventually the $OH^-(H_2O)_2(CD_3CN)$ cluster as a final product.[39] Interestingly, experiments with isotopic deuterium reveal, that within this cluster a dynamical, proton transfer equilibrium is established:

$$(H_2O)_2(OH^-)(CH_3CN) \quad \leftrightarrow \quad (H_2O)_3(CH_2CN^-) \qquad (5)$$

When CD_3CN is used, repeated proton transfer processes according to equation (5) lead to a complete isotopic scrambling within the complex between the “organic” CH_3CN, and the aqueous, $OH^-(H_2O)_2$ parts. It is also interesting to note, that a single additional water molecule is sufficient to switch off this isotopic scrambling.

Table 1. Summary of the hydrated electron cluster reactions with different molecules.

Reactant	Product	Type of reaction	Final product	
			Number of water molecules n	Electron detachment
CO [f]	-	a		YES
C_2H_4 [f]	-	a		YES
$C_6H_5CH_3$ [f]	-	a		YES
N_2 [a]	-	a		not probed
CH_3F [a]	-	a		not probed
CH_3OH [f]	$(H_2O)_n(CH_3OH)_{1-6}^-$	b		YES
O_2 [a,b,d]	$O_2^-(H_2O)_n$	c	2	NO
CO_2 [a,b,d]	$CO_2^-(H_2O)_n$	c	2	YES
$CO_2 + O_2$ [d]	$O_2^-(H_2O)_n$	c	2	NO
$CO_2 + C_2H_2$ [f]	$CO_2^-(H_2O)_n$	c	2	YES
CH_3CHO [f]	$(CH_3CHO)^-(H_2O)_n$	c	3 [g]	YES
CD_3CDO [e]	$(CD_3CDO)^-(H_2O)_n$	c	3 [g]	YES
CH_3COCH_3 [f]	$(CH_3COCH_3)^-(H_2O)_n$	c	4	YES
C_6H_5CN [f]	$(CH_3COCH_3)_{1-5}^-(H_2O)_n$	c	0 [g]	YES
NO [a,b]	$NO^-(H_2O)_n$	c		not probed
N_2O [b,f]	$O^-(H_2O)_n$	d	3	NO
	$OH^-(H_2O)_m$	d	3	NO
CH_3CN [c]	$OH^-(H_2O)_n$	d	[g]	NO
CD_3CN [e]	$OH^-(H_2O)_n$	d	[g]	NO
Br_2 [a]	$Br^-(H_2O)_n$	d		not probed
CH_3Br [a]	$Br^-(H_2O)_n$	d		not probed

[a] Reference [42].
[b] Reference [41].
[c] Reference [23].
[d] Reference [40].
[e] Reference [39].
[f] This work.
[g] Product undergoes further ligand exchange with the neutral reactant.

3.5. Conclusions

The studies of the hydrated electrons show, that they undergo many reactions known from pulsed radiolysis experiments and similar studies, but also exhibit properties specific for finite clusters. Studies of such clusters trapped in an FT-ICR experiment have the advantages of less ambiguity, complete elimination of the effects of impurities, and in view of the long lifetime of the solvated electron the ability to study even very slow and inefficient reactions. In this way, the inherent chemical properties of the solvated electron can be probed.

The processes occurring upon binary collisions of the $(H_2O)_n^-$ clusters with small gas phase molecules, can be classified, into at least four distinct categories, collisional activation, ligand exchange, core exchange, and rearrangement of covalent bonds. We present and discuss representative examples for each of these categories, and review the rich and multifaceted reactions of free electrons, the simplest free radicals of them all.

3.6 References

[1] W. Weyl, *Poggendorff's Annalen der Physik und Chemie* **1864**, *21*, 601.

[2] C.A. Kraus, *J. Am. Chem. Soc.* **1908**, *30*, 1323.

[3] E.J. Hart, J.W. Boag, *J. Am. Chem. Soc.* **1962**, *84*, 4090

[4] J.W. Boag, E.J. Hart, *Nature* **1963**, *197*, 45.

[5] J.P. Keene, *Nature* **1963**, *197*, 47.

[6] G.V. Buxton, C.L. Greenstock, W.P. Helman, A.B. Ross, *J. Phys. Chem. Ref. Data* **1988**, *17*, 513.

[7] A. Migus, Y. Gauduel, J.L. Martin, A. Antonetti, *Phys. Rev. Lett.* **1987,** *58*, 1559.

[8] Y. Kimura, J.C. Alfano, P.K. Walhout, P.F. Barbara, *J. Phys. Chem.* **1994,** *98*, 3450.

[9] U. Schindewolf, *Angew. Chem. Int. Edit.* **1968,** *7*, 190.

[10] J. Jortner, M. Ottolenghi, G. Stein, *J. Phys. Chem.* **1964,** *68*, 247.

[11] D.C. Walker, *Can. J. Chem.* **1966,** *44*, 2226.

[12] J. Jortner, *J. Chem. Phys.* **1959,** *30*, 839.

[13] F.H. Long, H. Lu, K.B. Eisenthal, *Phys. Rev. Lett.* **1990,** *64*, 1469.

[14] P.J. Rossky, J. Schnitker, *J. Phys. Chem.* **1988,** *92*, 4277.

[15] H. Haberland, H. Langosch, H.G. Schindler, D.R. Worsnop, *J. Phys. Chem.* **1984,** *88*, 3903.

[16] H. Haberland, C. Ludewigt, H.G. Schindler, D.R. Worsnop, *J. Chem. Phys.* **1984,** *81*, 3742.

[17] H. Haberland, H.G. Schindler, D.R. Worsnop, *Ber. Bunsen Ges. Phys. Chem.* **1984,** *88,* 270.

[18] J.V. Coe, G.H. Lee, J.G. Eaton, S.T. Arnold, H.W. Sarkas, K.H. Bowen, C. Ludewigt, H. Haberland, D.R. Worsnop, *J. Chem. Phys.* **1990,** *92*, 3980.

[19] P. Ayotte, C.G. Bailey, J. Kim, M.A. Johnson, *J. Chem. Phys.* **1998,** *108*, 444.

[20] P. Ayotte, M.A. Johnson, *J. Chem. Phys.* **1997,** *106*, 811.

[21] M.K. Beyer, B.S. Fox, B.M. Reinhard, V.E. Bondybey, *J. Chem. Phys.* **2001,** *115*, 9288.

[22] V.E. Bondybey, M.K. Beyer*, Int. Rev. Phys. Chem.* **2002,** *21*, 277.

[23] O.P. Balaj, I. Balteanu, B.S. Fox-Beyer, M.K. Beyer, V.E. Bondybey, *Angew. Chem.* **2003,** *115*, 5675; *Angew. Chem. Int. Edit.* **2003,** *42*, 5516.

[24] A.L. Sobolewski, W. Domcke, *Phys. Chem. Chem. Phys.* **2003,** *5*, 1130.

[25] A.L. Sobolewski, W. Domcke, *Phys. Chem. Chem. Phys.* **2002,** *4*, 4.

[26] D.C. Clary, D.M. Benoit, *J. Chem. Phys.* **1999,** *111*, 10559.

[27] F. Weigend, R. Ahlrichs, *Phys. Chem. Chem. Phys.* **1999,** *1*, 4537.

[28] J. Kim, J.Y. Lee, K.S. Oh, J.M. Park, S. Lee, K.S. Kim, *Phys. Rev. A* **1999,** *59*, R930.

[29] R.N. Barnett, U. Landman, S. Dhar, N.R. Kestner, J. Jortner, A. Nitzan, *J. Chem. Phys.* **1989,** *91*, 7797.

[30] R.N. Barnett, U. Landman, C.L. Cleveland, J. Jortner, *J. Chem. Phys.* **1988,** *88*, 4421.

[31] R.N. Barnett, U. Landman, C.L. Cleveland, J. Jortner, *J. Chem. Phys.* **1988,** 88, 4429.

[32] U. Landman, R.N. Barnett, C.L. Cleveland, D. Scharf, J. Jortner, J. *Phys. Chem.* **1987,** *91*, 4890.

[33] N.R. Kestner, J. Jortner, *J. Phys. Chem.* **1984,** *88*, 3818.

[34] B.K. Rao, N.R. Kestner, *J. Chem. Phys.* **1984,** *80*, 1587.

[35] J.M. Weber, E. Leber, M.W. Ruf, H. Hotop, *Eur. Phys. J.* **1999,** *D 7*, 587.

[36] M. Knapp, O. Echt, D. Kreisle, E. Recknagel, *J. Phys. Chem.* **1987,** *91*, 2601.

[37] M. Knapp, O. Echt, D. Kreisle, E. Recknagel, *J. Chem. Phys.* **1986,** *85*, 636.

[38] P.J. Campagnola, L.A. Posey, M.A. Johnson, *J. Chem. Phys.* **1991,** *95*, 7998.

[39] O.P. Balaj, C.-K. Siu, I. Balteanu, B.S. Fox-Beyer, M.K. Beyer, V.E. Bondybey, *J. Phys. Chem.* **2004**, *108*, 7506.

[40] O.P. Balaj, C.-K. Siu, I. Balteanu, M.K. Beyer, V.E. Bondybey, *Chem. Eur. J.* **2004**, *10*, 4822-4830.

[41] S.T. Arnold, R.A. Morris, A.A. Viggiano, M.A. Johnson, *J. Phys. Chem.* **1996,** *100*, 2900.

[42] L.A. Posey, M.J. Deluca, P.J. Campagnola, M.A. Johnson, *J. Phys. Chem.* **1989,** *93*, 1178.

[43] R.C. Dunbar, *J. Phys. Chem.* **1994,** *98*, 8705.

[44] R.C. Dunbar, T.B. McMahon, *Science* **1998,** *279*, 194.

[45] B.S. Fox, M.K. Beyer, V.E. Bondybey, *J. Phys. Chem. A* **2001,** *105*, 6386.

[46] T. Schindler, C. Berg, G. Niedner-Schatteburg, V.E. Bondybey, *Chem. Phys. Lett.* **1996,** *250*, 301.

[47] P.D. Schnier, W.D. Price, R.A. Jockusch, E.R. Williams, *J. Am. Chem. Soc.* **1996,** *118*, 7178.

[48] M. Sena, J.M. Riveros, *Rapid Commun. Mass Spectrom.* **1994,** *8*, 1031.

[49] D. Tholmann, D.S. Tonner, T.B. McMahon, *J. Phys. Chem.* **1994,** *98*, 2002.

[50] P. Weis, O. Hampe, S. Gilb, M.M. Kappes, *Chem. Phys. Lett.* **2000,** *321*, 426.

[51] J. Kim, I. Becker, O. Cheshnovsky, M.A. Johnson, *Chem. Phys. Lett.* **1998,** *297*, 90.

[52] J.M. Weber, J.A. Kelley, S.B. Nielsen, P. Ayotte, M.A. Johnson, *Science* **2000,** *287*, 2461.

[53] J.M. Weber, J.A. Kelley, W.H. Robertson, M.A. Johnson, *J. Chem. Phys.* **2001,** *114*, 2698.

[54] C.E. Klots, *J. Chem. Phys.* **1979,** *71*, 4172.

[55] T. Tsukuda, M. Saeki, R. Kimura, T. Nagata, *J. Chem. Phys.* **1999,** *110*, 7846.

[56] M. Saeki, T. Tsukuda, S. Iwata, T. Nagata, *J. Chem. Phys.* **1999,** *111*, 6333.

[57] G.E. Adams, R.L. Willson, *Trans. Faraday Soc.* **1969,** *65*, 2981.

[58] G.V. Buxton, R.M. Sellers, D.R. McCracken, *J. Chem. Soc., Faraday Trans.* **1976,** *172*, 1464.

[59] B.S. Wang, H. Hou, Y.S. Gu, *J. Phys. Chem. A* **2001,** *105*, 156.

4. Reaction of Hydrated Electrons $(H_2O)_n^-$ with Carbon Dioxide and Molecular Oxygen: Hydration of the CO_2^- and O_2^- Anions

4.1 Introduction

Most chemical reactions involve a transfer or redistribution of electrons between the reacting species, and free electrons themselves can be considered to be the simplest chemical reactants. Indeed, the reactions of electrons in bulk solutions have been studied quite extensively, for instance in experiments using the pulsed radiolysis techniques,[1] and Marcus pioneered the theory of electron transfer reactions in solution.[2] We have recently pointed out, that reactivity studies in finite clusters of solvated electrons, rather than in bulk solutions could provide very useful complementary information.[3] This approach has the advantage, that the elemental composition of clusters can be unambiguously established based on their exact mass, and side reactions which limit the lifetime of the hydrated electrons are absent.

All the species involved in the current work, that is molecular oxygen, water, and carbon dioxide, are important components of the atmosphere, and also electrons are extremely ubiquitous, being formed by radioactive processes, cosmic and vacuum UV radiation, as well as by electric discharges and lightening. In view of the abundance and frequent occurrence of these species, and their importance for atmospheric chemistry, the reactions of aqueous electrons with oxygen and carbon dioxide, and the properties and chemistry of the solvated anions investigated here may be of more than just academic interest.

The CO_2^- molecular anion, also known as formate radical, was repeatedly observed in rare gas matrices and characterized by infrared spectroscopy.[4-9] Free CO_2^- was generated in a crossed beam experiment by collision of alkali metal atoms with CO_2,[10] establishing its adiabatic electron affinity as -58 ±19 kJ/mol, while its vertical electron affinity was determined from electron scattering measurements as -350 kJ/mol.[11] Calculations by

Yoshioka and Jordan confirmed the charge-transfer nature of alkali metal-CO_2 complexes.[12,13] The idea that solvation can stabilize the CO_2^- anion was developed on $(CO_2)^-$ clusters.[14-16] Klots found that already one water molecule is sufficient to prevent electron autodetachment from $CO_2^-(H_2O)$.[17] Recently, photoelectron spectroscopy[18] and *ab initio* calculations[19] by Nagata, Iwata and coworkers confirmed and quantified these early observations. Similar results on the stabilization of COS^- by a single water molecule were recently reported by Sanov and coworkers.[20]

The superoxide radical O_2^- is ubiquitous in radiation chemistry, and plays an important role in biological radiation damage.[21] CO_2^- can serve as an intermediate in its formation.[22] In contrast to CO_2, the electron affinity of O_2 is positive, and no solvent is needed to stabilize the radical anion. Recent infrared spectroscopic studies by Johnson and coworkers indicate that the first solvation shell of $O_2^-(H_2O)_n$ is completed at n = 4.[23, 24]

Hydrated electrons in the gas phase, $(H_2O)_n^-$, were first reported by Haberland and coworkers,[25-28] and extensively characterized spectroscopically by different groups.[29, 30] A series of experiments by the groups of Johnson and Viggiano[31, 32] in molecular beam and flow reactor setups has revealed an interesting variety in their behavior towards different gaseous reactants. As typical electron scavengers, diatomic O_2, as well as the usually extremely stable and unreactive CO_2 molecules are "dissolved" in the $(H_2O)_n^-$ with nearly collisional efficiency.

We have previously reported that a laser vaporization cluster source is an effective source for solvated electrons.[33] This allowed us to investigate in some detail the stability of the solvated electrons, and the competition between their fragmentation and electron detachment induced by ambient black body infrared radiation. In the present work, we use Fourier Transform Ion Cyclotron Resonance (FT-ICR) mass spectrometry, and focus our investigation on O_2 and CO_2. The experimental study of the formation and stability of these hydrated anions is complemented by quantum chemical computations.

4.2 Experimental Section

The hydrated electron clusters, $(H_2O)_n^-$, are produced in a laser vaporization cluster source[34-36] developed in our laboratory.[37,38] In the source a pulsed Nd:YAG laser beam impinges upon a metal target in the presence of a high pressure of an inert carrier gas, usually helium (10 bar). The flow of the gas, containing water with its room-temperature vapor pressure as partial pressure, is controlled by a piezoelectric valve, whose opening is synchronized with the laser pulse. Depending on the exact conditions, the source produces a relatively wide distribution of the solvated electron clusters, where the number of ligands can range from n = 15 to nearly 100. A rapid fragmentation of the aqueous clusters due to absorption of the infrared black body ambient radiation limits the upper end of the distribution, while the formation of smaller clusters below about n = 20 becomes increasingly inefficient due to their low electron affinity, and rapid electron detachment.[33]

The ion clusters which form in the source and during the adiabatic expansion into high vacuum are guided along the magnetic field axis through several stages of differential pumping into the ICR cell. This is located inside the bore of a 4.7 T superconducting magnet of our Bruker/Spectrospin CMS47X FT-ICR mass spectrometer, which is equipped with an APEX III data station. At the start of each measurement, clusters produced in about twenty vaporization pulses are accumulated in the ICR cell.

To study chemical reactions, the reactant gases, in the present case mainly carbon dioxide or oxygen, are admitted into the instrument via a leak valve, to raise the pressure of the high vacuum section from the background value in the low 10^{-11} mbar range to a stable value usually in the range of about $2\text{-}5\times10^{-9}$ mbar. To obtain information about the cluster formation, their reactions, and kinetics of their fragmentation, mass spectra are acquired at a

nominal time t = 0, that is right after the completed accumulation, and then after allowing varying times ranging up to typically fifty seconds.

The simultaneous presence of hydrated metal anions in a previous study[33] did not interfere with the experiment, and in fact provided a useful means to proof that the electrons are indeed detaching from the clusters. In the present work, however, which is aimed at exploring chemical reactions of the electrons, the formation of $M^-(H_2O)_n$ can be avoided by employing targets made of metals with closed shell structure and a low or zero electron affinity. As shown in the previous chapter, use of zinc results in exclusive formation of the desired $(H_2O)_n^-$ clusters.

4.3 Results and Discussion

4.3.1 Reactions of $(H_2O)_n^-$ clusters with Carbon Dioxide

A typical initial mass spectrum of the hydrated electron clusters produced in our source at a nominal time t = 0, that is right after the ion accumulation, is shown in Figure 1a). As noted above, the distribution of the $(H_2O)_n^-$ clusters generated is somewhat dependent on the source setting, that is the laser power and its focusing, pressure of the carrier gas, pressure of the entrained water vapor, and in particular on the relative timing of the laser pulse and the opening of the valve controlling the gas flow. Even though the exact size range, which in this particular experiment extends between about n = 27 and n = 62, may differ slightly from experiment to experiment, some features of the distribution appear well reproducible. This statement is true, for instance, for the relatively pronounced maximum of the n = 50 cluster, which is almost a factor of two more intense than the n = 51 and n = 49 peaks, and for the even-odd intensity alternation exhibited by the peaks just above n = 50.

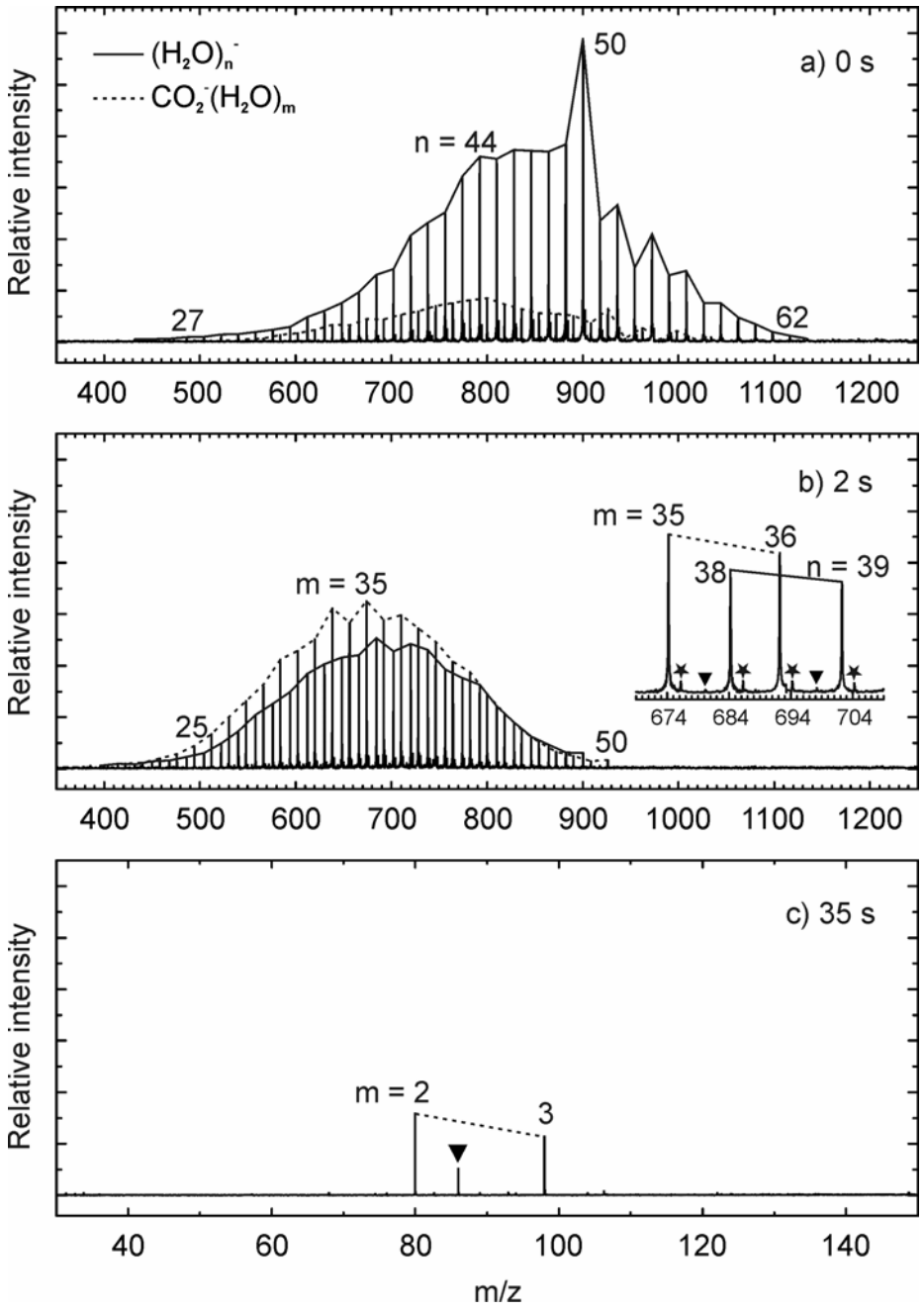

Figure 1. Mass spectra of the reaction of $(H_2O)_n^-$ with CO_2. a) At 0 s, some clusters have already reacted during the accumulation of the hydrated electrons in the ICR cell, and the product species $CO_2^-(H_2O)_m$ are present to some extent. After b) 2 s, more than 50% of the initial $(H_2O)_n^-$ are converted into products. In parallel, black-body radiation and collision induced dissociation occurs, and the clusters shrink by loss of single water molecules. For $n < 30$, also electron loss from $(H_2O)_n^-$ occurs, but since only few $(H_2O)_n^-$ reach this size region before conversion to $CO_2^-(H_2O)_m$, this reaction is negligible. Only one CO_2 enters the cluster, and the fragmentation proceeds until the cluster $CO_2^-(H_2O)_2$ is reached, as seen in c) 35 s. These species slowly disappear from the mass spectrum due to electron detachment. In the detail the peaks marked with star are due to the natural abundance of ^{18}O in the water molecules. $O_2^-(H_2O)_p$ impurity peaks, marked with ▼, are present after long reaction delays.

It is easy to see, that even in the nominally t = 0 spectrum, some products of the reaction with carbon dioxide are already present. As explained in the experimental section, the $(H_2O)_n^-$ clusters produced in the source are usually accumulated over twenty pulses that is nearly 2 s at the 10 Hz laser repetition rate, and since a constant pressure of 7.7×10^{-9} mbar of CO_2 is maintained in the cell, the reaction takes place already during this accumulation period. Since the laser is warming up in the first few shots and some previously trapped ions are lost again in the accumulation cycle, the nominal time t = 0 corresponds to about 0.5 s reaction time.

The reaction consists simply in one and only one carbon dioxide molecule being taken up by the clusters, and resulting in $CO_2^-(H_2O)_m$. A more careful examination of the spectrum after 2 s, Figure 1b), reveals, that the product clusters have a very similar, maybe slightly lower mass than the reactant species. Since the mass of CO_2 with 44 amu corresponds to 2.44 water molecules, this indicates that two to three water molecules are lost upon intake of the CO_2 molecule into the cluster:

$$(H_2O)_n^- + CO_2 \rightarrow CO_2^-(H_2O)_{n-x} + x\ H_2O,\ x = 2\text{-}3 \qquad (1)$$

An interesting detail concerning the intensity alternation above the intensity maximum is that it is, in fact, considerably more pronounced in the products of reaction (1) than in the reactant clusters. While the odd numbered solvated electrons in the range of n = 51-55 are, on the average, maybe 5-15% weaker than the neighboring even clusters, the intensity ratios are much larger for the products, with the odd clusters being favored more like by a factor of three or four. Probably a combination of kinetic and thermochemical effects is responsible for the observation of pronounced magic numbers in $CO_2^-(H_2O)_m$, $45 < m < 55$.

Comparison of the integrated intensities of the hydrated electrons with those of the carbon dioxide containing $CO_2^-(H_2O)_n$ products indicates that in the Figure 1b), after less than

two second, more than half of the initially present clusters has already reacted. This observation, combined with the known CO_2 pressure and the calculated collision rates from ADO theory[39-41] leads to the conclusion, that the reaction efficiency reaches almost 300%. This is not unreasonable, since the collision rate is calculated in a point charge model, while the reactant cluster has a considerable size, and its collision cross section is therefore larger than that of a point charge.

After the initial exchange, only a gradual fragmentation, due mainly to cluster heating by the room temperature black body background radiation, is taking place, with the water ligands being lost one by one. The final stage of the reaction and of this cluster fragmentation process are documented in the Figure 1c), which shows the mass spectrum after 35 second reaction. At this point, only weak peaks due to the last two, smallest carbon dioxide containing clusters, n = 2 and n = 3, remain. Also visible in the spectrum are the fragmentation products of impurity clusters containing molecular oxygen, $O_2^-(H_2O)_n$, with mainly n = 3 and minor quantities of n = 4 and n = 2 clusters being present. No n = 1 $CO_2^-(H_2O)$ cluster is detected, and after a few additional seconds all the signals due to the CO_2-containing clusters vanish, but without any new signals appearing. This is due to electron detachment, with neither the electron itself, nor the remaining, weakly bound neutral cluster, being directly observable in the FT-ICR instrument.

4.3.2Reactions of $(H_2O)_n^-$ Clusters with O_2.

The reactions with molecular oxygen are similar to those with carbon dioxide, in that one and only one O_2 molecule is taken up by each cluster. For the products the entire distribution seems to be shifted to smaller values of n. After 2 s reaction time, Figure 2b), the $(H_2O)_n^-$ distribution has its maximum around n = 35, while the most intense product cluster is

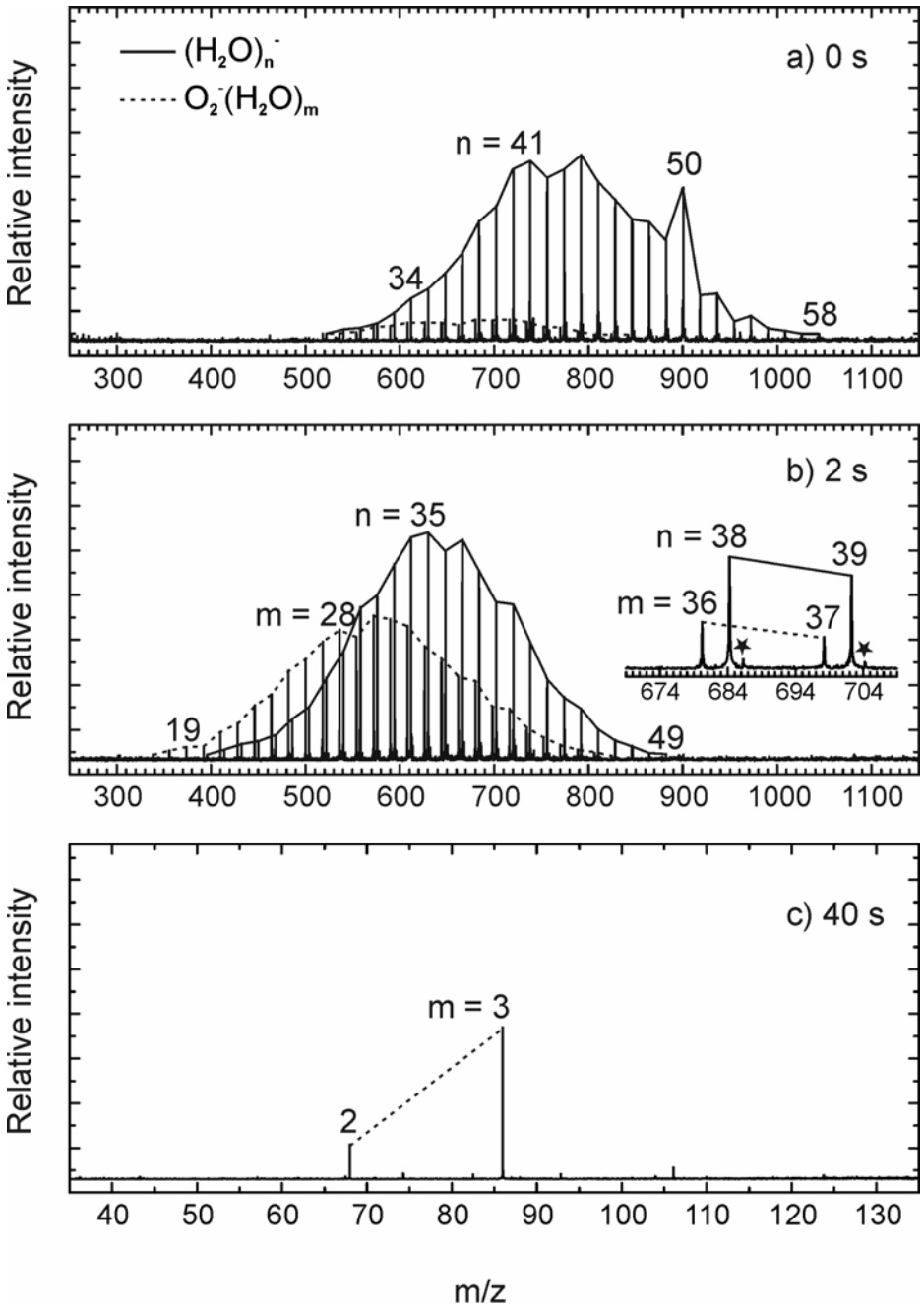

Figure 2. Mass spectra of the reaction of $(H_2O)_n^-$ with O_2. In a) 0 s, some clusters have already reacted during the accumulation of the hydrated electrons in the ICR cell, and the product species $O_2^-(H_2O)_m$ are present to some extent. After b) 2 s, only about 30% of the initial $(H_2O)_n^-$ are converted into products. In parallel, black-body radiation and collision induced dissociation occurs, and the clusters shrink by loss of single water molecules. For $n < 30$, also electron loss from $(H_2O)_n^-$ occurs, but since only few $(H_2O)_n^-$ reach this size region before conversion to $O_2^-(H_2O)_m$, this reaction is negligible. Only one O_2 enters the cluster, and the fragmentation proceeds until the cluster $O_2^-(H_2O)_2$ is reached, as seen in c) 40 s. These species are stable against further fragmentation as well as electron detachment. The peaks marked with star are due to the natural abundance of ^{18}O in the water molecules.

n = 30, with the shift suggesting that in the case of oxygen, the reaction proceeds according to the equation:

$$(H_2O)_n^- + O_2 \rightarrow O_2^-(H_2O)_{n-x} + x\ H_2O,\ x \approx 5\text{-}6 \qquad (2)$$

In other words, the dissolution of the O_2 molecule in the cluster is accompanied by the evaporation of several water ligands. As we will discuss below this is consistent with the thermochemistry of these processes and with the considerably higher exothermicity of the reaction with molecular oxygen. After 2 s, Figure 2b), only 30-40% of the hydrated electrons are converted into products, in spite of the, compared to CO_2, higher O_2 pressure of 1.86×10^{-8} mbar. This yields an ADO collision efficiency of 100%, about 1/3 the value of CO_2. The relative values are in agreement with earlier flow tube results,[32] while the absolute values deviate by a factor of 3. However, the different reaction gas temperature, 100 K in the flow tube vs. 300 K in the present study, may very well explain this discrepancy. Also the number of water molecules lost is in good agreement with the flow tube results.

Like in the case of carbon dioxide, after the first step, no further O_2 molecules are taken up by the clusters, and again only their gradual fragmentation is observed, with the distribution shifting towards smaller cluster sizes. After some 15 seconds almost every cluster has dissolved one O_2, with the unreacted solvated electron clusters being barely observable, and the size distribution of the $O_2^-(H_2O)_n$ products ranges from about n = 4 to n = 12. The fragmentation continues further but with decreasing rates, so that after some 40 seconds of reaction time, the n = 3 cluster is dominant, and loses only very reluctantly an additional ligand to form the $O_2^-(H_2O)_2$ final product, Figure 2c). Unlike in the case of CO_2, however, even after 60 seconds, which is the longest time studied, the signals do not disappear, but the n = 2 and 3 species remain with comparable intensities.

4.3.3 Ionic core exchange reactions.

In order to learn more about the relative stability of $CO_2^-(H_2O)_n$ and $O_2^-(H_2O)_n$, and to learn if the formation of O_2^- from CO_2^- can proceed directly in solution, we have studied the exchange of the ionic core in a third experiment. CO_2 was introduced into the UHV at a relatively high partial pressure of 1.3×10^{-7} mbar, together with O_2 at a partial pressure of 5.7×10^{-8} mbar. After 0.5 s, Figure 3a), the $(H_2O)_n^-$ distribution is completely gone, and $CO_2^-(H_2O)_n$ predominate in the spectrum. After 3 s, Figure 3b), $O_2^-(H_2O)_m$ have become the dominant species, and have almost completely replaced the $CO_2^-(H_2O)_n$ after 10 s, Figure 3c). In a crude estimate, the ADO efficiency of the core exchange is 50%, assuming that the reverse reaction does not take place in significant abundance. This is significantly lower than the efficiency of the O_2 recombining with the solvated electron, so formation of the superoxide radical anion is not promoted by the presence of CO_2 in our experiment. With similar arguments as above, the number of water molecules lost in the core exchange reaction is estimated to 3-4, so that the reaction can be summarized as follows:

$$CO_2^-(H_2O)_n^- + O_2 \rightarrow O_2^-(H_2O)_{n-x} + CO_2 + x\ H_2O,\ x \approx 3\text{-}4 \qquad (3)$$

4.3.4. Quantum Chemical Computations of Hydrated CO_2^- and O_2^- Anions.

Obviously, it is of interest to understand why CO_2 or O_2 react rapidly with the solvated electrons, while N_2, CO and ethylene do not react at all. Similarly, at first sight it might not be clear, why these species which dissolve so readily and with nearly collisional efficiency in the $(H_2O)_n^-$ clusters, are completely unreactive towards the seemingly quite similar $OH^-(H_2O)_n$, $H^+(H_2O)_n$ and other hydrated species. In order to obtain some additional insights into the

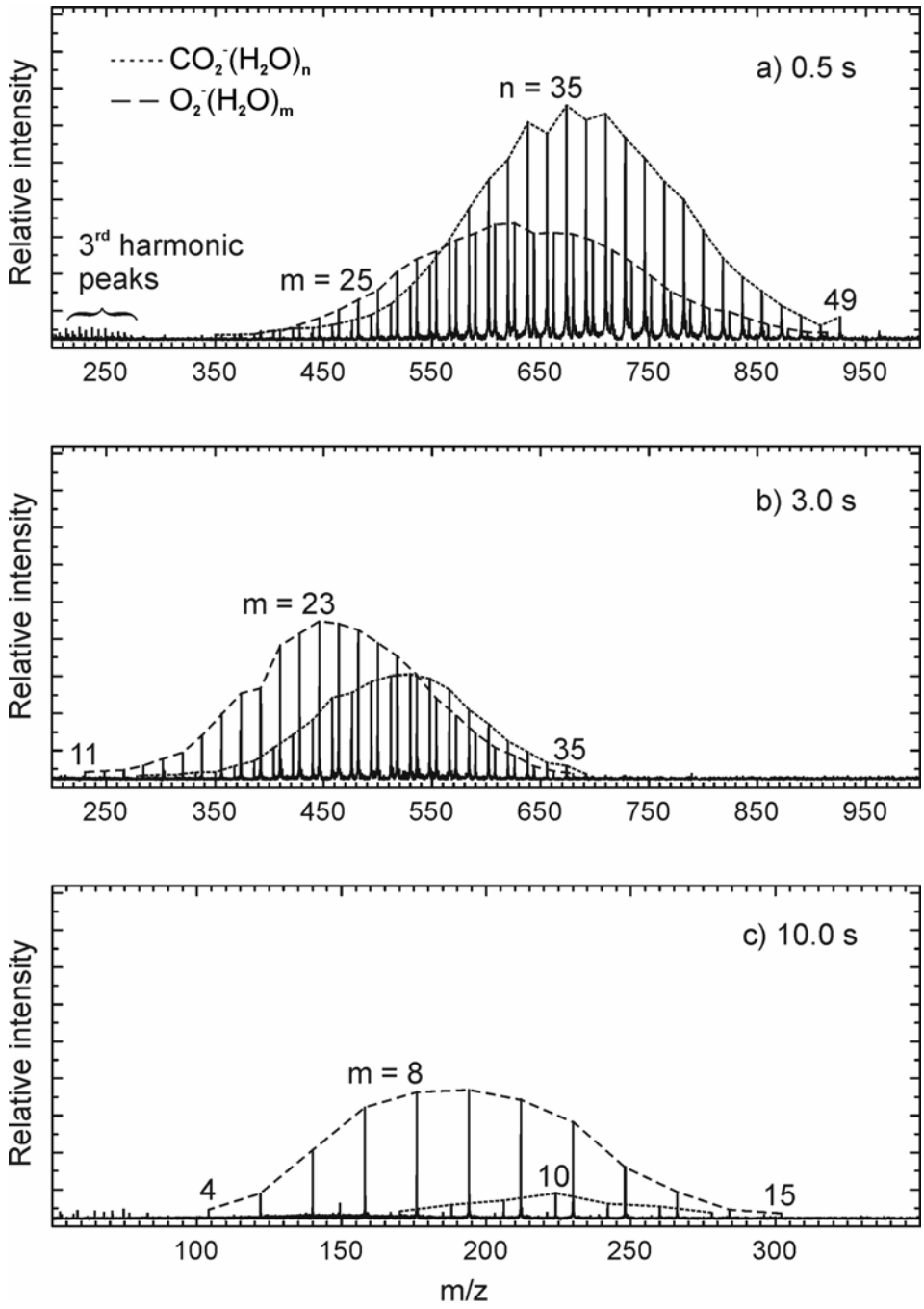

Figure 3. Mass spectra of the reaction of $(H_2O)_n^-$ with a roughly 2:1 mixture of CO_2 and O_2. In a) 0.5 s, $(H_2O)_n^-$ are completely converted to $CO_2^-(H_2O)_m$ and $O_2^-(H_2O)_m$, in a ratio of again roughly 2:1, despite the smaller reaction efficiency of O_2 with $(H_2O)_n^-$. This indicates that already core exchange has occurred, and most $O_2^-(H_2O)_m$ come from reactions with $CO_2^-(H_2O)_m$. After b) 3 s, the $O_2^-(H_2O)_m$ already dominate with 2:1 over $CO_2^-(H_2O)_m$. Again, black-body radiation and collision induced dissociation lead to a gradual shrinking of the clusters. After c) 10 s this process is almost complete, and $O_2^-(H_2O)_m$ are by far the dominant species in the mass spectrum.

structures and energetics of these ions, and facilitate the interpretation of our observations, we have carried out a series of computations on the stability, internal structure and other properties of the $CO_2^-(H_2O)_n$ and $O_2^-(H_2O)_n$ species. The calculations were done using the commercial Gaussian98 program package,[42] employing the hybrid, three parameter density functional B3LYP method, as described by Becke,[43] with the Lee-Yang-Parr correlation functional,[44] as implemented in the Gaussian package. After pre-optimization with a smaller basis set, the full 6-311++G(3df,3pd) triple zeta basis set treating all electrons explicitly, and employing one diffuse and four polarization functions on each atom was used for geometry optimizations and frequency calculations. The basis set superposition error of this large basis set employed is negligible, which is only about 5% of the total hydration energy, estimated from the neutral clusters using the counterpoise method.

To obtain the structures, binding energies, as well as electron affinities, we have carried out calculations with the same methods on the H_2O fragment, as well as on the $CO_2(H_2O)_n$, $CO_2^-(H_2O)_n$, $O_2(H_2O)_n$ and $O_2^-(H_2O)_n$ clusters, for n = 0-5. To ascertain that the optimized structures really are local minima, the vibrational frequencies were also computed for these species. Many of the clusters can exist in several "isomeric" forms, and in case of doubt, computations departing from several different starting geometries were carried out, to make reasonably sure that the global minimum was identified. The structures shown in Figure 4 and Figure 5 are the optimized geometries with the lowest energy for $CO_2^-(H_2O)_n$ and $O_2^-(H_2O)_n$, respectively, with n = 0-5. The results of our computations most relevant for discussing the experimental observations presented here, more specifically the dissociation energies and electron affinities of the hydrated clusters, and the thermochemistry of the ionic core exchange reaction, are summarized in Table 1 and Table 2, respectively.

As already noted, carbon dioxide is a very stable molecule due to its closed shell structure with 16 valence electrons and a completely filled highest occupied bonding π_g orbital. This according to Walsh's rules strongly favors linear configuration and gives the

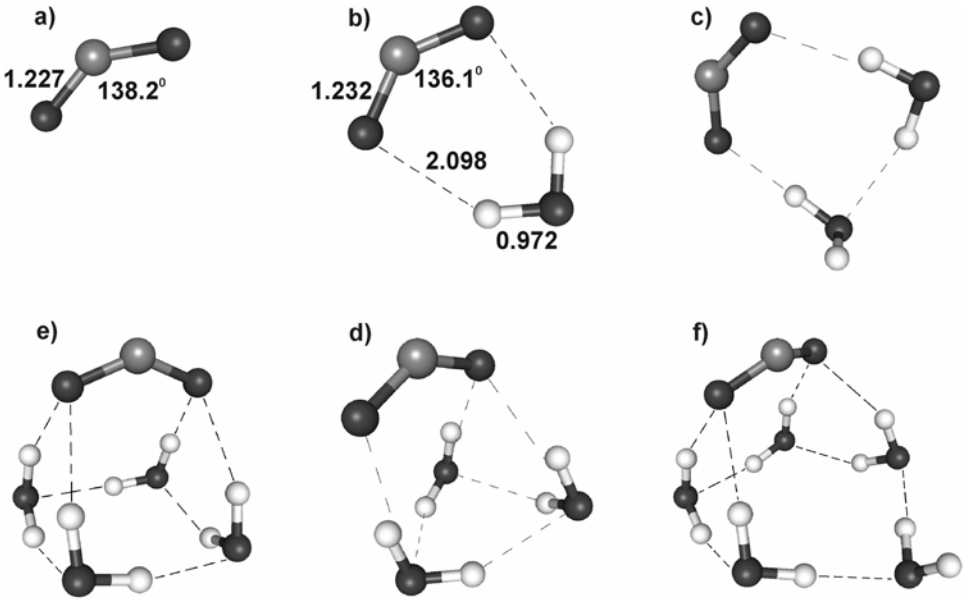

Figure 4. Optimized geometries of the most stable isomer of $CO_2^-(H_2O)_n$, n = 1-5 (Bond distances in Å and bond angles in degrees). The geometries are evaluated by the B3LYP/6-311++G(3df,3pd) level of theory using the Gaussian98 program. The CO_2^- is solvated on the cluster surface. The energies of a water loss for the $CO_2^-(H_2O)_n$ and the electron affinities of the corresponding neutral clusters are shown in Table 1.

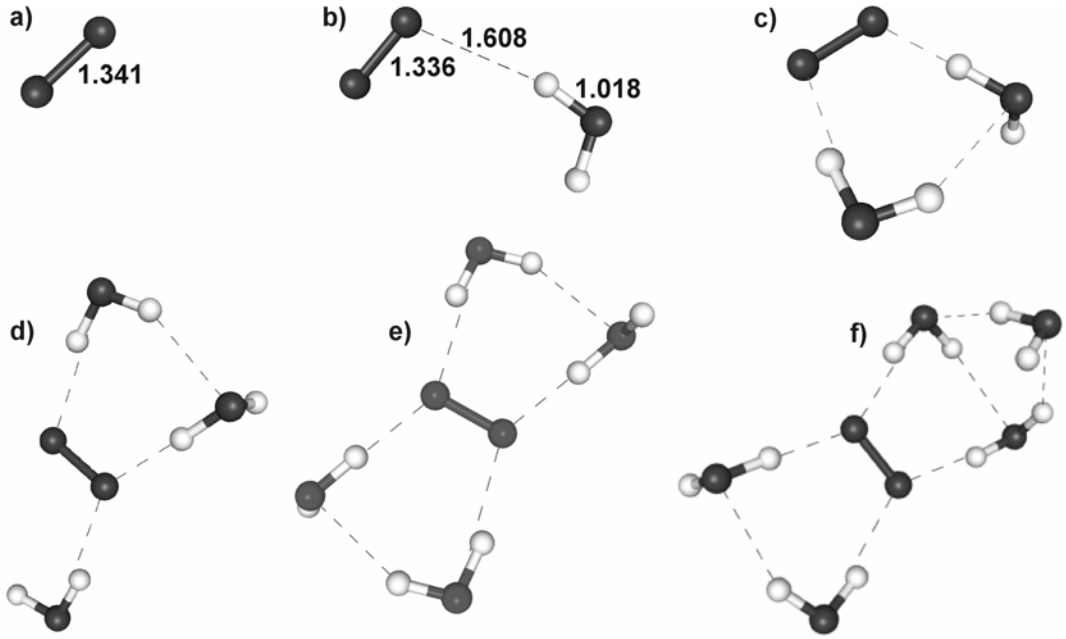

Figure 5. Optimized geometries of the most stable isomer of $O_2^-(H_2O)_n$, n = 1-5 (Bond distances in Å and bond angles in degrees). The geometries are evaluated by the B3LYP/6-311++G(3df,3pd) level of theory using the Gaussian 98 program. The O_2^- is internally solvated. The energies of a water loss for the $O_2^-(H_2O)_n$ and the electron affinities of the corresponding neutral clusters are shown in Table 1.

molecule a considerable rigidity, and a rather high bending vibrational frequency v_2 = 668 cm^{-1}. Consistent with experiment, the computation predict that it requires a considerable energy to place an additional electron into the next higher, empty "LUMO" orbital. This orbital is of π_u symmetry, and according to Walsh's rules favors strongly a bent configuration. The resulting bent CO_2^- anion (Figure 4a) has a valence angle (138.2°) similar to that of the isoelectronic NO_2 (134.5°), both predicted by the UB3LYP/6-311++G(3df,3pd) level of theory calculation, but is quite unstable with respect to electron detachment, our computation predicts the formation of the anion to be endothermic by 32.8 kJ/mol.

The situation is, however, quite different in aqueous solution. Already in the presence of a single H_2O the $CO_2…H_2O$ complex has a positive electron affinity. The complex of neutral CO_2 with water, OCO…HOH, is only tenuously bound by a very weak hydrogen bond to one of the oxygen atoms of the carbon dioxide. The binding energy is predicted to be less than 6 kJ/mol, and similarly weak binding energies are also predicted in the larger $CO_2…(H_2O)_n$ clusters. In the presence of the extra electron, however, the linear and non-polar carbon dioxide is converted into a bent, polar CO_2^- anion, which can form two strong hydrogen bonds to the two protons of the water molecule, forming a cyclic planar $CO_2^-…H_2O$ with a C_{2v} symmetry (Figure 4b). The binding energy of the cyclic complex, computed to be 54.1 kJ/mol, more than offset the endothermic nature of the free anion, so that $CO_2…H_2O$ complex has an electron affinity of 15.9 kJ/mol.

The larger neutral complexes are found to be essentially undistorted $(H_2O)_n$ clusters, the n = 2 dimer, and the cyclic n = 3, 4, and 5 polymers, with the CO_2 hydrogen-bonded to one of the free, dangling OH groups. Again, in each case the binding energy is very weak (less than 10 kJ/mol), and the potential surface is extremely flat. Much more strongly bound are the anionic species. The n = 2 anion in Figure 4c is a distorted water dimer, with each of the water molecules forming a hydrogen bond to one of the oxygen atoms of the CO_2^- anion. Similarly, the n = 3 and 4 species in Figure 4d and Figure 4e can be viewed as the cyclic

water trimer and tetramer, respectively. In this case, however, the water $(H_2O)_n$ species are strongly distorted compared with the free clusters. Unlike in the free $(H_2O)_3$ or $(H_2O)_4$, all the "dangling" OH bonds are facing out of the plane defined by the water oxygen atoms in the same direction, so that they can interact with and form hydrogen bonds to the negatively charged oxygen atoms of the CO_2^- anion. The n = 5 anion is again a cyclic water pentamer,

Table 1. Energies (in kJ/mol) of a H_2O dissociation together with electron affinities (in kJ/mol) of $CO_2^-(H_2O)_n$ and $O_2^-(H_2O)_n$ including zero-point corrected (ZPC) energies, thermal enthalpies (ΔH) and thermal free energies (ΔG) at ambient conditions. All the energies are evaluated based on the optimized geometries for the most stable isomer at each cluster size n using the Gaussian 98 program at the B3LYP/6-311++G(3df,3pd) level of theory. The numbers in parentheses are experimental values.[a]

	$CO_2^-(H_2O)_n$					
n	Dissociation Energy (D_o) $CO_2^-(H_2O)_n \rightarrow CO_2^-(H_2O)_{n-1} + H_2O$			Electron Affinity $CO_2^-(H_2O)_n \rightarrow CO_2(H_2O)_n + e^-$		
	$\Delta E_{+\Delta ZPC}$	$\Delta H_{298K,1\ atm.}$	$\Delta G_{298K,1\ atm.}$	$\Delta E_{+\Delta ZPC}$	$\Delta H_{298K,1\ atm.}$	$\Delta G_{298K,1\ atm.}$
0				-32.8	-33.7	-26.0
1	54.1	56.9	22.1	15.9	19.2	1.3
2	45.2	48.0	12.7	45.2	47.4	43.9
3	40.1	44.3	0.2	63.7	66.7	48.0
4	41.4	44.4	5.3	64.3	66.1	56.3
5	31.2	34.3	-5.7	67.7	70.5	53.5
	$O_2^-(H_2O)_n$					
n	Dissociation Energy (D_o) $O_2^-(H_2O)_n \rightarrow O_2^-(H_2O)_{n-1} + H_2O$			Electron Affinity $O_2^-(H_2O)_n \rightarrow O_2(H_2O)_n + e^-$		
	$\Delta E_{+\Delta ZPC}$	$\Delta H_{298K,1\ atm.}$	$\Delta G_{298K,1\ atm.}$	$\Delta E_{+\Delta ZPC}$	$\Delta H_{298K,1\ atm.}$	$\Delta G_{298K,1\ atm.}$
0				50.1	50.1(43.5)	49.6
1	82.3	86.0(77.0)	55.9(52.3)	113.4	138.5	119.9
2	62.7	66.3 (72.0)	27.2 (35)	184.5	191.8	163.0
3	53.0	54.4 (64.4)	21.6 (22)	208.7	212.0	195.0
4	45.8	48.8	9.8 (14)	216.0	218.1	202.7
5	35.0	38.5	-0.5	223.6	227.0	209.0

[a] NIST Chemistry WebBook, NIST Standard Reference Database Number 69, March 2003 (http://webbook.nist.gov/chemistry/)

but in this case due to steric reasons, only four water molecules of the water pentamer are directly bound to the CO_2^- anion. Similar to the anion with n = 1, the anions with n > 1 are stable with respect to electron detachment, and they are then further stabilized by additional water ligands, with the solvation energies and the electron affinities increasing with n, as can be clearly seen in Table 1.

The major differences in the energetics of the solvated molecular oxygen clusters are, as already mentioned, due to the fact that in contrast to carbon dioxide, in O_2 the antibonding $2p_{xy}$ π_g^* orbital is only partially occupied with two electrons, and can easily accommodate a third one, which results in the appreciable electron affinity of molecular oxygen. The value we computed, E_A = 50.1 kJ/mol, is in reasonable agreement with the experimental value of 43.5 kJ/mol.

The neutral complexes of O_2 with water are even more tenuously bound than those of CO_2, with computed binding energies being less then 1 kJ/mol for n = 1-5. In the n = 1, $O_2…H_2O$ the oxygen molecule is bound by a hydrogen bond to one of the water protons with the O_2 being inclined about 126.8° with respect to the nearly linear (174.1°) and rather long (2.454 Å) OH…O hydrogen bond. Also the structures of the larger, n = 2-5 $O_2(H_2O)_n$ species are quite similar to the corresponding neutral carbon dioxide complexes, and they consist of essentially undistorted neutral $(H_2O)_n$ clusters, with in this case the O_2 molecule being hydrogen bonded to one of the dangling OH bonds.

The anionic $O_2^-…H_2O$ is, unlike the corresponding complex of CO_2^-, not cyclic, but has a planar C_s symmetry, with the O_2^- asymmetrically bound to one of the water protons (Figure 5b). The H…O bond in $O_2^-…H_2O$ is much shorter (1.608 Å) than that in the neutral complex with the OOO angle being 98.0°. The lowest energy structures of the larger $O_2^-(H_2O)_n$, n = 2-4, complexes are in agreement with the recent ab initio studies.[23, 24] One of the water protons of each water molecule hydrogen bonds to one of the four lobes of the in plane $2p_{xy}$ π_g^* orbital of O_2^-. The completion of the first hydration shell contains four water

molecules $O_2^-(H_2O)_4$, which can be viewed as two water dimers interacting with the O_2^- (Figure 5e). As suggested by recent photo-fragmentation experiment $O_2^-(H_2O)_5$ was found to have more complicated water network than in the case of $O_2^-(H_2O)_4$.[23, 24] The most stable structure of $O_2^-(H_2O)_5$ obtained (Figure 5f), indeed, contains a water dimer and a water trimer interacting separately with the ionic core O_2^-, so that the IR vibration pattern of $O_2^-(H_2O)_5$ is more complicated than that of $O_2^-(H_2O)_4$.

As already noted, the hydration again increases appreciably the electron affinities due to formation of the strong hydrogen bonds between the water ligands and the oxygen anion. As can be seen in the Table 1, already for the n = 1 complex, $O_2\ldots H_2O$, the electron affinity is computed to be 113.4 kJ/mol, and it increases further considerably to more than 200 kJ/mol for the $n \geq 3$ species. On the other hand, the dissociation energies for the loss of water ligands in $O_2^-\ldots(H_2O)_n$ decrease in the same order as those in $CO_2^-\ldots(H_2O)_n$ from 82.3 kJ/mol for the n = 1 complex to less than 40 kJ/mol for n = 5. In any event, for all the hydrated O_2^- clusters the energies needed for electron detachment clearly exceed considerably those needed for a loss of ligand.

4.3.5 Mechanism of the $(H_2O)_n^-$ Cluster Reaction with O_2 and CO_2

With the results of the quantum chemical computations, and with a better knowledge and understanding of the structures and bonding of the $O_2^-(H_2O)_n$ and $CO_2^-(H_2O)_n$ species, one can now consider in more detail the mechanism of the reactions observed here. It is also instructive to compare and contrast them with some of the other reactions we have studied. We have already noted the striking difference between the efficient reactions of the carbon dioxide or O_2 molecules with the solvated $(H_2O)_n^-$ clusters, when compared with other similarly nonpolar molecules, such as for instance N_2 or ethylene, C_2H_4, or even the somewhat polar CO, which are found not to react at all.

The key property is their electron affinity, or to be more precise, the ability to bind exothermically the electron, and forming then very stable anion hydrates. Unlike the closed shell N_2 and CO species with completely filled bonding $2p_{xy}$ π_u orbitals which have no suitable empty orbitals, the highest, doubly occupied antibonding $2p_{xy}$ π_g* orbitals of O_2 can accommodate a third electron, resulting in the appreciable, 50.1 kJ/mol, electron affinity of molecular oxygen. Upon collision with $(H_2O)_n^-$ the O_2^- which immediately forms is further strongly stabilized by the water ligands. In the case of CO_2, whose two highest π_g molecular orbitals are fully occupied by four electrons, its electron affinity is, in contrast with O_2, negative (-32.8 kJ/mol). CO_2 has, however, an empty, low lying π_u orbital which can accept an extra electron, resulting in a bent, polar CO_2^- anion, isoelectronic with NO_2. This anion alone is unstable with respect to auto-detachment, but it can be stabilized by hydration. Already in the presence of a single water ligand a cyclic $CO_2^-\ldots H_2O$ anion complex is formed, since the binding energies of its two strong hydrogen bonds more than compensate for the endothermic nature of the free CO_2^-, and the anion is stabilized further by additional water ligands.

Clearly, the key difference here is the existence of low lying unfilled or partially filled orbitals in the case of CO_2 and O_2, and their absence in the other species such as N_2, CO, or ethylene, C_2H_4, which do not react with hydrated electron clusters at all. These molecules, with no low lying, unoccupied orbitals, cannot bind an extra electron. Their presence is evidenced only by their slight contribution to the rates of collisional cluster fragmentation. Apparently, the crucial first step of the reaction involves an attachment of the electron, and the negative ion is then stabilized by the formation of strong hydrogen bonds to the water ligands. While the exact location of the negative charge in the $(H_2O)_n^-$ solvated electron clusters is still controversial, it is undoubtedly fairly diffuse and probably localized at or near the cluster surface. During the collision of the gaseous reactant molecule with the solvated electron, a charge transfer takes place, with the O_2^- or CO_2^- anion formed being immediately

stabilized by strong hydrogen bonds to the cluster surface. The fact, that the process occurs efficiently not only for molecular oxygen, but also for CO_2, whose electron affinity is negative, suggests that the charge transfer and the anion stabilization by hydrogen bond formation have to be considered as concurrent, rather than consecutive reaction steps.

Since the mechanism described above which allows the nonpolar CO_2 or O_2 species to enter the water cluster requires the availability of a free electron, one can also easily understand the fact that one and only one molecule of CO_2 or O_2 can be taken up by the cluster anion. Once the electron is intimately bound to form the anion, and stabilized by the water ligands, it is no longer available to enable a further molecule to enter the cluster. With the same argument, one can also explain the lack of reactivity of carbon dioxide with a large number of other hydrated ions, whether positively or negatively charged, where a free electron is not available. The course of the reaction of carbon dioxide or O_2 and their behavior towards the $(H_2O)_n^-$ species is clearly fundamentally different from that we have observed for instance for methanol and a number of similar species. Similar to CO_2, methanol also reacts with $(H_2O)_n^-$ by replacing one or two water ligands. In this case, however, if the reaction is followed for longer times, one finds that the first ligand exchange is followed by a second, third, and so on, resulting in mixed solvated electron clusters of the type $(CH_3OH)_m(H_2O)_n^-$, with the exchange having been followed at least to m = 4. In this case, the water solvation shell is simply being replaced, or partially replaced by methanol, which like water is able to form extensive hydrogen bonded networks. The reason for this different behavior is obvious: CO_2 or O_2 do not replace one of the solvent ligands, but bind tightly the electron, so that there is a fundamental change in the cluster structure, and in its ionic core, and therefore regardless of the reaction time one and only one reactant molecule can be taken up by the cluster. In the case of water/methanol clusters, the electron is not bound to a specific molecule, and is not intimately involved in the reaction mechanism. Multiple exchanges therefore can take place.

With the results of the computations, one can also immediately understand, why a one for one ligand exchange occurs in the reaction of carbon dioxide, but several water molecules are lost in the molecular oxygen reaction. As seen in Table 1, the dissociation energies of the hydrated O_2^- and CO_2^- clusters are fairly similar. The electron affinities of $O_2\ldots(H_2O)_n$ are, however, some 150 kJ/mol higher than those of $CO_2\ldots(H_2O)_n$, which means that much more energy will be released during the reaction of O_2 with the hydrated electron, and this is responsible for the evaporation of several water ligands. In addition, the thermodynamics of the reactions can also explain some features of the cluster fragmentation. As can be seen in the Table 1, for both the $CO_2^-(H_2O)_n$ and $O_2^-(H_2O)_n$ the electron affinities increase, but the energies required for the loss of water ligand decrease, with the increasing n. For $CO_2^-(H_2O)_n$ with $n > 2$ the energies required to evaporate a water molecule are smaller than those needed to detach an electron, and this difference is even more pronounced, if the entropic effects are considered, as shown by the free energies in Table 1. Accordingly, for the larger clusters mainly fragmentation is observed, with no evidence of ion being lost in the FT-ICR experiments. On the other hand, for the small $CO_2^-(H_2O)_n$ complexes the situation is reversed, with the energies favoring electron detachment. These computational results are in excellent agreement with our experimental observations, with the small anions gradually disappearing from the cell, and with $CO_2^-\ldots H_2O$ (n = 1) not being detected at all. Ultimately, after about 40 s reaction time, all the ions have lost the electron and completely disappeared from the mass spectrum, whose lower detection limit is m/z = 14.5 amu.

Considerably different situation prevails for the $O_2^-(H_2O)_n$ anions, as can be seen in Table 1. Here even for the $O_2^-H_2O$ anion (n = 1) the computed ionization energy of 113.4 kJ/mol exceeds considerably the dissociation energy of 82.3 kJ/mol, and the ionization energies for the larger species are over 200 kJ/mol. As already noted, the dissociation energies decrease with n, and at least for n = 1 and 2 they are in the case of the smaller hydrated O_2^- anion considerably, some 15 kJ/mol, larger than those of the hydrated CO_2^- anion.

Accordingly, the fragmentation slows down considerably for the smallest ions, until near the end of the fragmentation process, $O_2^-(H_2O)_3$ is only very slowly converted to $O_2^-(H_2O)_2$, with no $O_2^-(H_2O)$ being detected. Electron detachment, if it occurs at all, must be even on the time scale of our experiment exceedingly slow. Accordingly, in experiments with molecular O_2, the $O_2^-(H_2O)_n$, n = 2 and 3 clusters effectively remain as final product even at the longest times studied. As already noted, in some experiments involving CO_2 where small amounts of O_2 impurities were present, these n = 2 and 3 oxygen containing clusters remained even after all the $CO_2^-(H_2O)_n$ anions have detached electron and disappeared.

The computed relative stabilities of $CO_2^-(H_2O)_n$ and $O_2^-(H_2O)_n$ are also confirmed by the mixed experiments, where both CO_2 and O_2 are added in the FT-ICR trap. The ionic core of $CO_2^-(H_2O)_n$ slowly exchanges from CO_2^- to O_2^-, which also suggests the larger exothermicity of the formation of $O_2^-(H_2O)_n$ comparing with the formation of $CO_2^-(H_2O)_n$. Table 2 shows the reaction energy of the ionic core exchange process. For the bare anions, the reaction energy of the ionic core exchange is the difference of the electron affinity between

Table 2. Energies (in kJ/mol) of ionic core exchange of $CO_2^-(H_2O)_n$ and $O_2^-(H_2O)_n$ including zero-point corrected (ZPC) energies, thermal enthalpies (ΔH) and thermal free energies (ΔG) at ambient conditions. All the energies are evaluated based on the optimized geometries for the most stable isomer at each cluster size n using the Gaussian 98 program at the B3LYP/6-311++G(3df,3pd) level of theory.

n	Ionic Core Exchange $CO_2^-(H_2O)_n + O_2 \rightarrow O_2^-(H_2O)_n + CO_2$		
	$\Delta E_{+\Delta ZPC}$	$\Delta H_{298K,1\ atm.}$	$\Delta G_{298K,1\ atm.}$
0	-82.9	-83.8	-75.6
1	-111.0	-112.8	-109.5
2	-128.5	-131.1	-124.0
3	-141.4	-141.2	-145.3
4	-145.8	-145.5	-149.9
5	-149.6	-149.7	-155.0

CO_2 and O_2, which is already highly exothermic by 82.9 kJ/mol. The ionic core exchange becomes more exothermic when the cluster size increases. The reaction is exothermic up to 150 kJ/mol for the cluster size of n = 5, which suggests that energy released in the exchange of anionic core is also sufficient for a loss of three to four water molecules.

Based on the current results, it is of course not possible to decide whether the molecular anion formed remains on the surface of the water cluster, or wanders inside it to become internally solvated. It seems that the solvation structure depends on the electronic structure and the geometry of the anionic core. For example, for the clusters with up to five water molecules, the bent CO_2^- prefers a solvation at the surface of a water cluster, while the O_2^- favors an internal solvation because of its symmetric electronic structure.

The observations reported here also have some relevance for the earlier studies involving hydrated Mg^+ cations,[45, 46] which took place in our laboratory. In order to explain some reactions of these species, we have argued that when placed into an aqueous cluster, a second ionization may take place, so that the $Mg^+(H_2O)_n$ species actually contain an Mg^{2+} ion and an electron.[47-50] The fact that these clusters were also found to be unreactive towards CO_2, and no carbonate formation could be detected, suggests that if such a second ionization does take place, the electron is not really free and available to enable the CO_2 molecule to enter the cluster.

4.4 Conclusions

The present chapter investigates the gas phase reactions of CO_2 and O_2 molecules with solvated electron clusters $(H_2O)_n^-$. The reactions proceed by the formation of CO_2^- or O_2^-, molecular anions, and their concurrent hydration, and stabilization by the aqueous shell. Since a single electron is present, one and only one molecule can be taken up by the cluster. These anionic clusters then gradually fragment under the influence of black body radiation and

collisions with the reaction gas. In the case of $CO_2^-(H_2O)_n$, the fragmentation proceeds down to the n = 2 clusters, which eventually detach the electron and vanish from the ICR trap. For the more stable $O_2^-(H_2O)_n$ fragmentation also results in the n = 2 species, which are, however, stable final products which do under the conditions of our experiments neither further fragment nor detach the electron. The experimental study is accompanied by a series of quantum chemical calculation of the structures, stability and energetics of the species studied, which facilitate the interpretation of our observations. The clusters with size up to n = 5, the CO_2^- is on the cluster surface, while O_2^- is internally solvated.

4.5 References

[1] G. V. Buxton, C. L. Greenstock, W. P. Helman, A. B. Ross, *J. Phys. Chem. Ref. Data* **1988**, *17*, 513-886.

[2] R. A. Marcus, *Reviews of Modern Physics* **1993**, *65*, 599-610.

[3] O. P. Balaj, I. Balteanu, B. S. Fox-Beyer, M. K. Beyer, V. E. Bondybey, *Angew. Chem.* **2003**, *115*, 5675-5677; *Angew. Chem. Int. Edit.* **2003**, *42*, 5516-5518.

[4] M. E. Jacox, D. E. Milligan, *Chem. Phys. Lett.* **1974**, *28*, 163-168.

[5] Z. H. Kafafi, R. H. Hauge, W. E. Billups, J. L. Margrave, *Inorg. Chem.* **1984**, *23*, 177-183.

[6] M. E. Jacox, W. E. Thompson, *J. Chem. Phys.* **1989**, *91*, 1410-1416.

[7] W. E. Thompson, M. E. Jacox, *J. Chem. Phys.* **1999**, *111*, 4487-4496.

[8] M. F. Zhou, L. Andrews, *J. Chem. Phys.* **1999**, *110*, 6820-6826.

[9] M. F. Zhou, L. Andrews, *J. Chem. Phys.* **1999**, *110*, 2414-2422.

[10] R. N. Compton, P. W. Reinhardt, C. D. Cooper, *J. Chem. Phys.* **1975**, *63*, 3821-3827.

[11] M. J. W. Boness, G. J. Schulz, *Phys. Rev. A* **1974**, *9*, 1969-1979.

[12] Y. Yoshioka, K. D. Jordan, *Chem. Phys. Lett.* **1981**, *84*, 370-374.

[13] K. D. Jordan, *J. Phys. Chem.* **1984**, *88*, 2459-2465.

[14] C. E. Klots, R. N. Compton, *J. Chem. Phys.* **1977**, *67*, 1779-1780.

[15] C. E. Klots, R. N. Compton, *J. Chem. Phys.* **1978**, *69*, 1636-1643.

[16] A. R. Rossi, K. D. Jordan, *J. Chem. Phys.* **1979**, *70*, 4422-4424.

[17] C. E. Klots, *J. Chem. Phys.* **1979**, *71*, 4172-4172.

[18] T. Tsukuda, M. Saeki, R. Kimura, T. Nagata, *J. Chem. Phys.* **1999**, *110*, 7846-7857.

[19] M. Saeki, T. Tsukuda, S. Iwata, T. Nagata, *J. Chem. Phys.* **1999**, *111*, 6333-6344.

[20] E. Surber, S. P. Ananthavel, A. Sanov, *J. Chem. Phys.* **2002**, *116*, 1920-1929.

[21] B. H. J. Bielski, D. E. Cabelli, R. L. Arudi, A. B. Ross, *J. Phys. Chem. Ref. Data* **1985**, *14*, 1041-1100.

[22] W. H. Koppenol, J. D. Rush, *J. Phys. Chem.* **1987**, *91*, 4429-4430.

[23] J. M. Weber, J. A. Kelley, S. B. Nielsen, P. Ayotte, M. A. Johnson, *Science* **2000**, *287*, 2461-2463.

[24] J. M. Weber, J. A. Kelley, W. H. Robertson, M. A. Johnson, *J. Chem. Phys.* **2001**, *114*, 2698-2706.

[25] G. H. Lee, S. T. Arnold, J. G. Eaton, H. W. Sarkas, K. H. Bowen, C. Ludewigt, H. Haberland, *Z. Phys. D At. Mol. Clusters*, 1991, *20*, 9-12.

[26] H. Haberland, C. Ludewigt, H. G. Schindler, D. R. Worsnop, *J. Chem. Phys.* **1984**, *81*, 3742-3744.

[27] H. Haberland, H. Langosch, H. G. Schindler, D. R. Worsnop, *J. Phys. Chem.* **1984**, *88*, 3903-3904.

[28] H. Haberland, H. G. Schindler, D. R. Worsnop, *Berichte Der Bunsen-Gesellschaft-Physical Chemistry Chemical Physics* **1984**, *88*, 270-272.

[29] L. A. Posey, M. A. Johnson, *J. Chem. Phys.* **1988**, *89*, 4807-4814.

[30] J. V. Coe, G. H. Lee, J. G. Eaton, S. T. Arnold, H. W. Sarkas, K. H. Bowen, C. Ludewigt, H. Haberland, D. R. Worsnop, *J. Chem. Phys.* **1990**, *92*, 3980-3982.

[31] L. A. Posey, M. J. Deluca, P. J. Campagnola, M. A. Johnson, *J. Phys. Chem.* **1989**, *93*, 1178-1181.

[32] S. T. Arnold, R. A. Morris, A. A. Viggiano, M. A. Johnson, *J. Phys. Chem.* **1996**, *100*, 2900-2906.

[33] M. K. Beyer, B. S. Fox, B. M. Reinhard, V. E. Bondybey, *J. Chem. Phys.* **2001**, *115*, 9288-9297.

[34] V. E. Bondybey, J. H. English, *J. Chem. Phys.* **1981**, *74*, 6978-6979.

[35] T. G. Dietz, M. A. Duncan, D. E. Powers, R. E. Smalley, *J. Chem. Phys.* **1981**, *74*, 6511-6512.

[36] S. Maruyama, L. R. Anderson, R. E. Smalley, *Rev. Sci. Instrum.* **1990**, *61*, 3686-3693.

[37] C. Berg, T. Schindler, G. Niedner-Schatteburg, V. E. Bondybey, *J. Chem. Phys.* **1995**, *102*, 4870-4884.

[38] M. Beyer, C. Berg, H. W. Görlitzer, T. Schindler, U. Achatz, G. Albert, G. Niedner-Schatteburg, V. E. Bondybey, *J. Am. Chem. Soc.* **1996**, *118*, 7386-7389.

[39] T. Su, M. T. Bowers, *J. Chem. Phys.* **1973**, *58*, 3027-3037.

[40] L. Bass, T. Su, M. T. Bowers, *Int. J. Mass Spectrom. Ion Processes* **1978**, *28*, 389-399.

[41] L. Bass, T. Su, W. J. Chesnavich, M. T. Bowers, *Chem. Phys. Lett.* **1975**, *34*, 119-122.

[42] M. J. Frisch, G. W. Trucks, H. B. Schlegel, G. E. Scuseria, M. A. Robb, J. R. Cheeseman, V. G. Zakrzewski, J. Montgomery, J. A., R. E. Stratmann, J. C. Burant, S. Dapprich, J. M. Millam, A. D. Daniels, K. N. Kudin, M. C. Strain, O. Farkas, J. Tomasi, V. Barone, M. Cossi, R. Cammi, B. Mennucci, C. Pomelli, C. Adamo, S. Clifford, J. Ochterski, G. A. Petersson, P. Y. Ayala, Q. Cui, K. Morokuma, D. K. Malick, A. D. Rabuck, K. Raghavachari, J. B. Foresman, J. Cioslowski, J. V. Ortiz, B. B. Stefanov, G. Liu, A. Liashenko, P. Piskorz, I. Komaromi, R. Gomperts, R. L. Martin, D. J. Fox, T. Keith, M. A. Al-Laham, C. Y. Peng, A. Nanayakkara, C. Gonzalez, M. Challacombe, P. M. W. Gill, B. G. Johnson, W. Chen, M. W. Wong, J. L. Andres, M. Head-Gordon, E. S. Replogle, J. A. Pople, Gaussian, Inc., Pittsburgh PA, **1998**.

[43] A. D. Becke, *J. Chem. Phys.* **1993**, *98*, 5648-5652.

[44] C. T. Lee, W. T. Yang, R. G. Parr, *Physical Review B* **1988**, *37*, 785-789.

[45] C. Berg, M. Beyer, U. Achatz, S. Joos, G. Niedner-Schatteburg, V. E. Bondybey, *Chem. Phys.* **1998**, *239*, 379-392.

[46] C. Berg, U. Achatz, M. Beyer, S. Joos, G. Albert, T. Schindler, G. Niedner-Schatteburg, V. E. Bondybey, *Int. J. Mass Spectrom.* **1997**, *167*, 723-734.

[47] K. Fuke, K. Hashimoto, S. Iwata, in *Adv. Chem. Phys., Vol. 110*, **1999**, pp. 431-523.

[48] B. M. Reinhard, G. Niedner-Schatteburg, *J. Chem. Phys.* **2003**, *118*, 3571-3582.

[49] C. K. Siu, Z. F. Liu, *Chem. Eur. J.* **2002**, *8*, 3177-3186.

[50] B. M. Reinhard, G. Niedner-Schatteburg, *Phys. Chem. Chem. Phys.* **2002**, *4*, 1471-1477.

5. The Hydrated Electron Nanodroplets in reaction with Acetonitrile.

5.1 Introduction

The studies done in the past have used especially the pulsed radiolysis technique[1] to characterize the hydrated electron, e_{aq}^-, and its reactions. Interpretation of the results is, however, complicated by the fact that even for pure water radiolysis, in a recent review[1] 33 distinct reactions are listed, which convert the primary species not only into new radicals, but also into each other. In order to study the reactivity of the hydrated electron, e_{aq}^-, the experiments are e.g. done in a buffer solution at pH = 12 to prevent formation of hydrogen atoms from the recombination of protons with the hydrated electrons.[2]

An alternative way to eliminate such problems is to solvate the electron in a nanodroplet. A laser vaporization source developed in our laboratory turns out the be a very efficient source of $(H_2O)_n^-$ species, which can be trapped and studied by high resolution FT-ICR mass spectrometry. The advantage of such clusters, whose sizes are typically in the range n = 13 - 80, is that their masses, and thus their elemental composition are exactly known, eliminating any effects due to impurities, and also the presence of H_3O^+ ions from the autoprotolysis of water can be ruled out in such clusters of typically less than a hundred water molecules.

Recently it was demonstrated that nanodroplets consisting of as few as 10 - 50 water molecules are sufficiently large to exhibit solution-phase behavior,[3,4] and a number of well-known bulk solution reactions were shown to have their counterparts in the nanodroplet.[3] More than 25 years ago the reaction of hydrated electron with acetonitrile was observed by ESR spectroscopy in solution, but the product was not identified.[2]

5.2 Experimental Section

The experiments were performed on a modified Bruker/Spectrospin CMS47X mass spectrometer, equipped with an Apex III data station and an external homebuilt laser vaporization source described previously.[4] Hydrated electrons $(H_2O)_n^-$, n = 25 - 60, were produced by laser vaporization of a solid zinc target with the 5 ns pulse of a frequency-doubled Nd:YAG laser (Continuum Surelite II, 10 Hz, 5 mJ pulse energy), followed by supersonic expansion of the hot plasma entrained in a 50 µs helium pulse, which was seeded with traces of water. The $(H_2O)_n^-$ ions formed were transferred by a series of electrostatic lenses through four stages of differential pumping, decelerated and stored in the ICR cell. The reactants, acetonitrile (Aldrich, 99.93+%) and acetonitrile-d3 (99.6% D, Aldrich), were degassed by freeze-pump-thaw-cycles. Admitted into the ultra high vacuum region of the ICR cell through a leak valve, the pressure was raised to the desired value. In the case of acetonitrile the base pressure was raised from 2×10^{-10} mbar to 9.6×10^{-9} mbar, which translates to a collision rate of 0.55 s^{-1}. The true collision rate is, however, probably larger due to the finite size of the nanodroplets. In the case of acetonitrile-d3 the pressure was raised to 5.0×10^{-9} mbar. The concentration of the reactant clusters and of their ionic reaction products was followed by acquiring mass spectra after defined reaction delays. Absolute rate constants are calculated from the number densities of the reactant ion, collision efficiencies are calculated as the ratio of the absolute rate constant and the collision rate, which in turn was calculated with average dipole orientation (ADO) theory.[5-8] Density functional calculations were carried out with the Gaussian98 program package,[9] using the BPW91 method with the 6-311++G** basis set. Partial charges were calculated using natural population analysis[10] as implemented in Gaussian98.

5.3 Results and Discussion

5.3.1 Addition of a Hydrogen Atom to Acetonitrile

The progress of the reaction was monitored at different intervals, as shown in Figure 1. As a constant pressure of the acetonitrile reactant is present in the instrument during the entire experiment, the reaction is already taking place during the accumulation of the $(H_2O)_n^-$ nanodroplets in the ICR cell, so that even at the nominal t = 0 time products are clearly observable. The product peaks are shifted by one unit to lower masses with respect to the solvated electron reactant, indicating that a hydrogen atom is lost from the cluster. The distribution of the products is broad and, except for a slight shift towards smaller values of n, similar to that of the reactant clusters, which suggests that the reaction rate is not strongly size-dependent. The overall reaction taking place can be described by the equation:

$$(H_2O)_n^- + CH_3CN \rightarrow OH^-(H_2O)_{n-m-1} + m\ H_2O + \ C_2H_4N,\ \ m = 1, 2 \qquad (1)$$

Clearly, one of the water molecules in the nanodroplet loses a hydrogen atom, and a hydrated hydroxide anion is formed. In addition, the shift in the distribution of the product towards a smaller number of ligands suggests that the overall reaction is sufficiently exothermic to evaporate one or several water molecules. After 0.5 s, almost exactly half of the ions have reacted, and after 10 s, virtually all the reactant $(H_2O)_n^-$ are converted into $OH^-(H_2O)_n$. However, even though the CH_3CN clearly is an essential participant of the reaction, in spite of a thorough search, no clusters containing acetonitrile were detected in the early stage of the reaction.

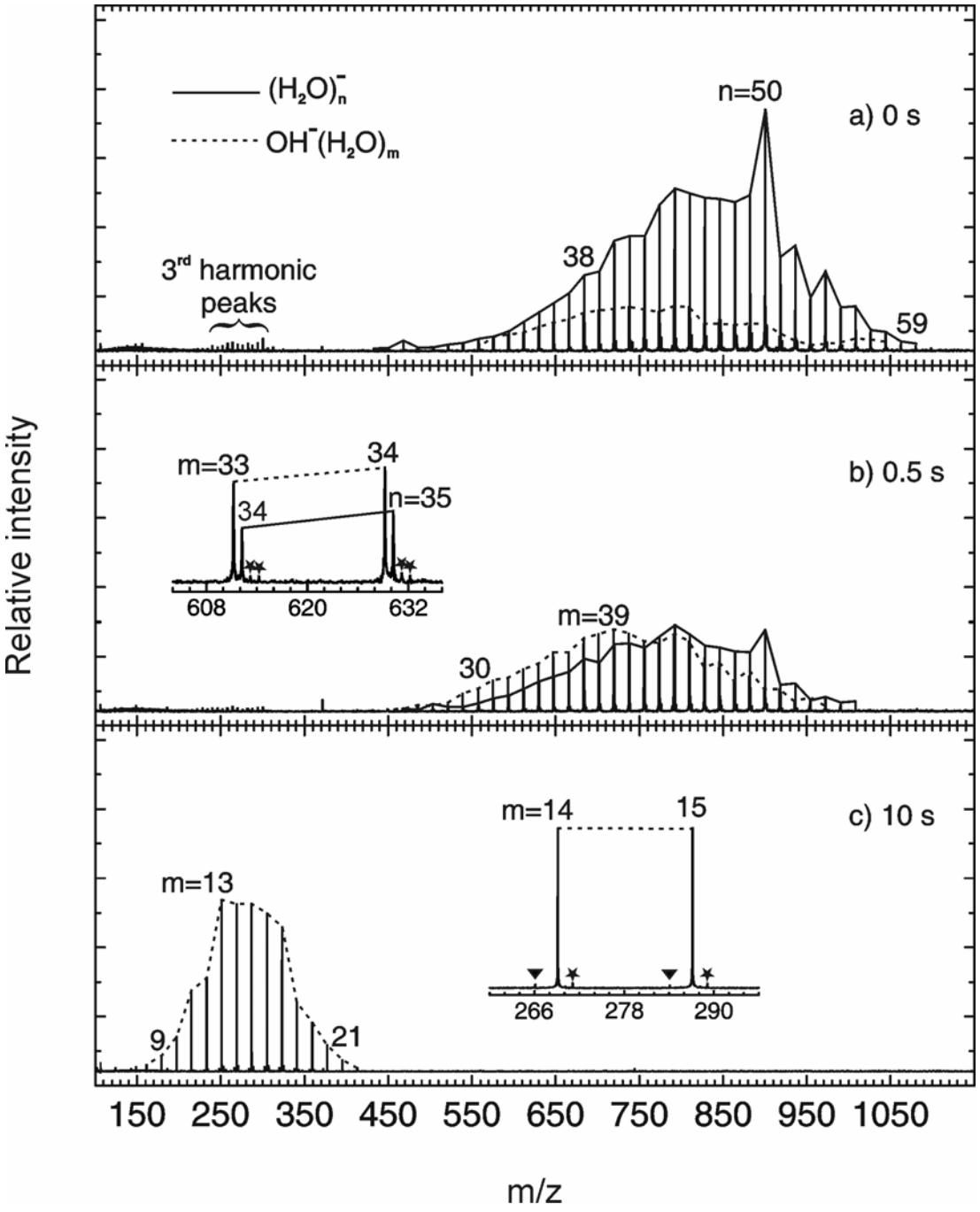

Figure 1: Mass spectrum of the reaction of $(H_2O)_n^-$ with acetonitrile after a) 0 s, b) 0.5 s and c) 10 s. One can clearly see already at 0 s, shifted lower by one AMU, the presence of the reaction products: $OH^-(H_2O)_m$. 0.5 s later about 50% of the ions have reacted and after 10 s reaction delay all of the initial $(H_2O)_n^-$ have been completely converted into products. The peaks marked with ★ are due to the natural abundance of ^{18}O in the water molecules. Also ▼ $O_2^-(H_2O)_p$ impurity peaks are present after long reaction delays.

The reaction is accompanied by collisional and black-body radiation-induced cluster fragmentation, which causes the nanodroplets to undergo sequential loss of single water molecules.[11] After even longer reaction times, when the number of water molecules drops below about n = 15, apparently the uptake of one acetonitrile molecule in the strongly basic $OH^-(H_2O)_n$ clusters becomes feasible, resulting in $OH^-(H_2O)_nCH_3CN$ species. The final product of their further fragmentation is an $OH^-(H_2O)_2CH_3CN$ complex, which appears stable under the conditions of our experiment. While the mass spectrometer unambiguously reveals the loss of a hydrogen atom, it cannot identify the neutral species formed in the reaction, and does not show if it is lost as a free atom, if it recombined with the acetonitrile molecule, or if other fragments, such as CN or HCN have been formed. However, the observed reaction must be both thermochemically allowed and mechanistically feasible. The potential energy surface of CH_3CN + H was recently studied by Wang et al. on the G3 level of theory, and the results were in excellent agreement with experimental data where available.[12] Among the eleven different possibilities investigated by these authors, the hydrogen addition product at the carbon atom, CH_3CHN, is clearly the thermochemically most favorable, and at the same time the product most likely to be produced from the mechanistic point of view, as it poses the smallest barrier for hydrogen addition.

Scheme 1 shows two ways to rationalize the observations, which differ in the initially activated species. Recent calculations suggest that structures containing the H_3O^+-OH^- ion pair are stable minima on the potential energy surface of $(H_2O)_n^-$ with n = 11 and n = 14.[13] Even though these structures are not the lowest energy species, the formation of such ion pairs in the collision complex could be promoted by the large dipole moment of CH_3CN of 3.924 D. Once formed, the H_3O^+ might recombine with the electron, and the resulting H atom is added to acetonitrile, as previously observed in radiolysis studies.[14,15]

The second, equally speculative mechanism, involves a solvent-stabilized covalent radical anion as the reactive intermediate. It is well-established for CO_2^- [16,17] and the uraci

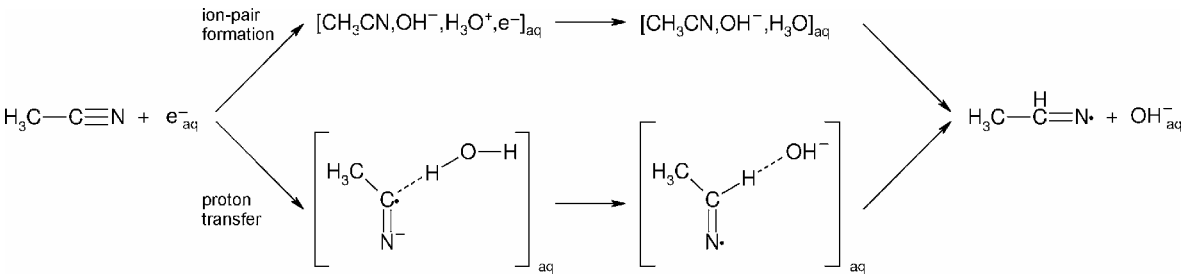

Scheme 1: Proposed mechanisms of $OH^-(H_2O)_m$ formation. In the first mechanism the large dipole moment of actonitrile induces H_3O^+-OH^- ion pair formation in the collision complex, followed by a hydronium-electron recombination. The resulting H is added to acetonitrile. The second mechanism involves a solvent-stabilized covalent radical anion as an intermediate. A proton can be transferred from a water molecule, the CH_3CHN and the $OH^-(H_2O)_m$ remains.

anion[18] that solvation with a single water molecule leads to a greatly increased electron affinity and, at least in the case of CO_2^-, with a significant change in their geometry and electronic structure. While CH_3CN^- is a dipole-bound anion in the gas phase,[19,20] it was recently shown that excess electrons in condensed acetonitrile lead to reactive species,[21-23] and calculations employing a polarizable continuum model yield a CCN angle of 125.4°.[23] It is quite conceivable that hydration may have a similar effect and transform CH_3CN^- into a covalent radical anion. When formed in the collision of CH_3CN with $(H_2O)_n^-$, this radical anion may be able to extract a proton from the nanodroplet, and a neutral CH_3CHN evaporates, leaving behind a hydrated OH^- cluster.

5.3.2 Base Catalyzed Hydrogen/Deuterium Exchange between Water and d3-Acetonitrile

In mass spectrometric experiments, hydrogen/deuterium reactions are frequently used as a probe of gas phase structures of peptides and proteins.[24-33] This exchange is specific to acidic or basic sites, and methyl groups are in general considered to be unaffected. However, flowing afterglow studies have shown that certain carbanions undergo efficient

H/D-exchange with H_2O.[34,35] CH_2CN^- was shown to sequentially exchange both H atoms against D in collisions with H_2O. In the reaction of acetonitrile-d3 with the hydrated electrons $OH^-(H_2O)_n$ products are also formed. At later stages, following the total conversion of the $(H_2O)_n^-$ into the products and their subsequent fragmentation, an H/D-exchange involving the methyl group of acetonitrile is observed.

The hydrated electron clusters react very efficiently with acetonitrile-d3 as seen in Figure 2. The reaction proceeds in a manner identical to normal acetonitrile with the exception that in this case the neutral, and therefore unobserved, product formed is CD_3CHN. The $OH^-(H_2O)_m$ products do not contain significant amounts of deuterium, and the proposed mechanism is consistent with the absence of isotopic scrambling. Also the fragmentation proceeds in the identical manner and with similar rates, so that after about 10 seconds all the hydrated electron clusters are replaced by the hydroxide clusters, $OH^-(H_2O)_m$. No exchange of hydrogen against deuterium is observed at this stage.

After about 15 seconds, as shown in the Figure 2b), the first evidence of the incorporation of acetonitrile-d3 into the hydrated hydroxide clusters is observed:

$$OH^-(H_2O)_m + CD_3CN \rightarrow OH^-(CD_3CN)(H_2O)_{m-x} + x\ H_2O \qquad (2)$$

where probably x = 1. The $OH^-(CD_3CN)(H_2O)_p$ product cluster sizes after 15 s range from p = 4 to p = 10, with the p = 7 cluster standing out, having about a factor of two higher intensity than the neighboring p = 6 and p = 8 species. Apparently, for larger clusters the incorporation of CD_3CN does not take place, but as the clusters lose water, it becomes progressively more favorable.

The latest stages of the reaction are shown in Figure 2, panels c), and d), which show spectra obtained after 30 and 50 seconds, respectively. In the 30 s spectrum, the most intense clusters correspond to p = 3, p = 2, m = 3, and m = 4 in that order. On the high mass side of

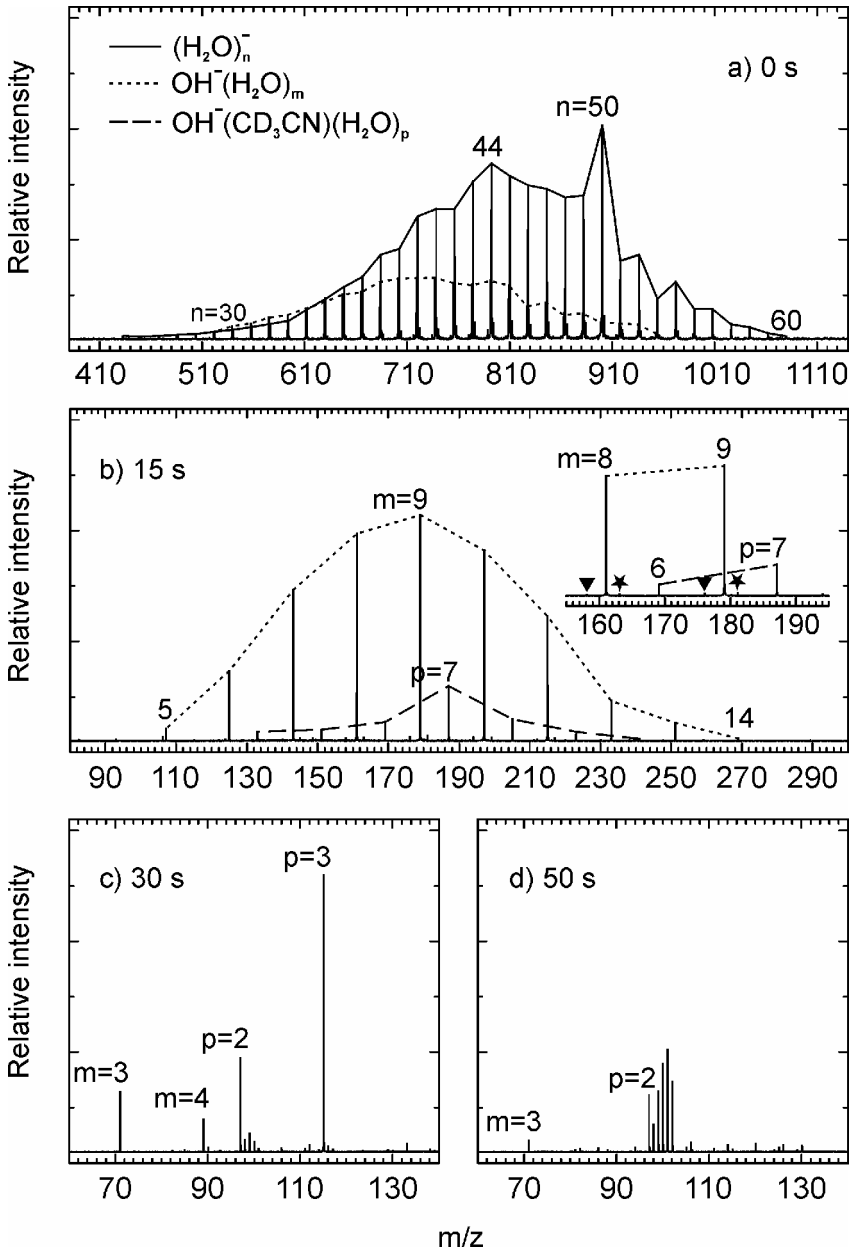

Figure 2. Mass spectra of the reaction of $(H_2O)_n^-$ with acetonitrile-d3. a) Since the reaction occurs already during the ion accumulation, the $OH^-(H_2O)_m$ products are visible already at 0 s. b) After 15 s the reaction products have become basic enough that the intake of one acetonitrile-d3 molecule is possible. Visible in the detail alongside $OH^-(H_2O)_{8,9}$ are $OH^-(CD_3CN)(H_2O)_{6,7}$ peaks. Species ▼$O_2^-(H_2O)_p$ are present due to minor impurities of O_2 in the expansion gas, ★ denotes peaks due to the natural abundance of ^{18}O in $OH^-(H_2O)_m$. c) The ions gradually lose ligands until after 30 s the main products are $OH^-(H_2O)_{3,4}$, $OH^-(CD_3CN)(H_2O)_2$ and $OH^-(CD_3CN)(H_2O)_3$. The peaks at 98, 99, 100, 101 and 102 AMU are due to the progressive deuteration of the $OH^-(CD_3CN)(H_2O)_2$ cluster through a reversible intracluster proton transfer reaction followed by an acetonitrile ligand exchange. d) The H/D isotopic exchange reaction proceeds until all the hydrogen atoms are replaced by deuterium.

the p = 2, that is $OH^-(CD_3CN)(H_2O)_2$ cluster at a nominal mass of 97 AMU, one can clearly observe weak peaks appearing at masses 98, 99, and 100 AMU, respectively. After additional ten seconds the 97 AMU peak does become the strongest peak in the spectrum, and its higher mass satellites at 98-100 AMU have gained considerably in intensity, with also peaks at 101 and 102 AMU now being clearly observable. Finally, in Figure 2d), corresponding to fifty seconds reaction time, the intensities shift further in favor of the higher masses, so that the 99-102 AMU peaks are now more intense than the original 97 AMU cluster.

Two conclusions may be drawn from these data:

1. The ligand exchange reaction (2) proceeds rather reluctantly, which suggests it might be thermoneutral or slightly endothermic.
2. During further collisions with the CD_3CN molecules, the $OH^-(CD_3CN)(H_2O)_2$ cluster is being progressively deuterated.

5.3.2.1 Uptake of CD_3CN by $OH^-(H_2O)_n$

In order to learn more about these processes, we mass selected the m/z = 115-117 species after 30 s, i.e. $OH^-(CD_3CN)(H_2O)_3$ including the ^{13}C, ^{18}O isotope peaks, and monitored its further reaction for additional 15 s. The time-intensity profile of this reaction is shown in Figure 3, together with a fit according to pseudo-first order kinetics. It is unambiguously shown that both CD_3CN and H_2O can be lost from the cluster, with a branching ratio of 0.72:0.28. In view of the higher number of H_2O molecules present in the cluster, this clearly indicates that CD_3CN is more weakly bound than H_2O, and that the ligand exchange reaction (2) is slightly endothermic. In addition, the absence of peaks with m/z = 72-78, corresponding to partially deuterated $OH^-(H_2O)_3$, peak is clear evidence that no isotopic scrambling takes place in $OH^-(CD_3CN)(H_2O)_3$.

The $OH^-(H_2O)_3$ fragment in turn undergoes the ligand exchange reaction (2), forming $OH^-(CD_3CN)(H_2O)_2$, which do not fragment any further. The product $OH^-(CD_3CN)(H_2O)_2$

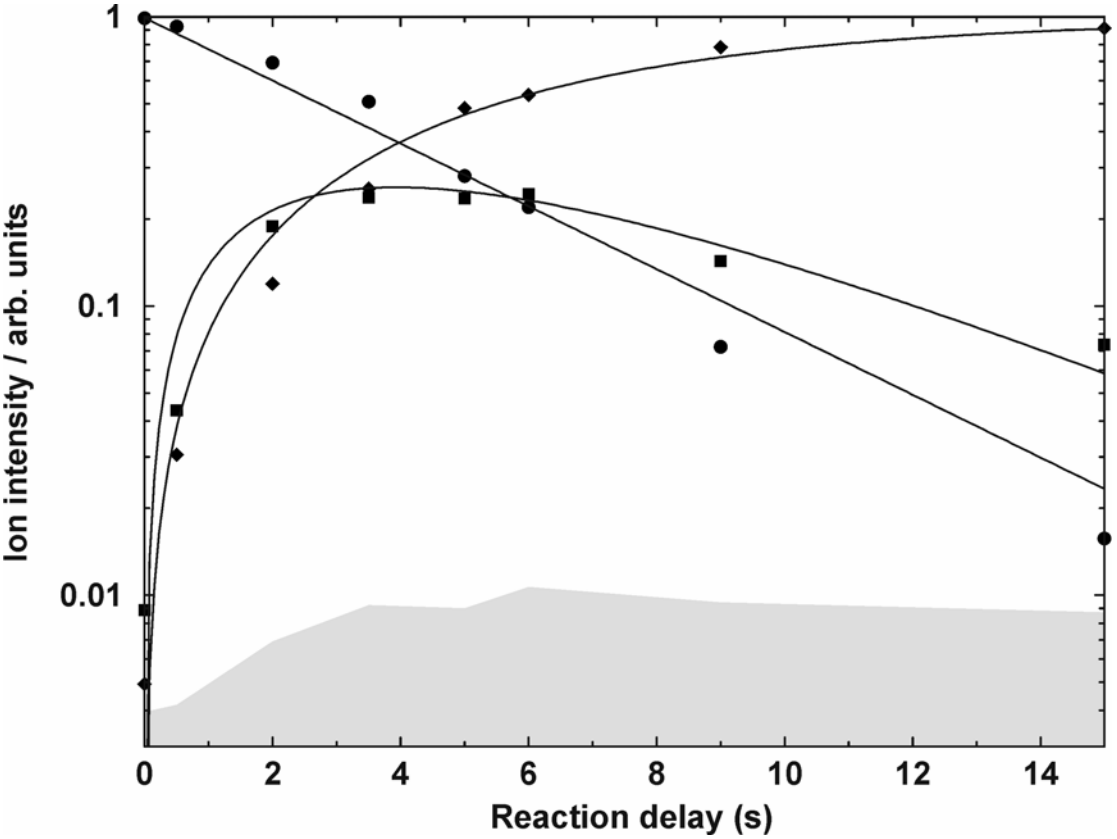

Figure 3. Kinetic fit of mass selected ● $OH^-(CD_3CN)(H_2O)_3$, which loses CD_3CN with a rate constant of k = 0.18 s^{-1} to form ■ $OH^-(H_2O)_3$ and H_2O with a rate constant of k = 0.07 s^{-1} to form ◆ $OH^-(CD_3CN)(H_2O)_2$. $OH^-(H_2O)_3$ undergo a ligand exchange to form $OH^-(CD_3CN)(H_2O)_2$ with k = 0.26 s^{-1}, which amounts to a bimolecular rate constant of 1.1×10^{-9} cm^3s^{-1} or 40% collision efficiency.[5-7] The intensity of subsequent H/D-exchange products was summed into that of $OH^-(CD_3CN)(H_2O)_2$. The gray shaded area denotes the noise level.

can thus be formed in two ways: As a primary product by water loss from $OH^-(CD_3CN)(H_2O)_3$, or as a secondary product by ligand exchange of $OH^-(H_2O)_3$ with CD_3CN.

These results suggest that the ligand exchange reaction (2) is in fact endothermic over the whole region where it occurs, and the CD_3CN are lost again with a high probability due to black-body radiation and collision induced dissociation. This explains why the ligand exchange products do not become the dominant species for a very long time, and why their intensities exhibit a fairly gradual onset around n = 10-11. Previous studies indicated that aqueous clusters containing OH^- can be viewed as strongly basic.[37] Conversely, acetonitrile is

known to be a very weak acid. As the number of water ligands decreases, the basicity of $OH^-(H_2O)_n$ increases, until it is sufficient to make incorporation of CH_3CN into the cluster energetically feasible.

5.3.2.2 H/D-exchange in $OH^-(CD_3CN)(H_2O)_2$

Returning to the H/D-exchange, the results so far indicate that only the "final" $OH^-(CD_3CN)(H_2O)_2$ clusters are being efficiently deuterated. We now performed a mass selection of the 97-102 AMU region of the mass spectrum after 35 s by resonant ejection of all ions outside this mass range, and followed the gradual deuteration of the $OH^-(CD_3CN)(H_2O)_2$ for an additional 5 s. The time-intensity profile of the results of this experiment is shown in Figure 4, where the intensities of the higher masses have been corrected for the ^{13}C, ^{16}N and ^{18}O contributions from lower-mass peaks.

It is immediately interesting to note, that the ion which grows in first and fastest is not 98 AMU, but 99 AMU, corresponding to exchange of two hydrogen atoms for deuterium. In order to rationalize this process, one has to assume that a reversible intracluster reaction is taking place, which exchanges protons between the "organic" part, that is the CD_3CN, and the "aqueous" part, that is the $OH^-(H_2O)_2$ (or $H_5O_3^-$). The initial step is described by reaction (3), which redistributes a proton and a deuteron between the two parts:

$$\begin{aligned} OH^-..CD_3CN(H_2O)_2 &\rightarrow HOD..CD_2CN^-(H_2O)_2 \rightarrow \\ &\rightarrow HOH..CD_2CN^-(H_2O)(HOD) \rightarrow OH^-..CD_2HCN(H_2O)(HOD) \end{aligned} \quad (3)$$

On the time scale of the ICR experiment of seconds, the cluster has enough time to undergo multiple intracluster H/D-exchanges of this type, which will essentially randomize the position of hydrogen and deuterium atoms, modified only by the different zero-point

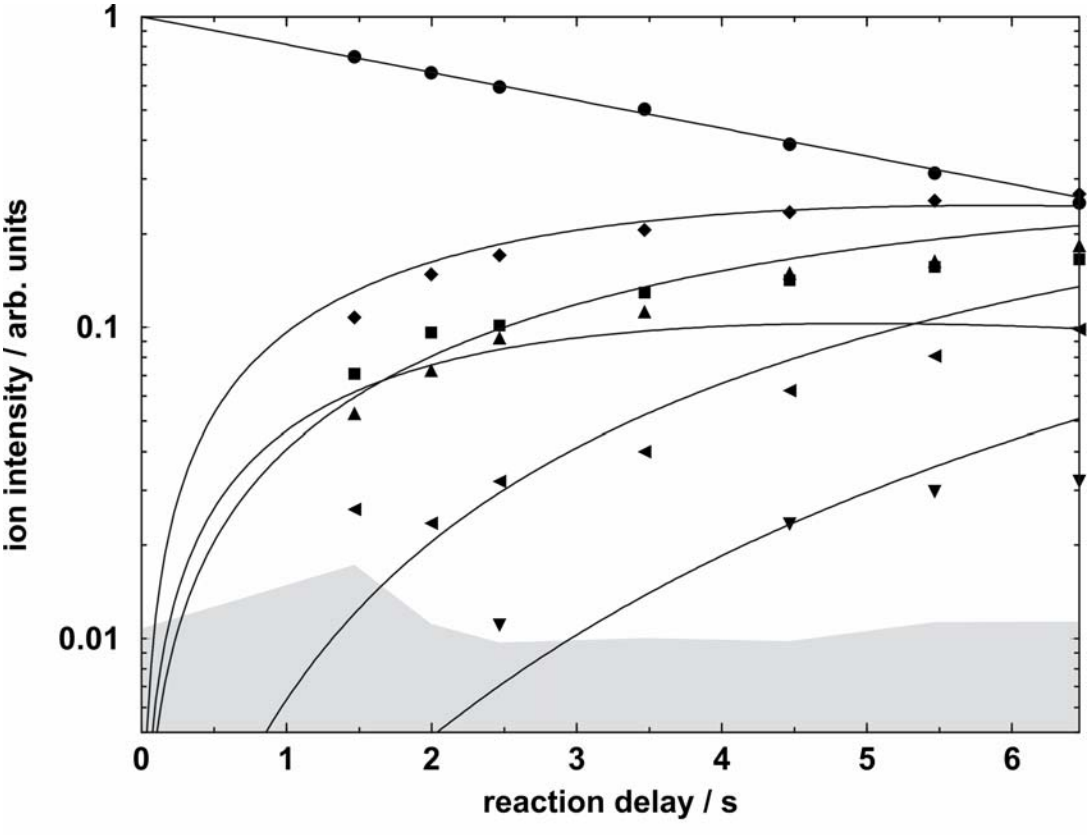

Figure 4. Kinetic fit for the progressive deuteration of the mass selected ● $OH^-(CD_3CN)(H_2O)_2$. The symbols denote the number of additional exchanges of H against D: ■ one, ◆ two, ▲ three, ◄ four and ▼ five, the latter corresponding to the completely deuterated final product $OD^-(CD_3CN)(D_2O)_2$. Since the H/D-exchange products overlap with other isotopes like ^{13}C and ^{18}O, the intensities were corrected for these contributions. The gray shaded area denotes the noise level.

energies of the various isomers.

In a subsequent two body collision with acetonitrile-d3, the isotopically scrambled $CD_{3-k}H_kCN$ may be replaced with a fully deuterated CD_3CN according to reaction (4):

$$H_{5-k}D_kO_3^-..CD_{3-k}H_kCN + CD_3CN \rightarrow H_{5-k}D_kO_3^-..CD_3CN + CD_{3-k}H_kCN,\ k = 0\text{-}3 \qquad (4)$$

The products of reaction (4) may in turn randomize the position of H and D in reaction similar to (3). In this way, full deuteration is gradually achieved.

If this picture is correct, the time-intensity profile shown in Figure 4 depends only on two factors: The rate with which the $CD_{3-k}H_kCN$ is exchanged against CD_3CN, and the probability $p_j(k)$ for a certain value of k in a cluster containing j H atoms and 8-j D atoms. This probability amounts to:

$$p_j(k) = \frac{\binom{j}{k}\binom{8-j}{3-k}}{\binom{8}{3}} \tag{5}$$

In the first exchange step, j = 5, and the probabilities for exchanging 0, 1, 2 or 3 D against H, i.e. k = 0, 1, 2, or 3, are 1/56, 15/56, 30/56 and 10/56, respectively. A least-square fit of the decay of the reactant m/z = 97 yields a relative rate constant of k_{rel} = 0.21 s^{-1}. The total exchange rate constant on which the complete fit must be based is then 56/55 k_{rel} = 0.22 s^{-1}, which corresponds to an absolute rate constant for the exchange of $k_{abs} = 9.4\times10^{-10}$ cm^3 s^{-1} or a collision efficiency of Φ = 36%. Table 1 compares the ideal rate constants calculated from these assumptions with the actual rate constants extracted from the fit. The rate constants for primary products are very well reproduced by this approach, especially the observation that

Table 1. Pseudo-first order rate constants k_{exp} for H/D-exchange processes of $OH^-(CD_3CN)(H_2O)_2$ in binary collisions with CD_3CN from the fit shown in Figure 4. The reactions describe the exchange of k H against D in a cluster containing j H. Theoretical numbers k_{rand} based on the assumption of total randomization in the cluster and a constant exchange rate of the acetonitrile molecule, as well as their statistical contribution are shown for comparison.

j,k	5,1	5,2	5,3	4,1	4,2	4,3	3,1	3,2	3,3	2,1	2,2	1,1
$10^2 k_{exp}$	6.2	11.8	3.8	3.5	3.5	0.5	8.5	4.0	0.3	9.5	2.0	8.0
$10^2 k_{rand}$	5.9	11.8	3.9	9.4	9.4	1.6	11.8	5.9	0.4	11.8	2.4	8.3
$56p_j(k)$	15	30	10	24	24	4	30	15	1	30	6	21

the probability for exchanging two H atoms in the first step is twice as high as for one H. The subsequent exchange steps, however, exhibit substantial deviations from this ideal picture, although the overall pattern is still well reproduced. In this simple approach, the energy differences due to the variations of vibrational frequencies with the position of H and D is neglected, which changes the relative probabilities as well as the rate constant for the exchange.

A second possibility is that scrambling may also occur to some extent in the collision complex, while full randomization in the collision complex can be excluded: The probability for exchange of one or two H atoms in the first step would be 5/11 or 4/11, respectively, while the data clearly indicate that exchange of two H atoms against D is preferred by a factor of 2. Given the simplicity of the approach, the agreement of the fit is quite remarkable, and indicates that the overall picture of the H/D-exchange process is correct.

The observed H/D-exchange also is indirect evidence that no base-catalyzed hydrolysis of acetonitrile to acetic acid takes place in these small gas phase clusters, which occurs under strongly basic conditions in aqueous solutions. However, the mechanism of this hydrolysis is very complicated and involves multiple proton transfer steps. If CD_3COO^- would form, the m = 2 product would have the composition $CD_3COO^-(NH_3)(H_2O)$, if scrambling is neglected. Under these conditions, replacement of a CD_3CN unit seems highly improbable.

5.3.2.3 Evidence of the OH^- role in the H/D exchange. Reactions of $(H_2O)_n^-$ with CD_3CDO.

To provide additional evidence that the presence of the hydroxide anion, and the basicity of the cluster are responsible for the H/D-exchange, we have carried out a similar experiment with perdeuterated acetaldehyde, CD_3CDO, instead of acetonitrile, as shown in Figure 5. The polar CD_3CDO is efficiently taken up by the hydrated electron clusters, and solvated $CD_3CDO^-(H_2O)_m$ anions are formed. Similar to other cases, like O_2 or CO_2 [38,39]

reactions, where the exchange of the ligand is accompanied by a change in the nature of the central ion, after a single molecule of the reactant has entered the cluster, no further uptake of acetaldehyde is observed for larger clusters. The clusters then only fragment and progressively lose ligands one by one, down to m = 3. However, when the clusters become very small, again an endothermic ligand exchange becomes feasible, and more and more $(CD_3CDO)_2^-(H_2O)_2$ is observed. Even after 30 s, however, no H/D-exchange peaks are detectable in these clusters, where no OH^- anions are present. After 50 s, the signal has disappeared due to slow, presumably collision-induced electron detachment.

The total absence of H/D-exchange peaks in $CD_3CDO^-(H_2O)_3$ after 30 s, when the exchange was in full progress in $OH^-CD_3CN(H_2O)_2$, provides additional strong evidence that the H/D-exchange mechanism requires the hydroxide anion, as suggested in reaction (3).

5.3.2.4 Density functional calculations of $OH^-(CH_3CN)(H_2O)_m$, m = 0 – 3.

We have further checked the feasibility of the H/D-exchange mechanism suggested by reactions (3) and (4) by a series of quantum chemical calculations on the $OH^-(CH_3CN)(H_2O)_m$, m = 0 – 3 clusters. Consistent with the proposed proton transfer, we find for most of the clusters two types of structures: $OH^-(CH_3CN)(H_2O)_m$ solvated hydroxide complexes which we denote in the Table and Figures with the letter A_{m-i}, and complexes $(CH_2CN^-)(H_2O)_{m+1}$ denoted B_{m-i}. In the latter, the acetonitrile has transferred one proton to OH^-, yielding a molecule of water, and resulting in a solvated H_2CCN^- anion. Obviously, the relative energies of these isomeric forms, and the barriers separating them are crucial for the proposed proton transfer and isotope exchange processes. To distinguish different isomers of the same A_m, B_m species, a second index i is introduced. The results are summarized in Table 2, which lists relative energies and the partitioning of the negative charge over the hydrogen bonded species in the cluster, according to natural population analysis.[10] The energetically lowest lying isomers of A_m and B_m for m = 0 - 3 are shown in Figures 6-8.

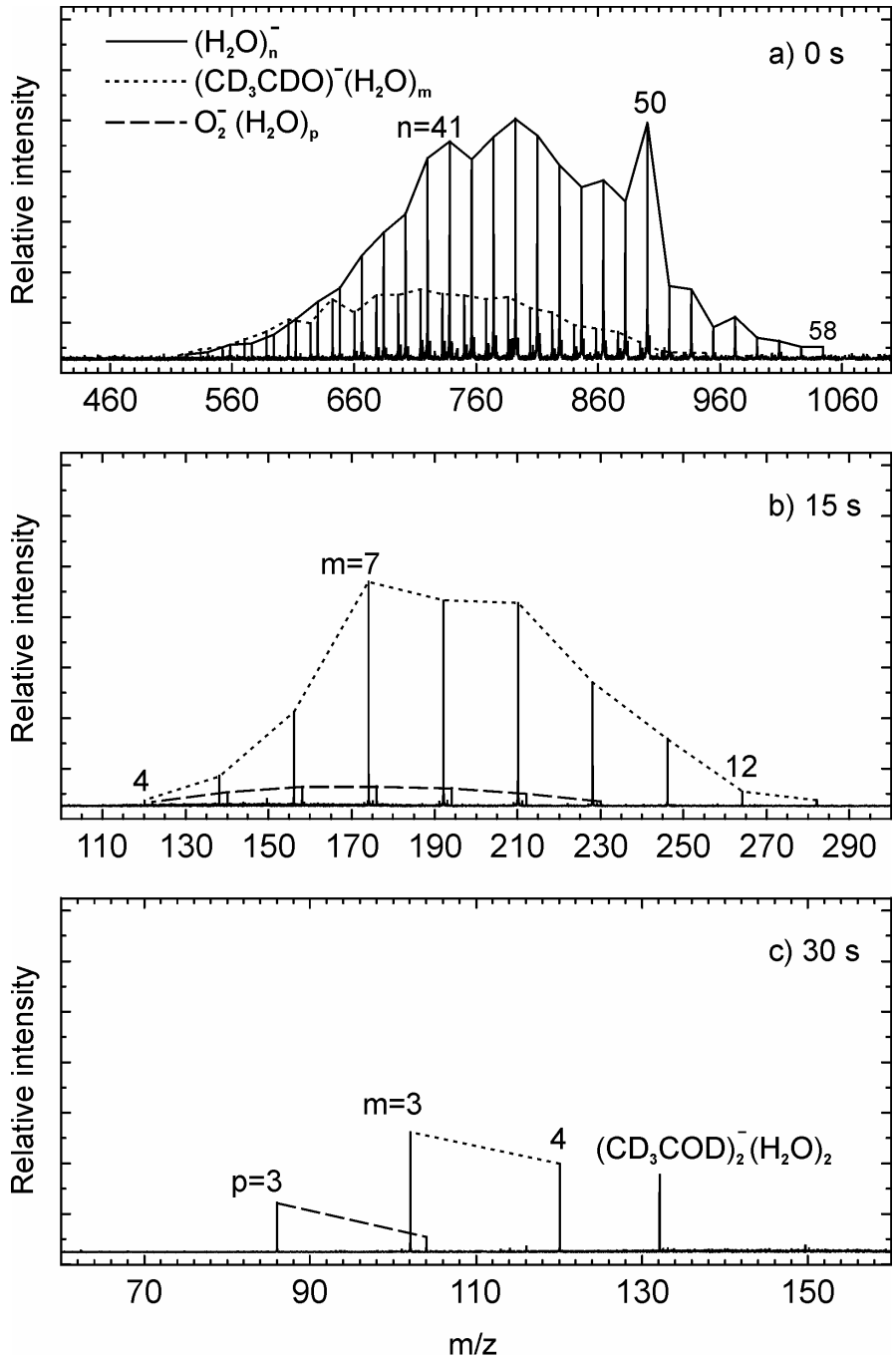

Figure 5. Mass spectra of the reaction of $(H_2O)_n^-$ with perdeuterated acetaldehyde. a) One CD_3CDO molecule is taken up by the hydrated electron clusters as can be seen already at nominally 0 s. b) The exchange is complete and fragmentation in full progress at 15 s. c) After 30 s the main products are $CD_3CDO^-(H_2O)_{3,4}$, $(CD_3CDO)_2^-(H_2O)_2$ and $O_2^-(H_2O)_3$ as impurity. No H/D exchange peaks are visible, which supports the role of the hydroxide anion in the suggested exchange mechanism.

A complex of OH^- with CH_3CN, which would in this notation be A_{0-1}, is found not to be stable; as soon as a hydroxide anion comes into contact with acetonitrile, a proton transfer takes place, resulting in the CH_2CN^- anion bound to a water ligand (B_{0-1} in Figure 6). The H_2O is bonded via a rather long, 1.838 Å hydrogen bond to the carbon atom of the CH_2-group, which carries a formal charge of -0.97e. The CCN bond angle with 175.8° deviates only slightly from linearity, and there is only little charge transfer from the CH_2CN^- to the water ligand, with the electron residing mostly on the organic anion (-0.88e).

Already a single additional water molecule stabilizes the OH^- anion, so that both kinds of structures represent local minima on the potential energy surface. The A_{1-1} complex (Figure 6) is a structure of $OH^-(CH_3CN)(H_2O)$ in which the OH^- is stabilized by two ligands, one molecule of water, and acetonitrile. In this complex, acetonitrile binds to the OH^- via one of the hydrogen atoms of the methyl group. The hydrogen-bonded C-H is appreciably lengthened to 1.183 Å, and the hydrogen bonding distance (1.614 Å) is remarkably short, comparable to the hydrogen bonding distance between the OH^- and H_2O (1.525 Å). A charge of -0.75e is computed to be localized on the OH^-, with -0.12e and -0.13e on the water ligand and on the acetonitrile, respectively. The proton transferred structure $(CH_2CN^-)(H_2O)_2$ (B_{1-1} in Figure 6) is also a stable dimer by two hydrogen bonds with C...H and N...H distances of 1.786 Å and 2.219 Å respectively.

Additional water ligands then further stabilize the hydroxide anion, reducing its basicity, and this is also reflected in the corresponding cluster structures, which are reproduced in Figures 7 and 8. The strength of the OH^- - acetonitrile hydrogen bond is reduced, and this is clearly evidenced by the H...O distance increasing with the added ligands from the unusually short value of 1.614 Å in A_{1-1} to 1.812 and 1.841 Å in A_{2-1} and A_{3-1}, respectively. Concurrently, the C-H bond length, which is unusually long in A_{1-1}, exhibits progressively less lengthening in the larger species.

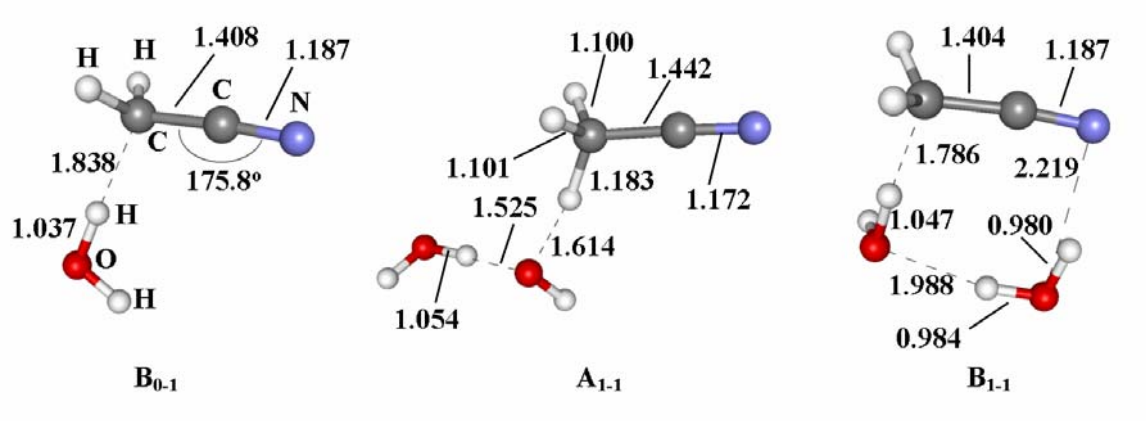

Figure 6. Optimized geometries for the isomers $OH^-CH_3CN(H_2O)_m$ (Structure **A**) and $CH_3CN(H_2O)_{m+1}$ (Structure **B**), for m = 0 and 1. The strong interaction between OH^- and CH_3CN with a short CH…H distance (1.614 Å) suggests a low barrier for the proton transfer from CH_3CN to OH^-.

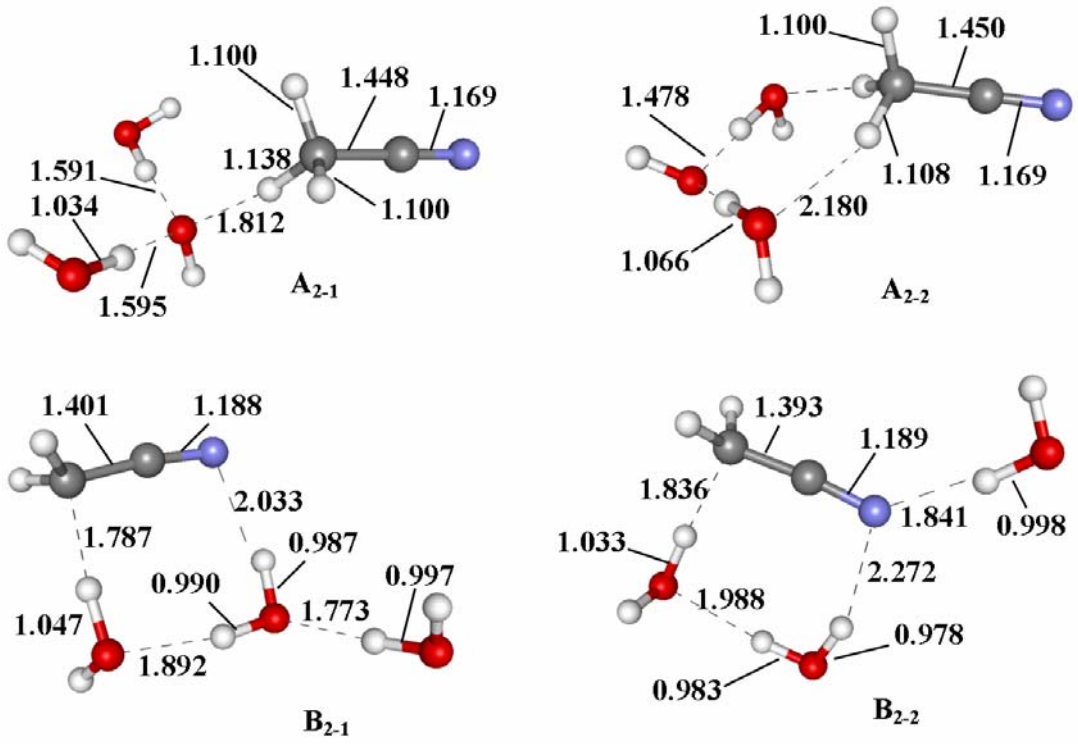

Figure 7. Optimized geometries for the isomers $OH^-CH_3CN(H_2O)_m$ (Structure **A**) and $CH_3CN(H_2O)_{m+1}$ (Structure **B**), for m = 2. Structures $\mathbf{A_{m-2}}$ are characterized by two hydrogen bonds from the methyl group to water molecules, with the OH^- ion moved to a more remote position. $\mathbf{B_{m-2}}$ structures feature two water molecules hydrogen bonded to the nitrile group.

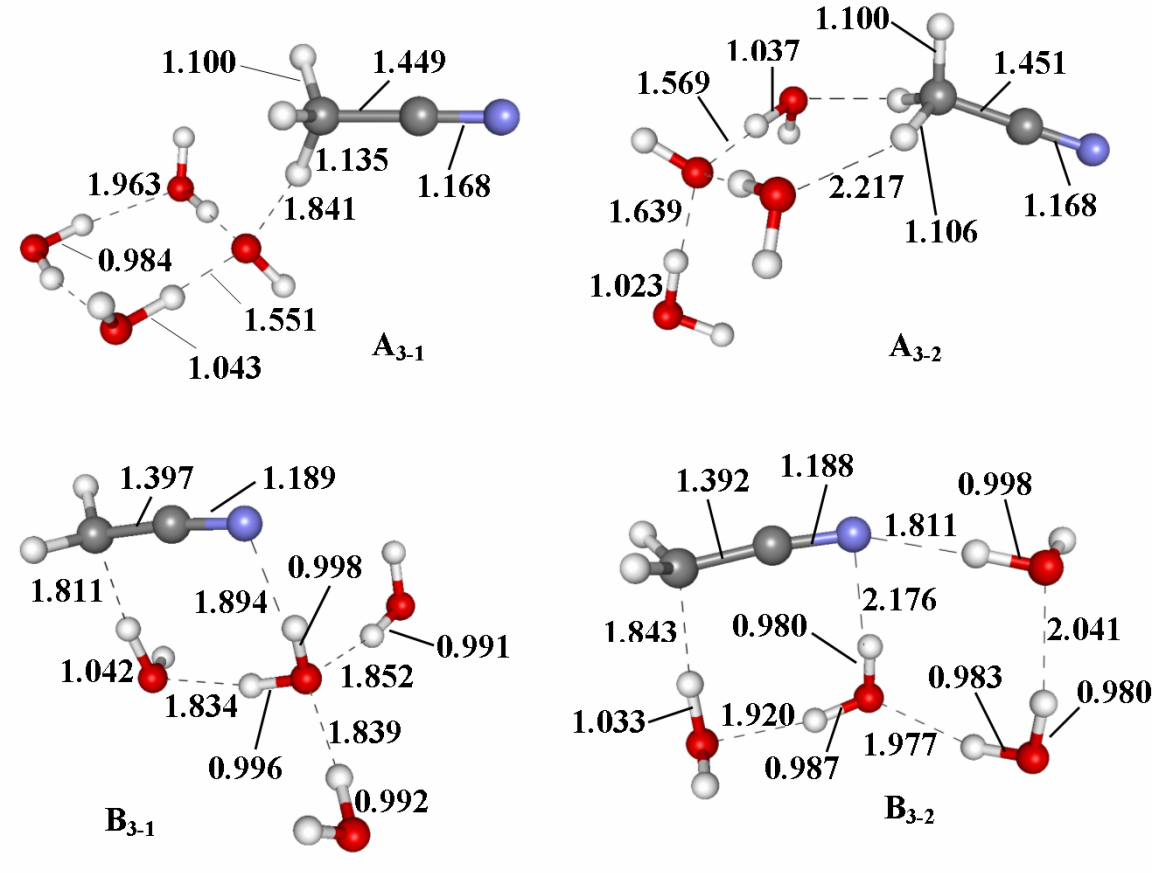

Figure 8. Optimized geometries for the isomers $OH^-CH_3CN(H_2O)_m$ (Structures **A**) and $CH_3CN(H_2O)_{m+1}$ (Structures **B**), for m = 3. The lower energy structures are here $\mathbf{A_{3\text{-}2}}$ and $\mathbf{B_{3\text{-}2}}$, the difference albeit being small. However, in $\mathbf{A_{3\text{-}2}}$ the OH^- does not directly attack the methyl group, and at the same time, no H/D-exchange is observed for the m = 3 clusters.

Clearly, the lengthened hydrogen bond, and shortened C-H bond will make proton transfer and isotopic exchange in the larger clusters much less favorable. The increased stability of the hydroxide anion is also reflected by a higher negative charge remaining on the $OH^-(H_2O)_m$ cluster, and correspondingly less transfer onto the acetonitrile molecule (Table 1). Obviously, with increasing number of water ligands, more local minima and isomers become possible, and this is exemplified in the Table and Figures by the structures $A_{2\text{-}2}$, $B_{2\text{-}2}$, $A_{3\text{-}2}$ and $B_{3\text{-}2}$.

The increasing stabilization of the OH^- anion also has the consequence, that with the number of water ligands the alternative, proton transferred structures become energetically less favorable, as may clearly be seen in Table 2. While the m = 1 species are close to

Table 2. Relative energy (kJ/mol) of $OH^-(CH_3CN)(H_2O)_m$ (Structure **A**) and $(CH_2CN^-)(H_2O)_{m+1}$ (Structure **B**). Dissociation energy (kJ/mol) of the most stable isomer for each size and natural population analysis (atomic unit) of selected fragments. The energies are evaluated by the BPW91/6-311++G** method with zero point energy correction.

$OH^-(CH_3CN)(H_2O)_m$ structure **(A)**		Relative Energy	Dissociation Energy		Natural Population Analysis				
$(CH_3CN)(H_2O)_{m+1}$ structure **(B)**			**$-CH_3CN$**	**$-H_2O$**	**CH_3CN**	**$OH^-(H_2O)_m$**	**OH^-**	**CH_2CN^-**	**$(H_2O)_{m+1}$**
m = 0	B_{0-1}	0.0						-0.88	-0.12
m = 1	A_{1-1}	0.0	72.6	53.9	-0.13	-0.87	-0.75		
	B_{1-1}	8.4						-0.85	-0.15
m = 2	A_{2-1}	0.0	58.1	64.2	-0.07	-0.93	-0.75		
	A_{2-2}	3.1			-0.04	-0.96	-0.73		
	B_{2-1}	31.0						-0.84	-0.16
	B_{2-2}	31.2						-0.83	-0.17
m = 3	A_{3-1}	6.0			-0.06	-0.94	-0.73		
	A_{3-2}	0.0	48.4	54.1	-0.03	-0.97	-0.73		
	B_{3-1}	51.2						-0.83	-0.17
	B_{3-2}	47.0						-0.83	-0.17

isoenergetic, with B_{1-1} being computed only 8.4 kJ/mol above A_{1-1}, the difference increases steeply to around 30 kJ/mol for m = 2, and almost 50 kJ/mol for m = 3. The computed isomers are still close enough in energy to be thermally accessible on the timescale of the ICR experiment, at least for m = 2 and 3. The H/D-exchange process is, however, observed only for m = 2. Actually, no clusters with only two ligands, that is either $OH^-(H_2O)_2$ or $OH^-(CH_3CN)(H_2O)$ are detected in our experiments. This is consistent with the relatively high 58.1 kJ/mol and 64.2 kJ/mol computed dissociation energies of the $OH^-(CH_3CN)(H_2O)_2$ cluster to lose CH_3CN and H_2O, respectively (see Table 2). For the next larger cluster,

$OH^-(CH_3CN)(H_2O)_3$, the dissociation energies to generate $OH^-(H_2O)_3$ and $OH^-(CH_3CN)(H_2O)_2$ are 48.4 kJ/mol and 54.1 kJ/mol respectively. This is thus approximately the maximum amount of energy a cluster anion of this size can absorb in the ICR chamber without falling apart. This energy is considerably higher than the about 30 kJ/mol difference between $OH^-(CH_3CN)(H_2O)_m$ and $(CH_2CN^-)(H_2O)_{m+1}$ for m = 2, the cluster size for which we observe the efficient H/D exchange process. However, already for m = 3 the energy difference between $OH^-(CH_3CN)(H_2O)_m$ and $(CH_2CN^-)(H_2O)_{m+1}$ is comparable to the energy required for cluster dissociation. As a consequence, for larger clusters such irreversible dissociation process should become dominant, and accordingly, essentially no H/D exchange process is detected for m > 2.

Figure 9 illustrates the potential energy surface of the relevant species, comparing ligand loss with isotopic scrambling. While for m = 2, the barrier for interconversion between A_{2-1} and B_{2-1} is readily overcome before ligand loss can occur, the situation is reversed for

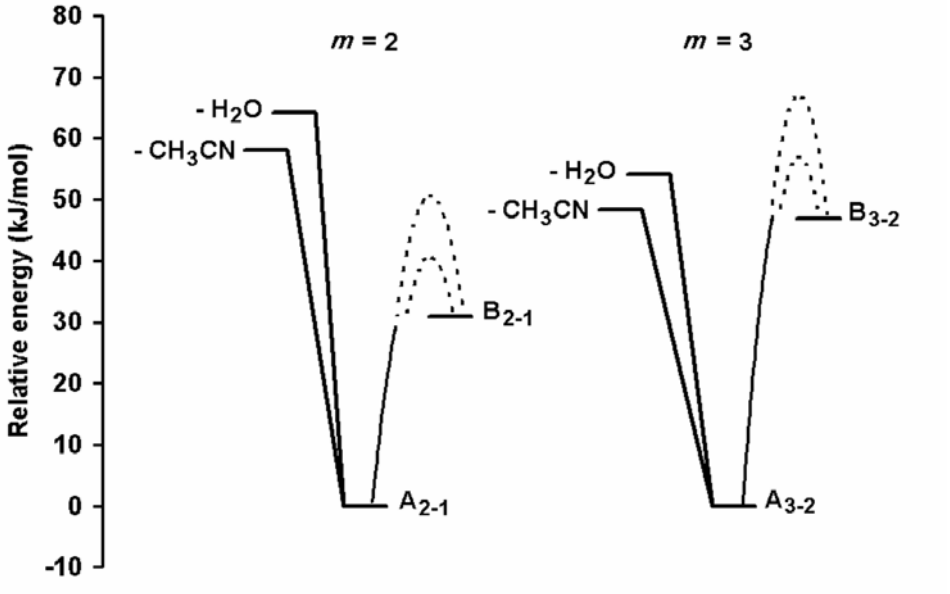

Figure 9. Potential energy surface of the H/D-exchange reaction for m = 2 and m = 3. For H/D-exchange to occur, an isomer of type **A** has to be converted to **B** and back. For m = 3, loss of the CH_3CN or H_2O is energetically more favorable than conversion from $\mathbf{A_{3-2}}$ to $\mathbf{B_{3-2}}$, while for m = 2, the situation is reversed. Consequently, H/D-exchange is only observed for m = 2.

m = 3.

Although we have not located the – probably multiple – transition states of this interconversion reaction, we can assume barriers of 10 – 20 kJ/mol for the rearrangement of hydrogen bonds in water clusters. The strength of one hydrogen bond of 20 kJ/mol[39] poses a conservative upper limit to the barrier, while a concerted mechanism can probably work with half this value. Since the isomerization from B_{m-1} to A_{m-1} starts with the rearrangement of one hydrogen bond, the ranges shown in the picture for the barriers are believed to be quantitative. The calculations consistently explain why isotopic scrambling is only observed for m = 2.

5.4 Conclusions

Hydrated electrons $(H_2O)_n^-$ are in collisions with acetonitrile and acetonitrile-d3 efficiently converted to hydrated hydroxide, $OH^-(H_2O)_m$ clusters, without isotopic scrambling. As the large clusters fragment and lose ligands, they become increasingly basic, so that when about m = 10-12 is reached, they are able take up an acetonitrile molecule. The fragmentation process continues with a parallel loss of acetonitrile-d3 and water and uptake of acetonitrile-d3 by ligand exchange, until $OH^-(CD_3CN)(H_2O)_2$ are formed. These species exhibit an interesting H/D isotopic exchange reaction, in which they are progressively deuterated in collisions with gaseous CD_3CN. This deuteration is due to repeated proton transfers and isomerizations within the $OH^-(CD_3CN)(H_2O)_2$ cluster, followed by ligand exchange, in which a partially deuterated $CD_{3-k}H_kCN$ is replaced by CD_3CN. This reaction proceeds until all the H atoms are replaced by deuterium, forming the final product $OD^-(CD_3CN)(D_2O)_2$. The feasibility of the proposed mechanisms of H/D-exchange was verified by detailed quantum chemical calculations of the structures and energetics of the clusters involved. To find further support for the role of OH^- and of the basicity of the

clusters, similar experiments were carried out with fully deuterated acetaldehyde. This is efficiently taken up by the cluster in the first reaction step, without formation of a hydroxide anion. Consequently, no trace of H/D-exchange is observed throughout the reaction. Density functional calculations map stationary points on the potential energy surface of the H/D-exchange reaction. The calculated energetics explain why H/D-exchange occurs only in the smallest cluster observed.

5.5 References

[1] G. V. Buxton, C. L. Greenstock, W. P. Helman, and A. B. Ross, *J. Phys. Chem. Ref. Data* **1988**, *17*, 513.

[2] N. C. Verma, and R. W. Fessenden, *J. Chem. Phys.* **1976**, *65*, 2139.

[3] V. E. Bondybey, and M. K. Beyer, *Int. Rev. Phys. Chem.* **2002**, *21*, 277.

[4] B. S. Fox, O. P. Balaj, I. Balteanu, M. K. Beyer and V. E. Bondybey, *Chem. Eur. J.* **2002**, *8*, 5534.

[5] L. Bass, T. Su, W. J. Chesnavich, and M. T. Bowers, *Chem. Phys. Lett.* **1975**, *34*, 119.

[6] L. Bass, T. Su, and M. T. Bowers, *Int. J. Mass Spectrom. Ion Processes* **1978**, *28*, 389.

[7] T. Su, M. and T. Bowers, *J. Chem. Phys.* **1973**, *58*, 3027.

[8] M. K. Beyer, C. B. Berg, and V. E Bondybey, *Phys. Chem. Chem. Phys.* **2001**, *3*, 1840.

[9] M. J. Frisch, G. W. Trucks, H. B. Schlegel, G. E. Scuseria, M. A. Robb, J. R Cheeseman, V. G.Zakrzewski, J. A. Montgomery, R. E. Stratmann, J. C. Burant, S. Dapprich, J. M. Millam, A. D. Daniels, K. N. Kudin, M. C. Strain, O. Farkas, J. Tomasi, V. Barone, M. Cossi, R. Cammi, B. Mennucci, C. Pomelli, C. Adamo, S. Clifford, J. Ochterski, G. A. Petersson, P. Y. Ayala, Q. Cui, K. Morokuma, D. K. Malick, A. D. Rabuck, K. Raghavachari, J. B. Foresman, J. Cioslowski, J. V. Ortiz, B. B. Stefanov, G. Liu, A. Liashenko, P. Piskorz, I. Komaromi, R. Gomperts, R. L. Martin, D. J. Fox, T. Keith, M. A. Al-Laham, C. Y. Peng, A. Nanayakkara, C. Gonzalez, M. Challacombe, P. M. W. Gill, B. G. Johnson, W. Chen, M. W. Wong, J. L. Andres, M. Head-Gordon, E. S. Replogle, and J. A. Pople, *Gaussian 98, Revision A.1*; Gaussian, Inc.: Pittsburgh PA, 1998.

[10] A. E. Reed, L. A. Curtiss, and F. Weinhold, *Chemical Reviews* **1988**, *88*, 899.

[11] V. E. Bondybey, and M. K. Beyer, *Int. Rev. Phys. Chem.* **2002**, *21*, 277.

[12] B. S. Wang, H. Hou, and Y. S. Gu, *J. Phys. Chem. A* **2001**, *105*, 156.

[13] A. L. Sobolewski, and W. Domcke, *Phys. Chem. Chem. Phys.* **2003**, *5*, 1130.

[14] I. Draganić, Z. Draganić, L. Petković, and A. Nikolić, *J. Am. Chem. Soc.* **1973**, *95*, 7193.

[15] P. Neta, R. W. Fessenden, and R. H. Schuler, *J. Phys. Chem.* **1971**, *75*, 1654.

[16] T. Tsukuda, M. Saeki, R. Kimura, and T. Nagata, *J. Chem. Phys.* **1999**, *110*, 7846.

[17] M. Saeki, T. Tsukuda, S. Iwata, and T. Nagata, *J. Chem. Phys.* **1999**, *111*, 6333.

[18] J. H. Hendricks, S. A. Lyapustina, H. L. de Clercq, and K. H. Bowen, *J. Chem. Phys.* **1998**, *108*, 8.

[19] C. G. Bailey, C. E. H. Dessent, and M. A. Johnson, *J. Chem. Phys.* **1996**, *104*, 6976.

[20] M. Gutowski, K. D. Jordan, and P. Skurski, *J. Phys. Chem. A* **1998**, *102*, 2624.

[21] I. A. Shkrob, and M. C. Sauer Jr., *J. Phys. Chem. A* **2002**, *106*, 9120.

[22] I. A. Shkrob, K. Takeda, and F. Williams, *J. Phys. Chem. A* **2002**, *106*, 9132.

[23] C.-G. Xia, J. Peon, and B. Kohler, *J. Chem. Phys.* **2002**, *117*, 8855.

[24] S. Campbell, M. T. Rodgers, E. M. Marzluff, and J. L Beauchamp,. *J. Am. Chem. Soc.* **1994**, *116*, 9765.

[25] C. J. Cassady, and S. R.Carr, *J. Mass Spectrom.* **1996**, *31*, 247.

[26] X. H. Cheng, and C. Fenselau, *Int. J. Mass Spectrom. Ion Processes* **1992**, *122*, 109.

[27] M. A. Freitas, and A. G.Marshall, *Int. J. Mass Spectrom.* **1999**, *183*, 221.

[28] M. K. Green, and C. B. Lebrilla, *Mass Spectrom. Rev.* **1997**, *16*, 53.

[29] E. H. Gur, L. J. Dekoning, and N. M. M. Nibbering, *J. Am. Soc. Mass Spectrom.* **1995**, *6*, 466.

[30] G. Koster, and C. Lifshitz, *Int. J. Mass Spectrom.* **1999**, *183*, 213.

[31] D. Suckau, Y. Shi, S. C. Beu, M. W. Senko, J. P. Quinn, F. M. Wampler, and F. W. McLafferty, *Proc. Natl. Acad. Sci. U. S. A.* **1993**, *90*, 790.

[32] B. E. Winger, K. J. Lightwahl, A. L. Rockwood, and R. D. Smith, *J. Am. Chem. Soc.* **1992**, *114*, 5897.

[33] T. Wyttenbach, B. Paizs, P. Barran, L. Breci, D. F. Liu, S. Suhai, V. H. Wysocki, and M. T. Bowers, *J. Am. Chem. Soc.* **2003**, *125*, 13768.

[34] C. H. DePuy, *Int. J. Mass Spectrom.* **2000**, *200*, 79.

[35] J. H. Stewart, R. H. Shapiro, C. H. Depuy, and V. M.Bierbaum, *J. Am. Chem. Soc.* **1977**, *99*, 7650.

[36] U. Achatz, S. Joos, C. Berg, T. Schindler, M. Beyer, G. Albert, and G. Niedner-Schatteburg, V. E. Bondybey, *J. Am. Chem. Soc.* **1998**, *120*, 1876.

[37] L. A. Posey, M. J. DeLuca, P. J. Campagnola, and M. A. Johnson, *J. Phys. Chem.* **1989**, *93*, 1178.

[38] S. T. Arnold, R. A. Morris, A. A. Viggiano, and M. A. Johnson, *J. Phys. Chem.* **1996**, *100*, 2900.

[39] J. S. Kim, J. Y. Lee, S. Lee, B. J. Mhin, and K. S. Kim, *J. Chem. Phys.* **1995**, *102*, 310.

6. Reactions of Hydrated Electrons with Hydrogen Chloride: Formation of Atomic Hydrogen

6.1 Introduction

Electrons are present in all chemical reactions, no matter when or where they are taking place. In redox reactions an electron is transferred from one atom or molecule to another, from solute to the solvent, from a catalyst surface to a reactant, or from a reactant to a catalyst surface. Even in mono-molecular reactions and isomerizations, electrons are transferred from one bond to another, an electron undergoes a transition from one molecular orbital to another. During chemical reactions charges move, separate and recombine, always involving the movement of electrons. An electron can therefore be viewed as the simplest, most elementary, prototypic chemical reactant.

Most processes essential for terrestrial life proceed in aqueous environment, and water is also the solvent for many technologically and industrially important reactions. This naturally makes the aqueous electron, its existence in solution, and its solvation topics of a particular interest. Solvated electrons have, in fact, been first observed already in the very early days of chemistry, almost two hundred years ago. It took, however, almost a century of research, among others by Weyl,[1] before this early observation by Humphrey Davy of a deep blue color appearing when liquefied NH_3 came in contact with sodium or potassium were correctly interpreted, as being due to electrons solvated by the ammonia.[2]

The fact that similar solvated electrons can also be generated, at least transiently, in water is a much more recent discovery. They can be produced by a variety of methods, and their properties have now become the object of a whole new area of physical chemistry.[3-5] In one type of such experiments, pulsed radiolysis, the liquid samples, mostly aqueous solutions,

are irradiated by intense pulses of energetic electrons, with energies of several MeV. Such radiolysis can, of course, also be done continuously, for instance by generating the energetic electrons in situ by γ-irradiation. Another, more recently introduced alternative is to generate the electrons by multiphoton ionization using short, intense, femtosecond laser pulses.[6] These allow investigations of the dynamics of electron solvation and kinetics of their chemical reactions by monitoring the appearance of their spectrum and of its subsequent decay, as well as the appearance of their reaction products in a variety of pump-probe experiments.

Such reactions of electrons in solution are not only a project of a purely academic interest, but are, in fact, of a considerable practical, technical, and industrial importance. For example, one important field of application lies in the purification of water. The extensive use of polychlorinated biphenyls, chlorinated aliphatic hydrocarbons, and other halogenated compounds represents a major environmental problem. Numerous of these compounds are highly toxic, and they often have a very long lifetime in the environment, but many of them can be very efficiently dechlorinated by means of radiolysis, and by reactions involving hydrated electrons.

In recent decades, it was demonstrated that besides bulk solutions, electrons solvated in small, finite clusters[7-9] can also be prepared in experiments with cold, supersonic beams. Such hydrated, charged clusters can be manipulated by electric or magnetic fields, and eventually stored and investigated in electromagnetic traps.[10]

In the last years we have used a very efficient laser vaporization source[11-14] to produce and study a large variety of hydrated ions.[10,15-22] Also we have succeeded in using the Fourier transform ion cyclotron resonance mass spectrometry technique (FT-ICR MS) to store and mass select the hydrated electron clusters, $(H_2O)_n^-$, and investigate, for instance, their stability, and the competition between their gradual fragmentation and the electron detachment induced by the absorption of infrared black-body radiation.[10]

Such finite clusters can, however, also be a very convenient medium for the studies of chemical reactions. Since the FT-ICR measurement yields unambiguous information about the chemical composition of the cluster, the effects of impurities which always plague experiments in bulk solutions can be completely eliminated. By letting hydrated clusters interact with various gaseous reagents, one or several of its molecules can be dissolved in the cluster, and their reactions investigated in microscopic detail.[15-17,19,21,23-35] In the present chapter, the behavior of the hydrated electron clusters in the presence of hydrogen chloride as reagent is examined.

6.2 Experimental Details

The experiments were performed using a 4.7 Tesla Bruker/Spectrospin CMS47X FT-ICR mass spectrometer equipped with an APEX III Data Station, a Bruker infinity cell, and a homebuilt laser vaporization source described in detail before.[10,12,22,25] Hydrated electrons were generated by laser vaporization of a rotating metal target and supersonic expansion of the hot plasma in a 50 μs gas pulse of helium seeded with water vapor.[10,22,25] The ions are accelerated, guided by electrostatic lenses, transferred through four stages of differential pumping, decelerated and finally trapped in the ICR cell at a background pressure of $3x10^{-10}$ mbar. The product formation is strongly dependent upon the vaporized target. The hydrated electron clusters can be produced by the laser vaporization of a metal target. In most cases, as for instance with Co or Au, also other anionic species are formed, and in particular abundant metal and metal cluster anions. These, however, cannot form, when a metal with closed shell and negative electron affinity is employed. In the present investigation we have used a target made from pressed Zn powder (Aldrich, 99.9%+) which generated an intense, clean, distribution of hydrated electron clusters, $(H_2O)_n^-$, essentially free of other anionic species.[10,25,26]

The reactant, in the present study hydrogen chloride (Aldrich, 99+%), is introduced into the ultra-high vacuum region through an adjustable needle valve, raising the pressure in the analysis cell to the desired value of 6.0×10^{-9} mbar. The mass spectra of the species accumulated in the ICR cell are taken at the end of the trapping cycle, and then after various reaction delays, in order to monitor the progress of the reaction, decay of the pure electron clusters, and the formation of products. As in all our experiments, the vacuum chamber enclosing the ICR cell was kept at a constant temperature of 290 ± 6 K by water flowing through a cooling jacket.

6.3 Results and Discussion

Our cluster source can generate $(H_2O)_n^-$ hydrated electron clusters with n values extending from about 15 to nearly 100. As we have previously shown, the low end limit is due to rapid electron detachment, while at the upper end the distribution is limited by the increasing rates of room temperature black body radiation induced fragmentation.[10] The range in a specific experiment depends on the conditions of the laser vaporization source and the time of flight parameters between the source and the cell, with a typical distribution in one of our experiments being exemplified in Figure 1, where the clusters extend over the range of n = 27 - 67. Similar to our previous studies with many other solvated ions, we find that also the $(H_2O)_n^-$ clusters react very avidly with hydrogen chloride, and allowing enough time, more than one HCl can be taken up by the clusters. There is, however, a conceptual difference between the reaction with the first HCl molecule, and the uptake of the second and following ones.

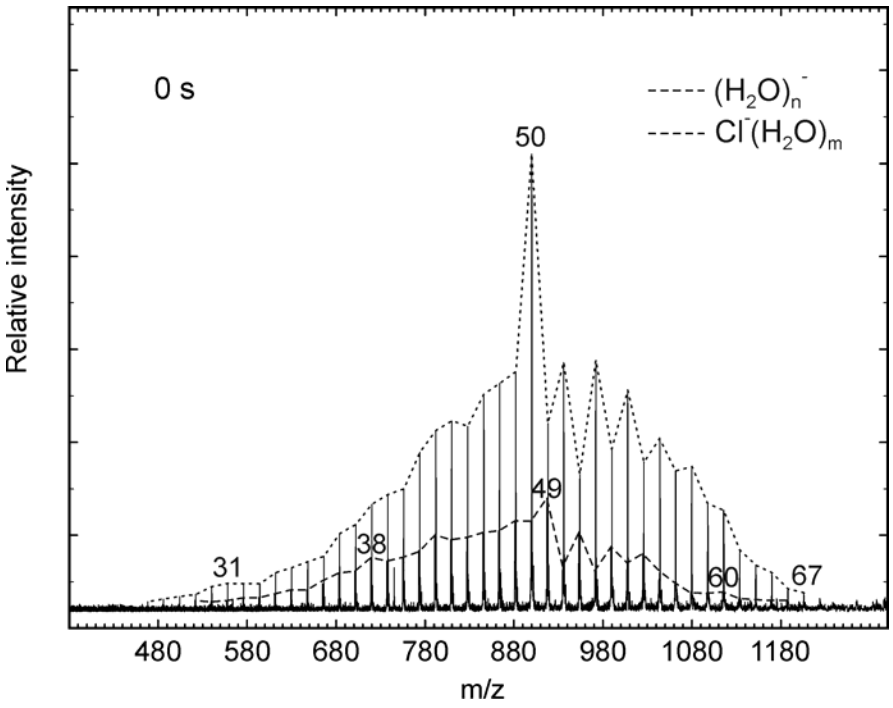

Figure 1. Mass spectra of the reaction of $(H_2O)_n^-$ with HCl. Already at 0 seconds, during the accumulation of the hydrated electrons in the FT-ICR "infinity" cell, the clusters have reacted and the product, $Cl^-(H_2O)_n$, is present.

6.3.1. Reaction with the first HCl molecule, and switch in the ionic cluster core.

In the experiment depicted in Figure 1, the clusters were reacted with a stationary pressure of 6×10^{-9} mbar of hydrogen chloride, with the trace 1a showing the measured distribution at a nominal time t = 0. The clusters produced in the pulsed supersonic expansion are usually accumulated over 20 pulses, and since during this time the reaction can already proceed, even at time zero, some products of the composition $Cl^-(H_2O)_n$ are detected. The interpretation is somewhat complicated by the fact, that the mass of the $H^{35}Cl$ molecule, 36 AMU, is equal to that of two molecules of water, so that in a low resolution spectrum the lines of an $(H_2O)_n^-$ solvated electron would not be clearly separated from that $(HCl)(H_2O)_{n-2}^-$ at the same nominal mass. Fortunately such problems do not arise for the heavier chlorine isotope with about 25% natural abundance, and their presence allows resolving any ambiguities which might otherwise result from bands of reactants and products overlapping.

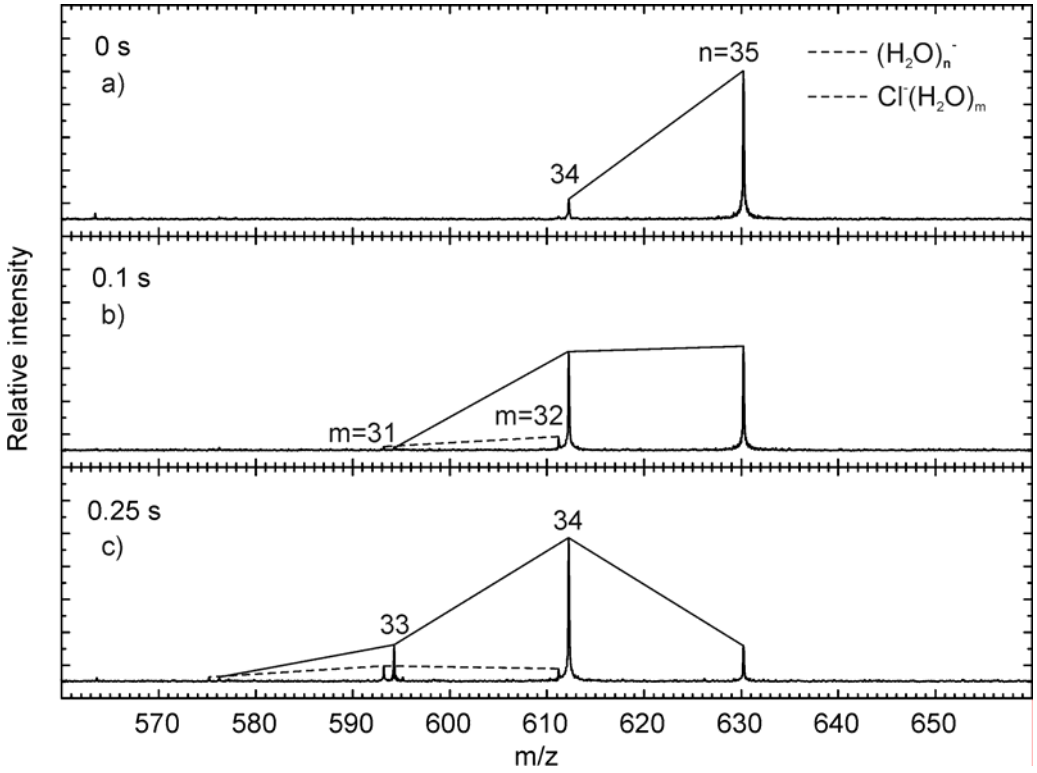

Figure 2. Mass spectra of the reaction of size-selected $(H_2O)_{35}^-$ with HCl after a) 0 s, b) 0.1 and c) 0.25 s reaction delay. The main fraction of the clusters fragment to form $(H_2O)_{34}^-$, but smaller fractions react and form $Cl^-(H_2O)_{32}$.

A typical sequence of spectra demonstrating in more detail the reactions of the solvated electron is shown in Figure 2, in an experiment where only a specific cluster with n = 35, that is $^-(H_2O)_{35}$ at a nominal mass of 630 AMU, was selected. $X^{\pm}(H_2O)_n$ hydrated ion clusters fragment due to absorption of room temperature black body radiation.[18,36-42] The rates of this fragmentation are to a fair approximation independent of the specific nature of the central species X, but are roughly proportional to the number of ligands n.[18,21,28,29,38,43] In the range around n = 35 the rate is of the order of 10 s^{-1}, and this makes it experimentally more difficult to mass select a single peak. Due to this process, there are already some 15% of the n = 34, that is $(H_2O)_{34}^-$ cluster at mass 612 AMU present in Fig. 2a, at a nominal time t = 0.

In the panel 2b showing the spectrum collected after a further 0.1 s reaction time, one can observe a considerable growth of the n = 34 fragmentation product at 612 AMU, with two additional peaks apparently due to a chemical reaction. A stronger peak appears at nominally

611 AMU, one unit lower in mass, and another one, one unit above the n = 34 cluster, at 613 AMU. If the HCl was simply dissolved in the cluster, with three water ligands being vaporized by the heat of the reaction, then a peak due to clusters containing $H^{35}Cl$ should be at a nominal mass of 612 AMU, identical to that of the n = 34 fragmentation product. The corresponding peak due to the $H^{37}Cl$ isotopic molecule is expected at 614 AMU, but none is observed. Absolute mass measurements are consistent with the assignment that the 611 and 613 AMU product species correspond to clusters with an elemental composition of $^{35}Cl^-(H_2O)_{32}$ and $^{37}Cl^-(H_2O)_{32}$, respectively. Since obviously, the $(H_2O)_{34}^-$ reactant must be responsible for the growth of these products, the following reactions are apparently taking place:

$$(H_2O)_{35}^- + h\nu \rightarrow (H_2O)_{34}^- + H_2O \quad (1)$$

$$(H_2O)_{35}^- + HCl \rightarrow (H_2O)_{34}^- + H_2O + HCl \quad (2)$$

$$(H_2O)_{35}^- + HCl \rightarrow Cl(H_2O)_{32}^- + H + 2\,H_2O \quad (3)$$

Here the reaction (1) corresponds to the black body, and reaction (2) to the collisional fragmentation, but from the shown spectrum alone, one can of course not distinguish between the two processes. However, we have previously studied the cluster size dependence of the former process extensively, and a comparison of the rate observed here with the rate measured for a cluster of the same size in the absence of collisions, indicates clearly that reaction (1), due to radiative heating is the dominant process, with the contribution of the collisional reaction (2) being quite small.

In reaction (3), the hydrogen chloride molecule is taken up by the hydrated electron clusters, and besides evaporation of two water ligands, also a hydrogen atom is lost, but the present data do not give information about the exact sequence of events involved in reaction (3). We know from our previous studies of numerous other hydrated ionic clusters, both

cationic and anionic, that hydrogen chloride is ionically dissolved in the clusters,[15,16,28-31,33] and it is natural to assume, that also in the present case, the dissolution and ionization of HCl in the large hydration shell, giving rise to aqueous H^+ and Cl^- ions is the first reaction step. In a subsequent step, the electron then would recombine with the proton, yielding a neutral hydrogen atom which interacts only weakly with the water solvation shell, and evaporates from the cluster on a timescale which cannot be resolved by ICR detection, i.e. less than 1 ms. An alternative course of the reaction would be rapid, direct transfer of the electron to the hydrogen chloride prior to its dissociation on the cluster surface, yielding HCl^-. This unstable anion would then nearly instantly dissociate to yield a chloride anion and a hydrogen atom, which would again evaporate from the surface.

Apparently the entire reaction, i.e. the dissolution of hydrogen chloride followed by reduction of hydrogen, is sufficiently exothermic to evaporate two molecules of water from the cluster, together with a thermochemically unfavorable hydrogen atom. If a reaction analogous to (3) but with the concurrent evaporation of three water molecules is taking place, based on the observed spectra the branching ratio of this process could not be larger than 10% of that of the reaction (3).

In spite of a rather careful search, we have also not been able to detect any products of the composition $(HCl)(H_2O)_n^-$, that is clusters where the HCl was dissolved, without loss of a hydrogen atom. Obviously, the intracluster charge transfer processes, the reduction of the proton, and elimination of atomic hydrogen must be very fast compared with the timescale of the experiment. The reaction products observed in Fig. 2b can react and fragment further, as can be seen in panel 2c, corresponding to a reaction time of 0.25 s. Here only about 25% of the $(H_2O)_{35}^-$ reactant is left, while the n = 34, $(H_2O)_{34}^-$ is now by far the strongest peak, and its consecutive fragmentation products n = 33 and n = 32 are can be seen. Also seen, although weak, are the $^{37}Cl^-(H_2O)_{32}$ chemical reaction redox product and analogous clusters with 31 and even 30 water ligands.

The key reaction apparent in Figs. 1 and 2 involves taking up of a hydrogen chlorine molecule by the cluster, its ionic dissociation followed by a reduction of the proton to yield a hydrogen atom. The hydrogen atom is lost from the cluster, and the entire reaction is accompanied by a switch in the ionic core of the cluster, with the free electron being replaced by a chloride anion, Cl^-.

6.3.2 Subsequent reactions of $Cl^-(H_2O)_n$ with HCl

The Figures 1 and 2 correspond to spectra recorded at very short lifetimes compared with the collisional rates, with most of the observed products there being the result of a single collision. Naturally, given enough time, the primary products can collide with additional molecules of HCl, and further reactions may take place. Examination of products at longer times reveals that such consecutive processes indeed take place, and the water clusters can "dissolve" additional hydrogen chloride, but such subsequent steps are conceptually different from the first one. Even though the additional molecules of HCl might again dissociate ionically to form the H^+ and Cl^- ions, the cluster now no longer contains a free electron, so that no neutralization of the proton and no redox reaction can take place.

Examination of the data indicates that there are limits to the ability of the clusters to take up hydrogen chloride. As the reaction is allowed to run further, the take up of the HCl proceeds concurrently with cluster fragmentation, and the overall distribution of the clusters continuously shifts to smaller sizes and smaller values of n. One finds, however, that after a certain time only the fragmentation takes place, with the clusters no longer being able to take up additional HCl molecules. Such a situation is exemplified in Figure 3, which shows the products after 9 s reaction delay. Examination of the spectrum reveals that each of the original, single peaks corresponding to the specific $(H_2O)_n^-$ clusters is replaced by a multiplet

of several lines. As noted above, chlorine has two isotopes with natural abundances occurring in ratio of about 3:1, and one can therefore from the pattern of each multiplet easily determine the number of chlorine atoms present in each product cluster. Thus for a single chlorine two lines in ratio of 3:1 are expected, two chlorine atoms should give roughly a 9:6:1 triplet, three a 27:27:9:1 quartet, and so on. These isotopic multiplets then provide fingerprints from which the elemental composition of each cluster size can easily be inferred. Calculated exact isotope patterns are shown in the detail of Figure 3 for the various numbers of Cl atoms in the clusters.

If one now examines the spectra with this in mind, an interesting pattern emerges, with clusters of any given size being able to take up a specific, well defined number of HCl molecules. For instance, in the region where in the original mass spectrum solvated electrons with 26-31 water molecules were present, there are now multiplets corresponding to clusters containing seven chlorine atoms. They exhibit a composition of $Cl^-(HCl)_m(H_2O)_n$, with m = 6, and n = 12-15. In other words, in these clusters 2 (m+1) = 14 water ligands seemed to be replaced by m+1 = 7 HCl molecules, of which, however, the first one recombined with the original electron to yield the Cl^- anion and to eliminate a neutral hydrogen atom, as discussed above. Proceeding then further towards lighter ions, one finds that in the range of n = 20-24 the hydrated electrons are now clusters with m = 5 and with 8-12 remaining water molecules, in the range where were originally $(H_2O)_n^-$ with n = 16-18 are now clusters with m = 4 and only 6-8 water ligands. Still towards lower masses one now finds clusters with four hydrogen chloride molecules and three or four water molecules, and finally, clusters with m = 3, and 5-6 water molecules.

Interestingly, these ranges differing by the value of m, that is by the number of HCl molecules, are clearly separated by gaps, where one of the chlorine multiplets is seemingly missing, or almost missing. One can understand this pattern better when one realizes, that the experiment started with a distribution of much larger $(H_2O)_n^-$ clusters, typically ranging from

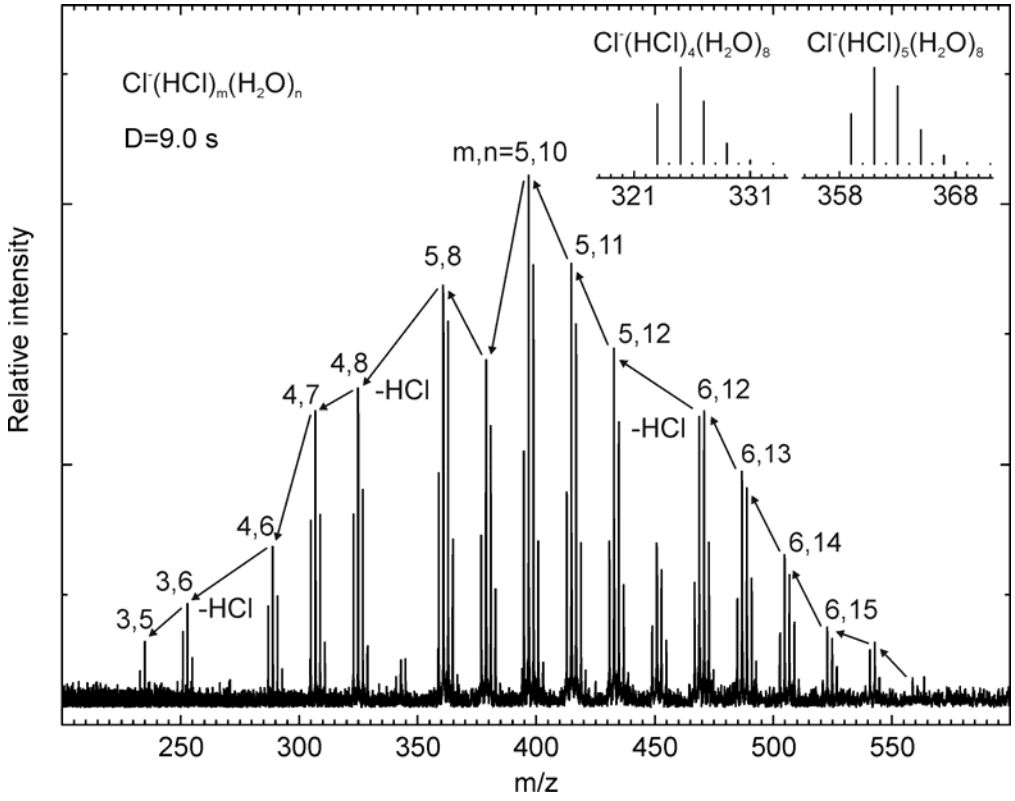

Figure 3. Mass spectrum of the reaction of $(H_2O)_n^-$, n = 28-57, with HCl taken with a reaction delay of 9 seconds. Following the initial core exchange reaction, the clusters saturate with HCl. Collisionally and black-body radiation induces dissociation are the dominant proceses, leading to the evaporation of either water or HCl. Loss of HCl preferentially occurs at n = 12, 8 and 6 water molecules.

n = 30-70. Since the collisional rate is of the order of 1 s^{-1}, after 10 - 30 s, these clusters are essentially "saturated" with the HCl. In the further course of reaction, they just lose ligands, either due to the above mentioned black body radiation, or to collisions. In either case, in the course of such a fragmentation, one can expect that at each stage, the weakest bound remaining ligand is most likely to be lost.

The order in which individual ligands are lost can be nicely followed in the Fig. 3. Starting, for instance from a $Cl^-(HCl)_m(H_2O)_n$ cluster with m = 6 and n = 15, the cluster will be gradually losing water ligands, one by one, each time losing a mass of 18 AMU. When the number of water molecules drops from n = 15 to n = 12, in the $Cl^-(HCl)_6(H_2O)_{12}$ apparently an HCl molecule is weaker bound than the remaining water ligands, and will evaporate from

the cluster, resulting in the loss of 36 AMU, and yielding an m = 5, n = 12 cluster. In this way a gap, or intensity minimum, will appear at a mass which would correspond to the loss of a single water ligand, 18 AMU. This gap is in the region of the original n = 25 $(H_2O)_n^-$ hydrated electron.

The $Cl^-(HCl)_5(H_2O)_{12}$ will then continue to fragment shedding water ligands. In this way, the smaller and smaller clusters alternate between loss of water, and loss of HCl. When only eight water molecules remain that is after the n = 8, m = 5 cluster is reached, again an HCl and a mass of 36 AMU will be lost, forming an m = 4, n = 8 cluster. This creates another gap in the distribution, near the original n = 19 cluster. The resulting $Cl^-(HCl)_4(H_2O)_8$ cluster then loses consecutively two water ligands before another HCl, is lost, forming $Cl^-(HCl)_3(H_2O)_6$, The process visible in the spectrum after 15 s reaction delay is loss of an additional water, followed by the evaporation of another HCl molecule from the cluster. After 20 seconds reaction delay, the most intense group of peaks in the spectrum is due to the presence of only 3 chlorine atoms, corresponding to $Cl^-(HCl)_2(H_2O)_5$. At this point the loss of water takes over and three H_2O molecules are lost one after the other, producing $Cl^-(HCl)_2(H_2O)_4$, $Cl^-(HCl)_2(H_2O)_3$ and $Cl^-(HCl)_2(H_2O)_2$.

Very interesting, after 30 seconds reaction delay, present in the spectrum are clusters containing 3, 4 and even 5 chlorine atoms. Overlapping $Cl^-(HCl)_2(H_2O)_{2\text{-}5}$, but distinct under a closer scrutiny, the $Cl^-(HCl)_3$, $Cl^-(HCl)_3(H_2O)$, $Cl^-(HCl)_4$ and $Cl^-(HCl)_3(H_2O)_3$ patterns are visible. Clearly, the presence of 5 chlorine atoms points to a ligand exchange process, the clusters are giving away water for HCl. Interesting is the fact that, there is no hint of a ligand exchange prior to the $Cl^-(HCl)_2(H_2O)_5$ formation. Predominant are the two groups of peaks at m/z = 143, 145, 147 and 149, indicating the presence of $Cl^-(HCl)_3$ and $Cl^-(HCl)_2(H_2O)_2$ in almost equal abundance. The clusters continue to exchange or fragment the water molecules until none is left.

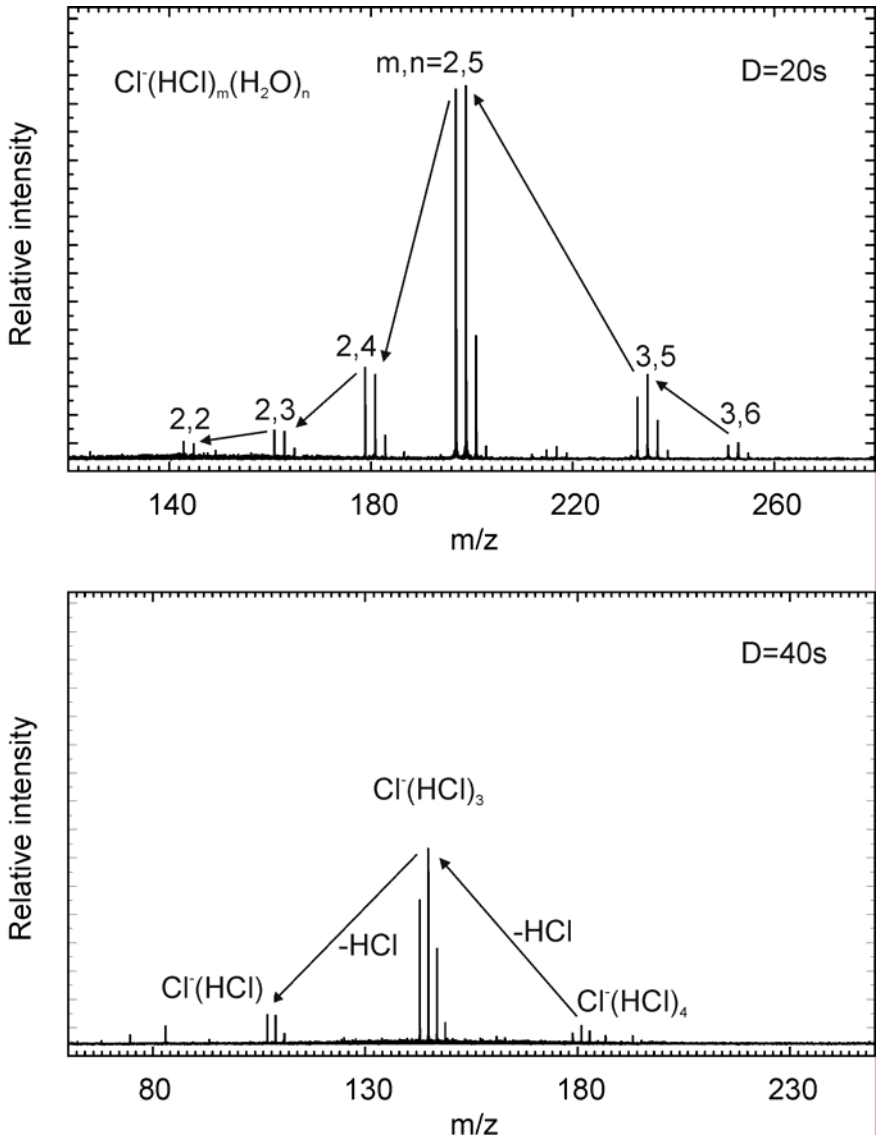

Figure 4. Mass spectra of the final stages of the reaction between hydrated electron clusters and HCl. The last time a HCl molecule is lost from the clusters occurs after 20 seconds reaction delay, forming $Cl^-(HCl)_2(H_2O)_5$. A very slow endothermic ligand exchange at later stages of the reaction, concurrent with fragmentation, will lead to the total loss of water molecules from the clusters. After 40 seconds reaction delay, the most intense peak is due to $Cl^-(HCl)_3$, surrounded by much smaller $Cl^-(HCl)_2$ and $Cl^-(HCl)_4$.

In our ligand exchange study of silver ions solvated with ammonia and water,[17] we have observed a similar behavior, with a very slow, endothermic ligand exchange in the last stage of the reaction. In the present case, a more or less thermoneutral or possibly slightly endothermic exchange of water against HCl may occur, and this is irreversible, since HCl is present in 100% excess as the only reactant.

Finally, after 40 seconds reaction delay, the only patterns present are due to $Cl^-(HCl)_{2,3,4}$. The most intense peaks correspond to the C_{3v} $Cl^-(HCl)_3$ complex ion, as can be seen in the Fig. 4. This then only very reluctantly further fragments losing HCl, to form the m = 2, C_{2v} $Cl^-(HCl)_2$ cluster.

6.3.3 Solubility of HCl in Aqueous Clusters.

In our previous study of reactions of cationic clusters of the type $M^+(H_2O)_n$, where M can be H or a metal like Na,[30,33] with gaseous hydrogen chloride, we have found out that the "solubility" of HCl in such clusters is finite, and that, for instance, clusters with $n \leq 10$ only fragment, but do not take up HCl at all. We have interpreted that in terms of ionic solubility - the cluster can only take up the acid, if there is enough solvent to solvate and stabilize the H^+ and Cl^- ions.[15,30,33] The saturation "concentration" of HCl in the present case of negative ions are, however, much higher than in the case of the cationic clusters, and even clusters much smaller than n = 10 clearly contain HCl. Obviously, one can hardly argue that, for instance, four HCl molecules are ionically dissolved in the above mentioned $Cl^-(HCl)_4(H_2O)_4$ cluster, and that four water molecule are sufficient to solvate and stabilize five chloride anions as well as four protons. Apparently, here the interpretation has to be sought elsewhere.

The difference clearly lies in the specific nature of the central ion. Protons, as well as most metal cations, have a high affinity for polar solvents. In the gas phase they surround themselves with a very stable, tight hydration shell, and also in solution they are known to be strongly stabilized by polar solvent. Specifically water has a rather high proton affinity of 7.2 eV, and will form with a proton a very stable, C_{3v}, symmetric H_3O^+ hydronium ion, where the positive charge is distributed upon the three hydrogen atoms. Furthermore, water forms extended, hydrogen bonded networks, where the individual H_2O molecules are bound on the average to four others, via two donor and two acceptor hydrogen bonds. The covalent

hydrogen chloride molecule, on the other hand, contains only a single proton, and does not fit well into such a three-dimensional water network. It will dissolve exothermically in water – or in the aqueous shell of a hydrated ion – only if enough water molecules are available to allow its ionic dissociation, and solvation of the two newly formed ions, H^+ and Cl^-

The situation is considerably different in anionic clusters, such as solvated electron, iodide or chloride. The charge in these species is quite diffuse, and they are only reluctantly solvated by water. There was, in fact, a considerable amount of discussion regarding these hydrated anions in molecular beams, and whether they are solvated in the interior of the clusters, or just attached to their surfaces.[20,44-54] The consensus seems to be, that quite a large number of water molecules is needed for the anion to be solvated internally. On the other hand, the halide anions interact very strongly with additional molecules of a hydrogen halide, and in fact the bihalide anions, such as the linear, centrosymmetric HCl_2^-, are characterized by one of the strongest hydrogen bonds known. The energetically favored outcome of the interaction of a $Cl^-(H_2O)_n$ cluster with an HCl molecule will not necessarily be a cluster with three independently solvated ions, H^+ proton and two Cl^- anions, but a solvated bichloride anion, $HCl_2^-(H_2O)_n$. The Cl^- anion does not need to interact with only a single HCl molecule, but forms readily $Cl^-(HCl)_m$ ions, with m = 2, 3, or 4. Density functional computations confirm the existence of rather stable, strongly bound C_{2v} $Cl(HCl)_2^-$, C_{3v} $Cl(HCl)_3^-$, or even tetrahedral $Cl(HCl)_4^-$ anions. Unlike the hydrated cationic cluster, where the hydrogen chloride molecules are ionically dissociated, the anionic clusters are characterized by a stable $Cl(HCl)_n^-$ ionic core, with undissociated HCl ligands, and this is also reflected in the fragmentation pattern of the anionic clusters.

6.4. Conclusions

Hydrated electron clusters $(H_2O)_n^-$, n = 19-45, have been generated by laser vaporization of a Zn target and supersonic expansion of a helium-water mixture, and their reactions with hydrogen chloride analyzed using Fourier transform ion cyclotron resonance (FT-ICR) mass spectrometry. HCl is taken up by the clusters, presumably ionically dissolved. The proton is reduced, through an electron transfer, to atomic hydrogen evaporating from the cluster. This process is accompanied by black-body radiation and collision induced loss of water molecules. The mass spectrometrically observed reaction products are $Cl^-(H_2O)_{n-3}$ clusters, whose further fragmentation and ligand exchange ultimately lead to saturation of the cluster with hydrogen chloride.

6.5. References

[1] W. Weyl, *Poggendorff's Annalen der Physik und Chemie* **1864**, *121*, 601-612.

[2] C. A. Kraus, *J. Am. Chem. Soc.* **1908**, *30*, 1323.

[3] M. Anbar, *Adv. Phys. Org. Chem.* **1969**, *7*, 115.

[4] U. Schindewolf, *Angew. Chem. Int. Edit.* **1968**, *7*, 190.

[5] G. V. Buxton, C. L. Greenstock, W. P. Helman and A. B. Ross, *J. Phys. Chem. Ref. Data* **1988**, *17*, 513-886.

[6] Y. Kimura, J. C. Alfano, P. K. Walhout and P. F. Barbara, *J. Phys. Chem.* **1994**, *98*, 3450-3458.

[7] H. Haberland, C. Ludewigt, H. G. Schindler and D. R. Worsnop, *J. Chem. Phys.* **1984**, *81*, 3742-3744.

[8] H. Haberland, H. Langosch, H. G. Schindler and D. R. Worsnop, *J. Phys. Chem.*, **1984** *88*, 3903-3904.

[9] H. Haberland, H. G. Schindler and D. R. Worsnop, *Ber. Bunsen-Ges. Phys. Chem.* **1984**, *88*, 270-272.

[10] M. K. Beyer, B. S. Fox, B. M. Reinhard and V. E. Bondybey, *J. Chem. Phys.* **2001**, *115*, 9288-9297.

[11] V. E. Bondybey and J. H. English, *J. Chem. Phys.* **1981**, *74*, 6978-6979.

[12] C. Berg, T. Schindler, G. Niedner-Schatteburg and V. E. Bondybey, *J. Chem. Phys.* **1995**, *102*, 4870-4884.

[13] T. G. Dietz, M. A. Duncan, D. E. Powers and R. E. Smalley, *J. Chem. Phys.* **1981**, *74*, 6511-6512.

[14] S. Maruyama, L. R. Anderson and R. E. Smalley, *Rev. Sci. Instrum.* **1990**, *61*, 3686-3693.

[15] V. E. Bondybey and M. K. Beyer, *Int. Rev. Phys. Chem.* **2002**, *21*, 277-306.

[16] B. S. Fox, O. P. Balaj, L. Balteanu, M. K. Beyer and V. E. Bondybey, *Chem. Eur. J.* **2002**, *8*, 5534-5540.

[17] B. S. Fox, M. K. Beyer and V. E. Bondybey, *J. Am. Chem. Soc.* **2002**, *124*, 13613-13623.

[18] B. S. Fox, M. K. Beyer and V. E. Bondybey, *J. Phys. Chem. A* **2001**, *105*, 6386-6392.

[19] U. Achatz, B. S. Fox, M. K. Beyer and V. E. Bondybey, *J. Am. Chem. Soc.* **2001**, *123*, 6151-6156.

[20] U. Achatz, S. Joos, C. Berg, M. Beyer, G. Niedner-Schatteburg and V. E. Bondybey, *Chem. Phys. Lett.* **1998**, *291*, 459-464.

[21] C. Berg, U. Achatz, M. Beyer, S. Joos, G. Albert, T. Schindler, G. Niedner-Schatteburg and V. E. Bondybey, *Int. J. Mass Spectrom.* **1997**, *167/168*, 723-734.

[22] M. Beyer, C. Berg, H. W. Görlitzer, T. Schindler, U. Achatz, G. Albert, G. Niedner-Schatteburg and V. E. Bondybey, *J. Am. Chem. Soc.* **1996**, *118*, 7386-7389.

[23] U. Achatz, S. Joos, C. Berg, T. Schindler, M. Beyer, G. Albert, G. Niedner-Schatteburg and V. E. Bondybey, *J. Am. Chem. Soc.* **1998**, *120*, 1876-1882.

[24] O. P. Balaj, E. P. F. Lee, I. Balteanu, B. S. Fox, M. K. Beyer, J. M. Dyke and V. E. Bondybey, *Int. J. Mass Spectrom.* **2002**, *220*, 331-341.

[25] O. P. Balaj, I. Balteanu, B. S. Fox-Beyer, M. K. Beyer and V. E. Bondybey, *Angew. Chem. Int. Edit.* **2003**, *42*, 5516-5518.

[26] O. P. Balaj, C.-K. Siu, I. Balteanu, M. K. Beyer and V. E. Bondybey, *Chem. Eur. J.* **2004**, *10*, 4822-4830.

[27] O. P. Balaj, C.-K. Siu, I. Balteanu, B. S. Fox-Beyer, M. K. Beyer and V. E. Bondybey, *J. Phys. Chem. A* **2004**, *108*, 7506-7512.

[28] C. Berg, M. Beyer, U. Achatz, S. Joos, G. Niedner-Schatteburg and V. E. Bondybey, *Chem. Phys.* **1998**, *239*, 379-392.

[29] M. Beyer, U. Achatz, C. Berg, S. Joos, G. Niedner-Schatteburg and V. E. Bondybey, *J. Phys. Chem. A* **1999**, *103*, 671-678.

[30] B. S. Fox, M. K. Beyer, U. Achatz, S. Joos, G. Niedner-Schatteburg and V. E. Bondybey, *J. Phys. Chem. A* **2000**, *104*, 1147-1151.

[31] B. S. Fox, O. P. Balaj, I. Balteanu, M. K. Beyer and V. E. Bondybey, *J. Am. Chem. Soc.* **2002**, *124*, 172-173.

[32] V. E. Bondybey, M. Beyer, U. Achatz, S. Joos and G. Niedner-Schatteburg, *Isr. J. Chem.* **1999**, *39*, 213-219.

[33] T. Schindler, C. Berg, G. Niedner-Schatteburg and V. E. Bondybey, *Chem. Phys. Lett.* **1994**, *229*, 57-64.

[34] T. Schindler, C. Berg, G. Niedner-Schatteburg and V. E. Bondybey, *J. Phys. Chem.* **1995**, *99*, 12434-12443.

[35] T. Schindler, C. Berg, G. Niedner-Schatteburg and V. E. Bondybey, *Chem. Phys.* **1995**, *201*, 491-496.

[36] R. C. Dunbar, *J. Phys. Chem.* **1994**, *98*, 8705-8712.

[37] R. C. Dunbar and T. B. McMahon, *Science* **1998**, *279*, 194-197.

[38] T. Schindler, C. Berg, G. Niedner-Schatteburg and V. E. Bondybey, *Chem. Phys. Lett.* **1996**, *250*, 301-308.

[39] P. D. Schnier, W. D. Price, R. A. Jockusch and E. R. Williams, *J. Am. Chem. Soc.* ***1996***, *118*, 7178-7189.

[40] M. Sena and J. M. Riveros, *Rapid Commun. Mass Spectrom.* **1994**, *8*, 1031-1034.

[41] D. Thölmann, D. S. Tonner and T. B. McMahon, *J. Phys. Chem.* **1994**, *98*, 2002-2004.

[42] P. Weis, O. Hampe, S. Gilb and M. M. Kappes, *Chem. Phys. Lett.* **2000**, *321*, 426-432.

[43] B. S. Fox, I. Balteanu, O. P. Balaj, H. C. Liu, M. K. Beyer and V. E. Bondybey, *Phys. Chem. Chem. Phys.* **2002**, *4*, 2224-2228.

[44] J. V. Coe, *Int. Rev. Phys. Chem.* **2001**, *20*, 33-58.

[45] J. V. Coe, *J. Phys. Chem. A* **1997**, *101*, 2055-2063.

[46] M. S. Johnson, K. T. Kuwata, C. K. Wong and M. Okumura, *Chem. Phys. Lett.* **1996**, *260*, 551-557.

[47] G. Markovich, S. Pollack, R. Giniger and O. Cheshnovsky, *J. Chem. Phys.* **1994**, *101*, 9344-9353.

[48] J. V. Coe, *Chem. Phys. Lett.* **1994**, *229*, 161-168.

[49] J. E. Combariza, N. R. Kestner and J. Jortner, *Chem. Phys. Lett.* **1994**, *221*, 156-160.

[50] J. E. Combariza, N. R. Kestner and J. Jortner, *J. Chem. Phys.* **1994**, *100*, 2851-2864.

[51] L. Perera and M. L. Berkowitz, *J. Chem. Phys.* **1994**, *100*, 3085-3093.

[52] G. Markovich, S. Pollack, R. Giniger and O. Cheshnovsky, *Zeitschrift Fur Physik D-Atoms Molecules and Clusters* **1993**, *26*, 98-100.

[53] J. E. Combariza, N. R. Kestner and J. Jortner, *Chem. Phys. Lett.* **1993**, *203*, 423-428.

[54] G. Markovich, R. Giniger, M. Levin and O. Cheshnovsky, *J. Chem. Phys.* **1991**, *95*, 9416-9419.

7. Reactions of hydrated aluminum ions with methanol and formic acid

7.1 Introduction

In the course of the last few years we have used an efficient cluster source developed in our laboratory to study the behavior of a large variety of hydrated ions.[1-9] The source can generate both anions and cations solvated with up to over one hundred water molecules or other ligands, which can be transferred into and stored under ultra-high vacuum in an electromagnetic FT-ICR trap. The stored clusters gradually fragment due to absorption of the infrared background radiation[1,9,10-12] and collisions, if a reaction gas is present.[1-3] Investigations of hydrated aluminum cations, $Al(H_2O)_n^+$ have revealed, in addition to fragmentation, also an interesting, exothermic intracluster reaction, in which the aluminium is oxidized yielding an Al^{3+} hydroxide and simultaneously reducing water, with molecular H_2 being released, and water molecules evaporating from the cluster. Interestingly, the reaction only proceeded over a limited size range, in clusters with 11 to 25 water ligands:

$$Al^+(H_2O)_n \rightarrow Al(OH)_2^+(H_2O)_{n-m-2} + H_2 + m\ H_2O,\ 11 \leq n \leq 25,\ m = 2, 3.$$

It should be emphasized, that the hydrated Al^+ clusters are formed in the source, with the reaction taking place hundreds of milliseconds later, in the high vacuum, collision-free environment of the FT-ICR instrument, activated simply by the 300 K background infrared radiation. We have proposed two possible mechanisms for this reaction, an insertion of the aluminum into an O-H bond, and a concerted proton transfer.[1]

Similar hydrogen elimination processes in metal-solvent clusters have now also been observed in molecular beam experiments in a number of different circumstances. In one of

these experiments, H_2 is formed when water clusters containing at least three sodium atoms are ionized.[13-15] Formation of $Mg(OH)^+(H_2O)_n$ hydroxide was observed in collisions of the monovalent alkaline earth metal ions, Mg^+ (or Ca^+) with neutral water clusters.[16-20] Similar hydrogen loss was observed with methanol[21-24], and ethanol[25], as recently reviewed by Fuke et al.[26], and in some cases, even methyl radicals are formed, as in Mg^+ solvated with dimethyl ether[27] and Sr^+ with methanol[21]. Also small hydrated aluminum ions have been previously studied both experimentally[28] and by theory[29], but no intracluster reactions were reported.

To clarify the mechanism of the intracluster reaction, we have carried out additional experiments, "dissolving" gaseous hydrogen chloride in the hydrated clusters. As soon as a molecule of hydrogen chloride is taken up by the cluster, the intracluster reduction-oxidation reaction and formation of molecular hydrogen proceeds, and the upper size limit disappears:

$$Al^+(H_2O)_n + HCl \rightarrow Al(OH)Cl^+(H_2O)_p + H_2 + q\ H_2O\ ,\ 11 \leq n,\ p+q = n-1 \qquad (1)$$

The lower size limit, n = 11 is, on the other hand, retained. It was shown previously that the hydrogen chloride dissolves in the cluster ionically[30-37], with at least 11 water molecules being needed for the HCl to dissolve, and the hydrated H^+ and Cl^- ions to form. This observation, that the hydrogen formation is promoted by the introduction of a proton into the cluster, provides a strong support for the proton transfer mechanism previously proposed[2] by our group. In a number of theoretical works by several different authors it was recently found that a concerted proton transfers through a water chain can significantly reduce the activation energy of a reaction.[38-43]

The question is to what extent the proton transfer and the hydrogen evolution can be fine-tuned by the introduction of various reactants, such as methanol or formic acid, with acidities intermediate between those of water and hydrogen chloride. The effect of these

reactants on the hydrogen formation reaction could thus give further insight, and support for or against the proton transfer mechanism.

7.2 Experimental and computational details

7.2.1 Experimental procedure

The experiments were performed on a modified FT-ICR mass spectrometer Bruker/Spectroscopin CMS47X[44], equipped with a superconducting 4.7 T magnet and a cylindrical 60 x 60 mm "infinity" cell. The cations were produced by laser vaporization of a rotating target disk made from aluminum (Aldrich, 99+%). The plasma is entrained by a carrier gas pulse, in our case helium seeded with water, supplied by a home-built piezoelectric valve with a 50 μs opening time, and cooled by flowing through a confining channel. Aluminum cations solvated by water are formed in the subsequent adiabatic expansion into vacuum where they are accelerated, and further guided by electrostatic lenses. They are transferred through four stages of differential pumping and finally decelerated and stored in the ICR cell, with a base pressure of ~ 4 x 10^{-10} mbar.

The temperature of the trapped cluster ions is determined by a competition between evaporative cooling and radiative heating by the ambient temperature background radiation.[9,45] To study the cluster chemistry, the reactants, in the present case formic acid (Aldrich 99%) and methanol (Aldrich 99%), were introduced into the ultra high vacuum region through a needle valve to raise the pressure to a desired value, typically 5 x 10^{-8} mbar in the present experiments. Mass spectra were taken at the completion of ion accumulation, and then after different reaction delays to monitor the progress of the reaction.

7.2.2 Theoretical Methods

Ab initio calculations have been carried out on the hydrogen elimination reactions, $Al^+(AH)(BH) \rightarrow AlAB^+ + H_2$, for A, B = OH, CH_3O, and HCOO, using the Gaussian98[46] program. For all the species involved, the geometry was optimised with the MP2 method using the 6-311G(2d,2p) basis set. With the optimised geometry, thermochemical constants were computed using the G2 and the RCCSD(T) methods. The calculations do not take into account the effects of solvation.

In all cases it was intended to evaluate thermodynamic constants at the G2 level, but it was not possible to complete the calculations with this method for $Al(OH)_2^+$, because the HF/6-31G* geometry of this ion was near linear and the MP2(full)/6-31G* geometry optimization did not converge. Because of this, the RCCSD(T)/aug-cc-pVTZ//MP2/6-311++G(2d,2p) relative energies, the MP2/6-311++G(2d,2p) geometries and vibrational frequencies were used for the case A = OH, B = OH to evaluate the reaction thermodynamic constants, instead of the G2 method. The RCCSD(T)/aug-cc-pVTZ//MP2/6-311++G(2d,2p) level is higher than the QCISD/6-311++G(3df,2p) level, which is the target of the composite method, G2. For some of the reactions considered, both the G2 and RCCSD(T)//MP2 levels of calculation were employed to evaluate their thermodynamic constants.

7.3 Results and Discussion

7.3.1 Reactions of $Al^+(H_2O)_n$ with methanol (CH_3OH).

Fig. 1 exemplifies a typical initial distribution of clusters at a nominal time t = 0. Since the reactions and ligand exchange can occur already during the ion accumulation, one

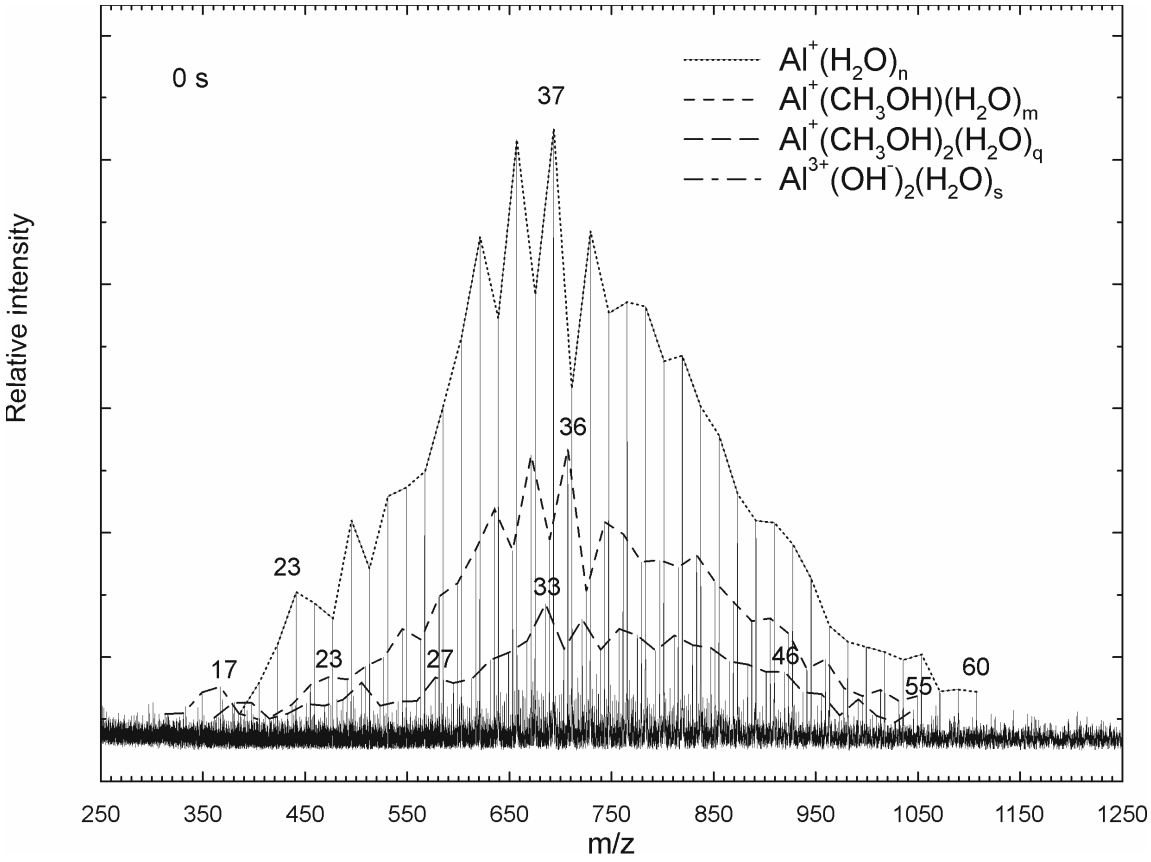

Figure 1. Mass spectrum of the initial cluster distribution $Al^+(H_2O)_n$, n = 20–60, for methanol reactions, with a nominal reaction delay of 0 s, after accumulating the ions for 2 seconds in the ICR-cell. The reactions proceed through ligand exchange. Up to two methanol molecules have already been taken up by the clusters.

observes here not only the hydrated Al^+ ion reactants (connected by the dotted line), but also some primary (dashed line) and even secondary products (longer dashes). The initial distribution here ranges from 20 to about 60 water ligands, with a maximum intensity around n ≈ 37. The reaction proceeds through a basically thermoneutral ligand exchange of water molecules for CH_3OH:

$$Al^+(H_2O)_n(CH_3OH)_m + CH_3OH \rightarrow Al^+(H_2O)_{n-k}(CH_3OH)_{m+1} + k\ H_2O,\ k \approx 1 \qquad (2)$$

Note the oscillations in the initial reactant cluster distribution around the intensity maximum, with the n = 33, 35, 37, and 39 clusters exhibiting appreciably higher intensities than the intervening n = 34, 36, and 38 species. The same pattern appears to be repeated in the primary product distribution, but shifted to higher masses by 14 AMU, the difference between the masses of methanol and water ligands, 32 and18 AMU, respectively, and a hint of the structure is observable even in the secondary exchange product. This suggests that the initial ligand exchange is extremely efficient, and competitive with the cluster fragmentation.

The initial stages of the reaction can be seen more clearly in Figure 2, which shows two sections of the mass spectra at higher resolution, at a nominal delay of 0 s, as well as after 0.7 and 1.5 s. At the right hand side the region of larger $Al^+(H_2O)_n$ clusters, in the range of about n = 35-37 is shown. Already at the nominal t = 0 ligand exchange products containing 1-3 methanol molecules can be seen, due to reactions occurring during the accumulation process. To the left of the peak labeled 0,37, that is cluster with 37 water and 0 methanol ligands, appear peaks shifted by 4 and 8 AMU to lower masses, which correspond to the 1,35 and 2,33 species. The exchange products with m CH_3OH ligands will be shifted 4m AMU to lower mass with respect to the hydrated Al^+ clusters, corresponding to the difference between the mass of two molecules of water, 36 AMU, and that of methanol, 32 AMU. In the two spectra at longer time delays one can observe that the reaction proceeds further, with the distribution maximum shifting to clusters with 2 and 4 methanol ligands after 0.7 and 1.5 s, respectively.

On the left-hand side of the Figure 2, a distribution of smaller clusters, in the range of n = 28-30 is shown. In this case, however, one can see in the 0.7 and 1.5 s panels that major products are not shifted 4m, that is 4, 8, 12 etc. AMU from the pure hydrated Al+ clusters, but 4m+2 AMU, that is 2, 6, 10, … AMU. As previously observed with pure hydrated aluminum ions,[1, 2] the ligand exchange is again accompanied by an intracluster reaction leading to the oxidation of aluminium to Al^{3+} forming aluminum hydroxide, while reducing hydrogen and

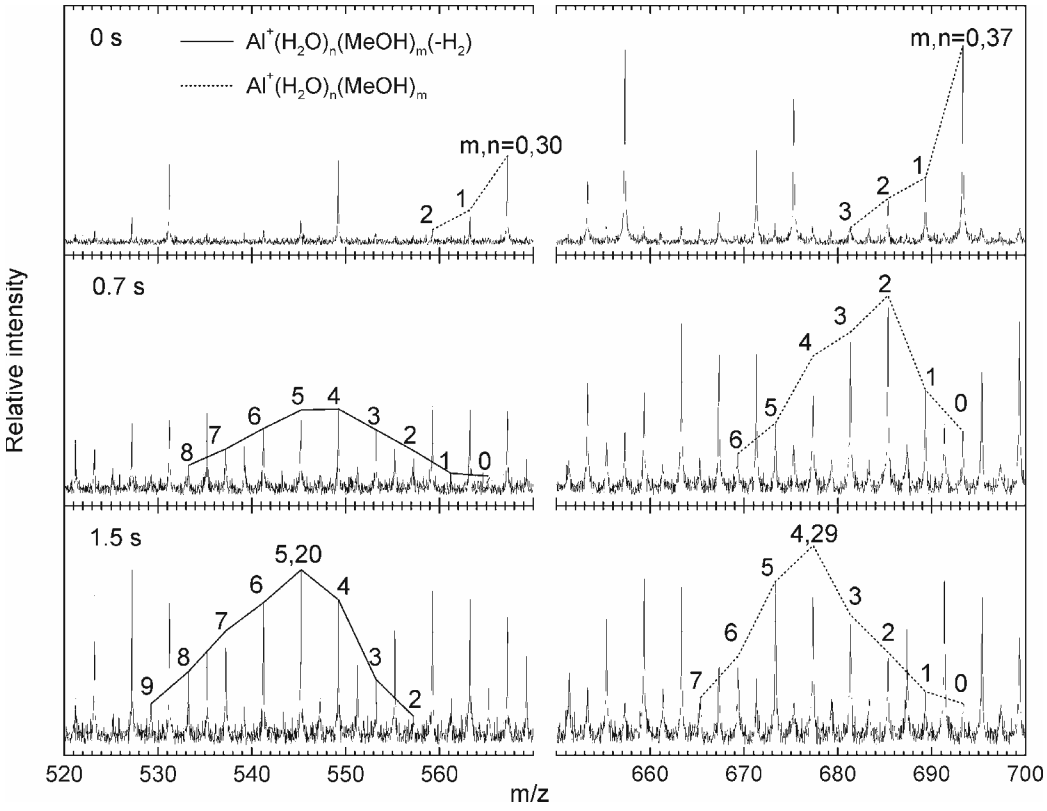

Figure 2: Representative sections of mass spectra illustrating the upper size limit for the intracluster reaction in the ligand exchange reaction with methanol. The peaks are labelled indicating the number of methanol molecules in the corresponding cluster. At 0 s, no hydrogen elimination product is present both on the left and right side. At longer times, exemplified at 0.7 s and 1.5 s, the ligand exchange pattern on the right side corresponding to larger clusters develops in time, while on the left side, displaying clusters containing less than 30 solvent molecules, H_2 elimination shifts the peak group by two mass units. The exact transition between these two regions is blurred, but the existence of an upper size limit around a total of 30 solvent molecules can unambiguously be established.

eliminating molecular H_2:

$$Al^+(H_2O)_n(CH_3OH)_m \rightarrow Al(OH)(CH_3O)^+(H_2O)_{n-p} + H_2 + (p-1)\ H_2O,\ m = 1 \qquad (3)$$

$$Al^+(H_2O)_n(CH_3OH)_m \rightarrow Al(CH_3O)_2{}^+(H_2O)_{n-p}(CH_3OH)_{m-2} + H_2 + p\ H_2O,\ m \geq 2 \qquad (4)$$

Compared to pure the $Al^+(H_2O)_n$ where the reaction does not occur in clusters with $n > 24$, however, the upper limit appears to be shifted to a somewhat higher value of n.

The exchange does not stop at one or two methanol ligands, but continues further, and there seems to be no apparent upper limit for the number of methanol molecules which can be taken up by the cluster. Its rate, however, slows down considerably above $m \approx 5$, while the fragmentation continues. After 5s, the largest clusters are $Al(CH_3O)_2^+(CH_3OH)_{13}(H_2O)_6$. The smallest cluster observed in this experiment which contains only methanol is, after 10 s, $Al(CH_3O)_2^+(CH_3OH)_7$. After 80 s essentially only two "final" cluster products remain, $Al(CH_3O)_2^+(CH_3OH)_2$ and $Al(CH_3O)_2^+(CH_3OH)_3$.

The initial cluster distributions contains, besides the hydrated aluminum clusters, also trace amounts of a whole range of hydrated proton clusters, $H^+(H_2O)_n$. These also exchange water for methanol, and since in the end the entire distribution is converted to a single product cluster, $H^+(CH_3OH)_4$, this becomes clearly observable among the final products.

Since all the major end-products contain Al^{3+} with two methanolate anions, $Al^{3+}(CH_3O^-)_2$, even though in the initial stages of the reaction also $Al(OH)_2^+(H_2O)_n$ ions were produced, clearly also the hydroxides were replaced by methanolate. There is therefore some ambiguity as to the true structure of some of the early products which can be either formulated as $Al(CH_3O)_2^+(H_2O)_{n-p}(CH_3OH)_{m-2}$, as shown in reaction (1), or alternatively as solvated hydroxides, $Al(OH)_2^+(H_2O)_{n-p-2}(CH_3OH)_m$. The total absence of hydroxides among the final products suggests that any hydroxide ions are presumably replaced by methanolate shortly after a methanol molecule enters the cluster, and also our accompanying *ab initio* calculations discussed in section 3.3 seem to favor the methanolate structure.

7.3.2 Reactions of $Al^+(H_2O)_n$ with formic acid.

Figure 3 shows mass spectra of the cluster distribution after 0.3 s and 1 s reaction time with formic acid. The clusters $Al^+(H_2O)_n$, n = 17-57, again exhibit fragmentation and ligand exchange reactions, which are, however, considerably slower than in the case of methanol.

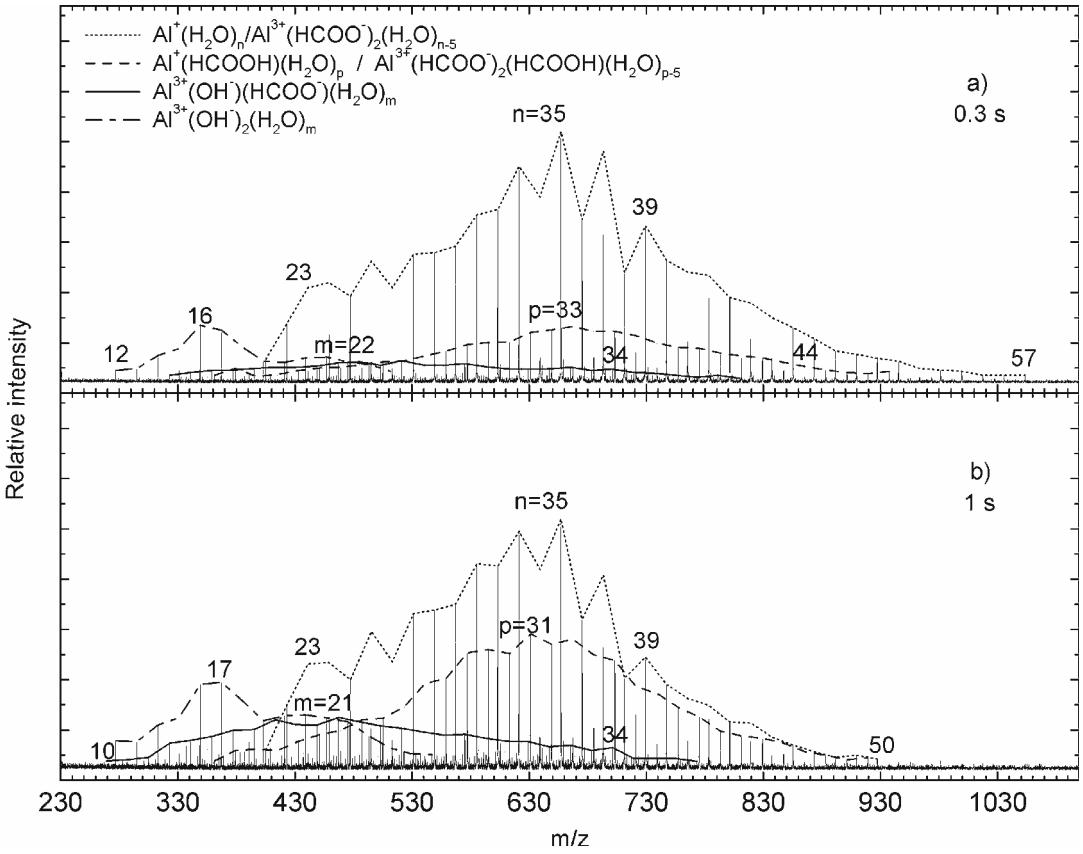

Figure 3: Mass spectrum of the reaction of $Al^+(H_2O)_n$ with HCOOH formic acid after (a) 0.3 s and (b) 1 s. Due to the same nominal mass of $(H_2O)_5$ and $(HCOO)_2$ of 90 AMU, clusters which have taken in two formic acid and eliminated H_2 overlap with the initial cluster distribution, and subsequent exchange products also overlap, as indicated in the figure legend. The compared to methanol slower progress of ligand exchange and the elimination of H_2 without an upper size limit are clearly identified.

The intracluster reaction leading to the formation of molecular hydrogen is again observed, but the data analysis is somewhat complicated by the fact that clusters containing two formic acid molecules after the H_2 elimination, $Al(HCOO)_2^+(H_2O)_{n-5}$, have the same

nominal mass as the initial $Al^+(H_2O)_n$ species. While in principle the mass resolution in FT-ICR should be adequate to distinguish these ions by their mass defect, this is not accomplished in broad-band mode in this mass range due to the limitations of the ASPECT3000 data station.

In spite of this difficulty, one can see clearly from Figure 3 that over the entire cluster size range studied an efficient intracluster aluminum oxidation and molecular hydrogen elimination proceeds:

$$Al^+(H_2O)_n(HCOOH) \rightarrow Al(OH)(HCOO)^+(H_2O)_{n-p} + H_2 + (p-1)\ H_2O,\ m = 1 \qquad (5)$$

At least up to about n = 57 the upper size limit seems to be removed by the presence of formic acid, similar to the case of HCl. Owing to the lower acidity of HCOOH as compared with HCl where the hydrogen elimination took place almost immediately, in the formic acid case the process seems to be at least an order of magnitude slower. One can clearly see in Figure 3 both the ligand exchanged cluster prior to the H_2 elimination, as well as the Al^{3+} acetate-hydroxide product formed by the reduction-oxidation reaction. Apparently the HCOOH must first diffuse, on the time scale of the ICR experiment, through one or two solvent "layers", in order to get in contact with the central aluminum ion, and initiate the reaction.

In further collisions the remaining hydroxide anion can be replaced by $HCOO^-$ with the HCOOH proton recombining with OH^-:

$$Al(OH)(HCOO)^+(H_2O)_n + HCOOH \rightarrow Al(HCOO)_2{}^+(H_2O)_{n-m+1} + m\ H_2O \qquad (6)$$

The lower overall rate of the exchange process is reflected in the smaller number of formic acid molecules taken up by the clusters. After about five seconds the largest number of

formic acid ligands is in an $Al(HCOO)_2^+(HCOOH)_8(H_2O)_3$ cluster, while the smallest cluster containing only formic acid is $Al(HCOO)_2^+(HCOOH)_4$, observed after 10 s.

At the late stages of the reaction, also the formation of formic acid anhydride becomes feasible, leading to the elimination of an additional water molecule. The "final" dominant product remaining after 80 s is an $Al(HCOO)_2^+HCOOH((HCO)_2O)$ ion, which seems to be stable with respect to further fragmentation at room temperature, and which is apparently formed according to the reaction:

$$Al(HCOO)_2^+HCOOH_3 \rightarrow Al(HCOO)_2^+HCOOH((HCO)_2O) + H_2O \qquad (7)$$

Apparently, formation of an anhydride from two formic acid molecules with the loss of water is favored, compared with the loss of an additional formic acid ligand. Like in the case of methanol, in the 80 s mass spectrum a final product of the reactions of the protonated water clusters with formic acid can again be found. The whole distribution of $H^+(H_2O)_n$ clusters initially present in trace amounts is now converted to a single product, the $H^+((HCO)_2O)_3$ cluster, a proton solvated by three formic acid anhydride molecules.

In all four cases studied, that is in pure $Al^+(H_2O)_n$, as well as in their reactions with HCl, HCOOH, and CH_3OH, the interesting hydrogen elimination can be rationalized with the previously suggested concerted proton transfer mechanism.[1,2] This is in Figure 4 exemplified by the specific case of the HCOOH reaction. It is initiated by the transfer of a proton originating from the formic acid molecule, which results in a transient formation of a hydroxonium cation in the second solvation shell of the Al^+. The s-electron pair of the Al^+ is then transferred outward, and the charge rearranged resulting in an $HCOO^-$-Al^{3+}-OH^- salt-bridge, with an H^-/H_3O^+ ion pair recombining to form H_2 and H_2O.

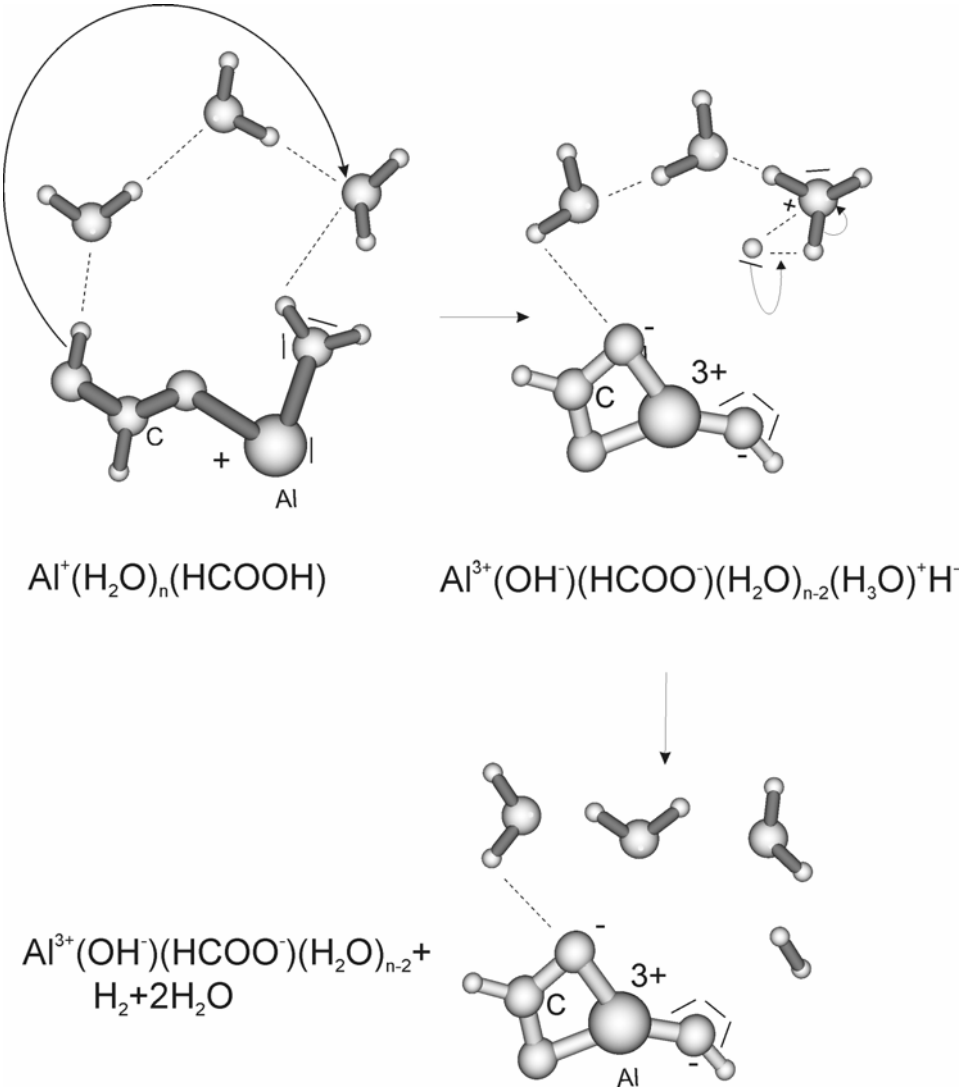

Figure 4. Proposed mechanism of the intracluster reaction exemplified in an $Al^{+}(HCOOH)(H_2O)_n$ cluster. Dissolving formic acid results in a proton transfer and charge separation into H_3O^{+} and $HCOO^{-}$ in the cluster. $HCOO^{-}$ comes in contact with the Al^{+} ion inducing the shift of the $3s^2$ lone pair, which results in the $HCOO^{-}$ - Al^{3+} - OH^{-} salt bridge and the formal H^{-} - H_3O^{+} ion pair. By recombination, molecular hydrogen is formed and additional water molecules are lost. The aluminum ion is assumed as hexacoordinated, with additional chains of water molecules between the first shell ligands. For clarity only the first hydration shell is shown in detail.

7.3.3 Theoretical results

To gain further insights into the mechanisms of molecular hydrogen elimination, we have carried out theoretical computations for reactions of the type:

$$Al^+(AH)(BH) \rightarrow Al(A)(B)^+ + H_2$$

Here AH, BH denote the Bronsted acids involved, that is H_2O, CH_3OH, or HCOOH, with the effect of the solvation shell not being explicitly considered. Although these reactions are fundamental for the redox chemistry of aluminum, to the best of our knowledge, they have not appeared in the literature so far. The only studies available so far deal with neutral and singly charged hydrated aluminum by Iwata and coworkers,[29,47] and Al^{3+}-water potentials have been derived computationally by Wasserman et al.[48] Detailed studies are available by several groups on the problem of aluminum insertion into the water O-H bond,[47,49,50] which involves change of the aluminum oxidation state from +I to +III, but H_2 elimination from large clusters has yet to be computationally treated. Our most recent results on competing H and H_2 elimination from hydrated vanadium ions,[51] $V^+(H_2O)_n$, might prove to be an even bigger challenge for theory.

We initially intended to carry out the evaluation of all the thermodynamic constants at the G2 level, but encountered problems for some of the species, since the HF/6-31G* geometry of $Al(OH)_2^+$ is nearly linear, and the MP2(full)/6-31G* geometry optimization failed to converge even after 60 cycles. Because of this, we have used RCCSD(T)/aug-cc-pVTZ relative energies, the MP2/6-311++G(2d,2p) geometries and vibrational frequencies to evaluate them instead. The RCCSD(T)/aug-cc-pVTZ//MP2/6-311++G(2d,2p) level is, in fact,

higher than the QCISD/6-311++G(3df,2p) level, which is the target of the composite G2 level.

The changes in electronic energy for the hydrogen elimination reactions computed at different levels of correlation with the aug-cc-pVTZ basis are summarized in the Table 1. The results suggest that the MP2 level is inadequate, but that the contribution from triple excitations is negligibly small. This suggests that if the assumption of additivity in the G2 method is valid, it is probably adequate for this type of reaction.

The thermodynamic constants obtained at the RCCSD(T)/aug-cc-pVTZ//MP2/6-311++G(2d,2p) level, within the harmonic oscillator rigid rotor approximation employing RCCSD(T) D_e values, MP2 optimized geometries and harmonic vibrational frequencies are shown in the Table 2, together with the corresponding G2 values where they could be computed. The results show that in the case of water, i.e. A = B = OH, the computed electronic energy change of the reaction is positive. The zero-point energy correction and reduces the energy change somewhat, with the reaction remaining slightly endothermic both at 0 and 289K. A positive reaction entropy results then overall in a negative free energy change. In the presence of one methanol molecule, that is A = CH_3O, B = HO, calculations could be carried out at both levels of theory, and allow an assessment of the reliability of the G2 level for this type of reactions. The differences between the G2 and RCCSD(T)//MP2 results may be considered as small, with the difference in the enthalpies being less than 3 kcal/mol. The differences in the computed entropy changes are less than 6 cal/mol.K, and in directions which make them cancel out each other in the evaluation of the Gibbs free energy. These differences lead overall to a very small difference of ca. 1 kcal/mole at 298 K in the Gibbs free energies computed at the two levels. The given entropy change at the G2 level is based on the scaled HF/6-31G* vibrational frequencies and optimized geometrical parameters.

Table 1. The computed electronic energy changes for the title reaction with the aug-cc-pVTZ basis set at different levels of correlation.

Reaction	Level	ΔE_e (kcal/mol)
$Al^+(H_2O)_2 \rightarrow Al^+(OH)_2 + H_2$	MP2	5.98
	CCSD	11.69
	CCSD(T)	11.53
$(CH_3OH)Al^+(H_2O) \rightarrow (CH_3O)Al^+(OH) + H_2$	MP2	4.88
	CCSD	10.66
	CCSD(T)	10.77
$(HCO_2H)Al^+(H_2O) \rightarrow (HCO_2)Al^+(OH) + H_2$	MP2	-13.6
	CCSD	-8.0
	RCCSD(T)	-8.5

Table 2: Summary of the computed thermodynamic constants (in kcal/mol) obtained at the G2 and RCCSD(T)/aug-cc-pVTZ//MP2/6-311++G(2d,2p) levels of theory, for the reactions: $Al^+(AH)(BH) \rightarrow Al^+(A)(B) + H_2$.

Level	AH, BH	ΔH (0 K)	ΔH (298 K)	ΔG (298 K)
RCCSD(T)//MP2	H_2O, H_2O	2.9	4.4	-2.9
G2	H_2O, CH_3OH	0.3	1.5	-5.2
RCCSD(T)//MP2	H_2O, CH_3OH	2.7	4.2	-4.3
G2	CH_3OH, CH_3OH	0.6	1.9	-5.8
G2	HCOOH, HCOOH	-38.7	-38.5	-41.6
G2	H_2O, HCOOH	-17.9	-17.0	-23.1
RCCSD(T)//MP2	H_2O, HCOOH	-16.2	-15.5	-21.3

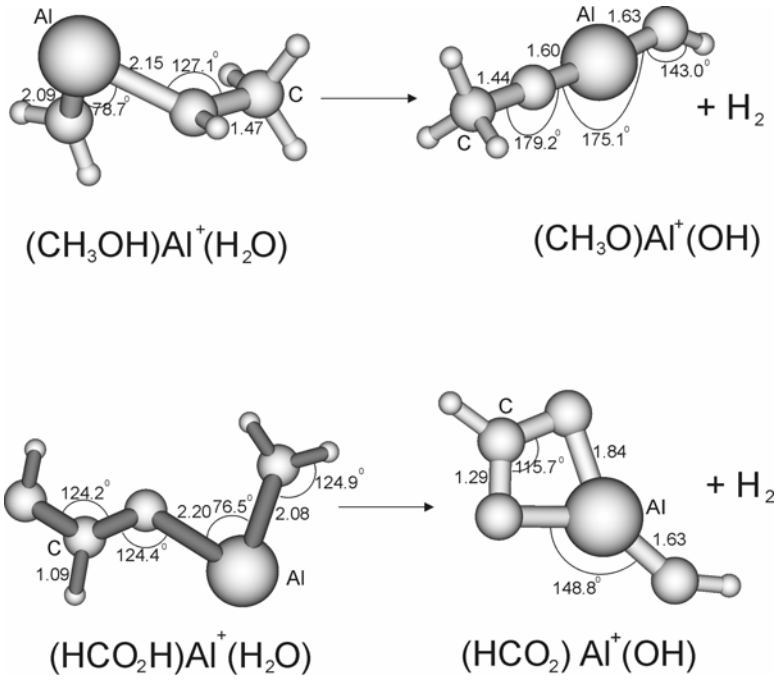

Figure 5. Selected optimized geometries for hydrogen elimination reaction. The Al^{3+} compounds prefer a linear structure due to the negative charge of the ligands. Also the bond lengths shrink due to increased attraction between the negatively charged oxygen atoms and the Al^{3+} ion.

Similarly small differences in the computed enthalpies and Gibbs free energies are found when one formic acid molecule is involved, A = HCOO, B = HO. In this case the difference in the computed enthalpy changes obtained at the two levels of calculation is less than 1.8 kcal/mol, the computed entropy changes less than 2 cal/mol.K at 298 K.

Table 2 reveals that all the reactions considered are thermodynamically possible. The most favorable conditions occur when at least one formic acid molecule is involved, and also the presence of methanol favors the hydrogen elimination reaction slightly compared with pure hydrated aluminum clusters. The calculations thus support the experimental observation that an increasing acidity of the reactant favors the intracluster hydrogen elimination, which occurs fastest with formic acid, followed by methanol, and is least favored in pure hydrated aluminum clusters.

The presence of solvent molecules is surely expected to change the thermochemistry of the intracluster reaction considerably in favor of the products. The interaction energies with the products, containing a triply charged Al^{3+} and two singly charged anions, is significantly enhanced over the initial singly charged Al^{+}, and the slightly positive enthalpy of some of the calculated reactions is very likely turned negative already by the addition of a single solvent molecule.

The calculated structures, exemplified in Fig. 5, reflect the loss of the hydrogen, with the Al-O bond length shrinking in both reactions shown, a consequence of the 3+ charge on the aluminum atom after oxidation. Also interesting are the linear structures of the compounds containing Al^{3+}. The conformational change is induced by the negative charges of the oxygen atoms directly coordinated to Al^{3+}, which result in ligand repulsion.

7.4 Conclusions

The reaction of hydrated aluminum cations containing up to 60 water molecules with methanol and formic acid were studied. In both cases an efficient ligand exchange is followed by an intracluster reaction oxidizing the aluminum atom, thereby eliminating molecular hydrogen. The observed trend of the reaction rate, which increases with the acidity of the reactant, from pure water over CH_3OH, HCOOH to HCl provides a strong support for the previously proposed proton transfer mechanism of the reaction. The theoretical computations agree with this interpretation, the reaction enthalpies follow the same trend.

7.5 References

[1] M. Beyer, C. Berg, W. Görlitzer, T. Schindler, U. Achatz, G. Albert, G. Niedner-Schatteburg, V.E. Bondybey, *J. Am. Chem. Soc.* **1996**, *118*, 7386.

[2] M. Beyer, U. Achatz, C. Berg, S. Joos, G. Niedner-Schatteburg, V.E. Bondybey, *J. Phys. Chem. A* **1999**, *103*, 671.

[3] C. Berg, U. Achatz, M. Beyer, S. Joos, G. Albert, T. Schindler, G. Niedner-Schatteburg, V.E. Bondybey, *Int. J. Mass Spectrom. Ion Proc.* **1997,** *167/168*, 723.

[4] C. Berg, M. Beyer, U. Achatz, S. Joos, G. Niedner-Schatteburg, V.E. Bondybey, *Chem. Phys.* **1998**, *239*, 379.

[5] U. Achatz, S. Joos, C. Berg, M. Beyer, G. Niedner-Schatteburg, V.E. Bondybey, *Chem. Phys. Lett.* **1998**, *291*, 459.

[6] U. Achatz, B.S. Fox, M.K. Beyer, V.E. Bondybey, *J. Am. Chem. Soc.* **2001**, *123*, 6151.

[7] B. S. Fox, M. K. Beyer, U. Achatz, S. Joos, G. Niedner-Schatteburg, V.E. Bondybey, *J. Phys. Chem. A* **2000,** *104*, 1147.

[8] T. Schindler, C. Berg, G. Niedner-Schatteburg, V.E. Bondybey, *Chem. Phys.* **1995**, *201*, 491.

[9] T. Schindler, C. Berg, G. Niedner-Schatteburg, V.E. Bondybey, *Chem. Phys. Lett.* **1996** *250*, 301.

[10] R.C. Dunbar, T.B. McMahon, *Science* **1998**, *279*, 194.

[11] M. Sena, J.M. Riveros, *Rapid Commun. Mass Spectrom.* **1994**, *8*, 1031.

[12] P.D. Schnier, W.D. Price, R.A. Jockusch, E.R. Williams, *J. Am. Chem. Soc.* **1996**, *118*, 7178.

[13] U. Buck, C. Steinbach, *J. Phys. Chem. A* **1998,** *102*, 7333.

[14] C.J. Mundy, J. Hutter, M. Parrinello, *J. Am. Chem. Soc.* **2000,** *122*, 4837.

[15] F. Mercuri, C.J. Mundy, M. Parrinello, *J. Phys. Chem. A* **2001,** *105*, 8423.

[16] K. Fuke, F. Misaizu, M. Sanekata, K. Tsukamato, S. Iwata, *Z. Phys. D* **1993,** *26*, S180.

[17] A.C. Harms, S.N. Khanna, B. Chen, A.W. Castleman, *J. Chem. Phys.* **1994,** *100*, 3540.

[18] H. Watanabe, S. Iwata, K. Hashimoto, F. Misaizu, K. Fuke, *J. Am. Chem. Soc.* **1995,** *117*, 755.

[19] M. Sanekata, F. Misaizu, K. Fuke, *J. Chem. Phys.* **1996**, *104*, 9768.

[20] D.C. Sperry, A.J. Midey, J.I. Lee, J. Qian, J.M. Farrar, *J. Chem. Phys.* **1999,** *111*, 8469.

[21] J. Qian, A.J. Midey, S.G. Donnelly, J.I. Lee, J.M. Farrar, *Chem. Phys. Lett*. **1995,** *244*, 414.

[22] C.A. Woodward, M.P. Dobson, A.J. Stace, *J. Phys. Chem. A* **1997**, *101*, 2279.

[23] W. Lu, S. Yang, *J. Phys. Chem. A* **1998**, *102*, 825.

[24] J.I. Lee, D.C. Sperry, J. M. Farrar, *J. Chem. Phys.* **2001**, *114*, 6180.

[25] N. Horimoto, J. Kohno, F. Mafuné, T. Kondow, *J. Phys. Chem. A* **1999**, *103*, 1518.

[26] K. Fuke, K. Hashimoto, S. Iwata, *Adv. Chem. Phys.* **1999,** *110*, 431.

[27] B. Soep, M. Elhanine, C.P. Schulz, *Chem. Phys. Lett.* **2000**, *327*, 365.

[28] F. Misaizu, M. Sanekata, K. Fuke, *Z. Phys. D* **1993,** *26*, S177.

[29] H. Watanabe, S. Iwata, *J. Phys. Chem.* **1996,** *100*, 3377.

[30] T. Schindler, C. Berg, G. Niedner-Schatteburg, V.E. Bondybey, *Chem. Phys. Lett.* **1994,** *229*, 57.

[31] C. Dedonder-Lardeux, G. Grégoire, C. Jouvet, S. Martrenchard, D. Solgadi, *Chem. Rev.* **2000,** *100*, 4023.

[32] R.S. MacTaylor, J.J. Gilligan, D.J. Moody, A.W. Castleman, Jr., *J. Phys. Chem. A* **1999,** *103*, 4196.

[33] D. Laria, R. Kapral, D. Estrin, G. Ciccotti, *J. Chem. Phys.* **1996**, *104*, 6560.

[34] D. Estrin, J. Kohanoff, D. Laria, R. O. Weht, *Chem. Phys. Lett.* **1997,** *280*, 280.

[35] H. Arstila, K. Laasonen, A. Laaksonen, *J. Chem. Phys.* **1998,** *108*, 1031.

[36] I. Kusada, Z. G. Wang, J. H. Seinfeld, *J. Chem. Phys.* **1998,** *108*, 6829.

[37] S. Re, Y. Osamura, K. Morokuma, *J. Phys. Chem. A* **1999,** *103*, 3535.

[38] P.E.M. Siegbahn, *J. Phys. Chem.* **1996,** *100*, 14672.

[39] M.T. Nguyen, G. Raspoet, L.G. Vanquickenborne, P.T. van Duijnen, *J. Phys. Chem. A* **1997,** *101*, 7379.

[40] M. Aida, H. Yamataka, M. Dupuis, *Chem. Phys. Lett.* **1998,** *292*, 474.

[41] M. Aida, H. Yamataka, *J. Mol. Struc.-Theochem* **1999,** *462*, 417.

[42] H. Yamataka, M. Aida, *Chem. Phys. Lett.* **1998,** *289*, 105.

[43] J. Andrés, M. Canle, M.V. García, L.F.R. Vázquez, J.A. Santaballa, *Chem. Phys. Lett.* **2001,** *342*, 405.

[44] C. Berg, T. Schindler, G. Niedner-Schatteburg, V.E. Bondybey, *J. Chem. Phys.* **1995,** *102*, 4870.

[45] B.S. Fox, M.K. Beyer, V.E. Bondybey, *J. Phys. Chem. A* **2001,** *105*, 6386.

[46] M.J. Frisch, G.W. Trucks, H.B. Schlegel, G.E. Scuseria, M.A. Robb, J.R. Cheeseman, V.G. Zakrzewski, J.A. Montgomery, Jr., R.E. Stratmann, J.C. Burant, S. Dapprich, J. M. Millam, A.D. Daniels, K.N. Kudin, M.C. Strain, O. Farkas, J. Tomasi, V. Barone, M. Cossi, R. Cammi, B. Mennucci, C. Pomelli, C. Adamo, S. Clifford, J. Ochterski, G.A. Petersson, P.Y. Ayala, Q. Cui, K. Morokuma, D. K. Malick, A. D. Rabuck, K. Raghavachari, J.B. Foresman, J. Cioslowski, J.V. Ortiz, A.G. Baboul, B.B. Stefanov, G. Liu, A. Liashenko, P. Piskorz, I. Komaromi, R. Gomperts, R.L. Martin, D.J. Fox, T. Keith, M.A. Al-Laham, C.Y. Peng, A. Nanayakkara, C. Gonzalez, M. Challacombe, P.M.W. Gill, B. Johnson, W. Chen, M.W. Wong, J.L. Andres, C.

Gonzalez, M. Head-Gordon, E.S. Replogle, J.A. Pople, *Gaussian 98,* Revision A.7; Gaussian, Inc.: Pittsburgh, PA, **1998**.

[47] H. Watanabe, M. Aoki, S. Iwata, Bull. *Chem. Soc. Jpn.* **1993,** *66*, 3245.

[48] E. Wasserman, J.R. Rustad, S.S. Xantheas, *J. Chem. Phys.* **1997,** *106*, 9769.

[49] S. Sakaki, K.D. Jordan, *J. Phys. Chem.* **1993,** *97*, 8917.

[50] J. Hrušák, D. Stöckigt, H. Schwarz, *Chem. Phys. Lett.* **1994,** *221*, 518.

[51] B.S. Fox, I. Balteanu, O.P. Balaj, M.K. Beyer, V.E. Bondybey, *Phys. Chem. Chem. Phys.* **2002**, *4*, 2224.

8. Development of a temperature controlled FT-ICR "infinity" cell

8.1 Introduction

Fourier transform ion cyclotron resonance mass spectrometry (FTICR-MS) has proven to be a powerful method used in the analytical and bio-analytical research. It is used in many different fields where it provides valuable information ranging from biomolecular structural studies to metallic and organometalic ion chemistry. Extensively used in the last years it has demonstrated to be invaluable in the identification and structural characterization of large biomolecules and individual components present in mixtures. However by being able to control the cell temperature it is possible, for example, to extract the activation energies from BIRD (Black-body infrared radiative dissociation) using master equation modeling. The BIRD experiments are mostly known to make use of elevated temperatures and they provide accurate information about ion dissociation energetics for a large variety of ions.[1-11] Non-covalent complexes studied in BIRD experiments[10,12] can, due to the low temperatures in a cooled cell, benefit of an increase of their the lifetime of and thus enhance resolution for large bio-molecules, which otherwise might undergo lifetime broadening. One can also study ion-molecule reactions under variable and well-defined collision-gas temperatures or use water clusters as model systems for polar stratospheric clouds and study their reactions under realistic conditions.

8.2 Construction details of the Garching "infinity" cooled cell.

The heart of the FT-ICR mass spectrometer is the analysis cell. Used to trap, excite and then detect the signal induced by the coherent packages of ions, it has known many different types of configurations. Starting with the original cubic cell,[13] continuing with the cylindrical[14,15], "infinity"[16] and open-ended cylindrical[17,18] cell they have been continually improved and modified. The vast majority of them are operating at room temperature.

Recent BIRD experiments made use of heated filaments placed close to the cell excitation-detection plates[19-21] or simply used the infrared radiation from a directly heated vacuum chamber.[5] Although the temperature of the filament can reach high values, around 2000 K, the temperature distribution within the cell is not homogeneous. In the latter case, depending on the target temperature, the indirect heating would require long times needed to get a cell with stable temperature. In both cases the temperature of the ion population is not accurately defined. Changing the temperature of the cell can be done also by direct contact to a cooling or heating system. In the last years experiments were also tried using cells operating at lower temperatures.[11,22,23]

The cell under development is an "infinity" cell provided by Bruker which is cooled by liquid nitrogen flowing through a 6 mm copper tube incorporated in a massive copper shield. The cooling shield "embraces" the cell fulfilling two objectives: to shield the cell from the black-body radiation coming from the ultra-high vacuum chamber walls and to cool the cell itself. The shield covers all the openings between the excitation/detection/trapping plates of the original "infinity" cell. In the same time it does not hinder the pumping of the cell interior. The high heat conductivity ceramics, aluminum/boron nitride Tokuyama SHAPAL-M soft, insure a uniform and rapid cooling of the excitation/detection/trapping plates. They are placed above the upper trapping plate, below the lower trapping plate and are also sustaining the excitation/detection plates. To insure a

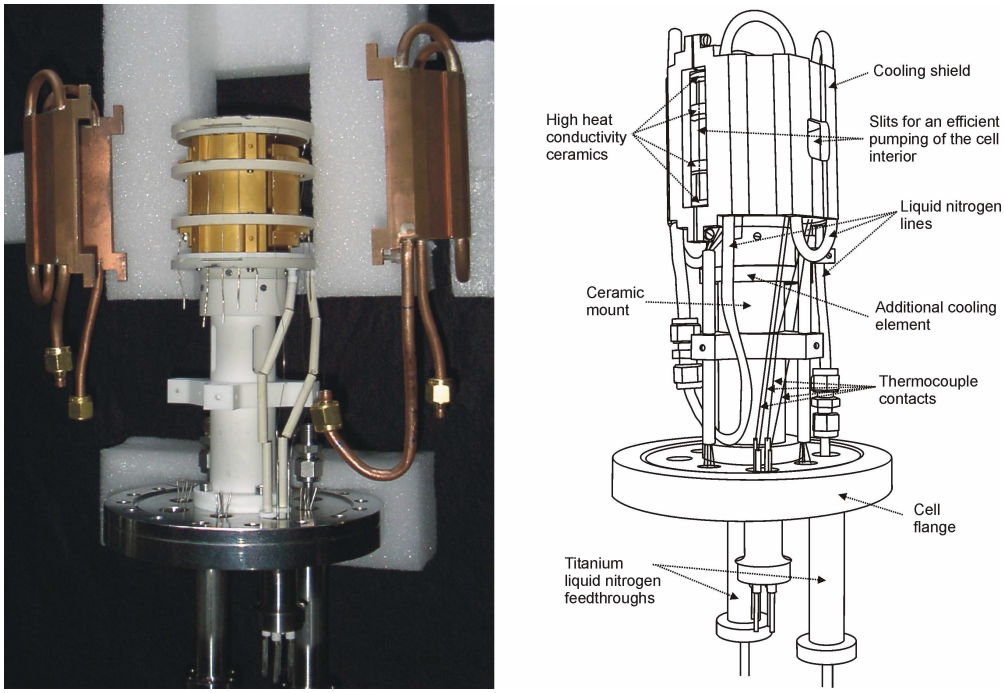

Figure 1. The "infinity" cell is in a thermal contact with the copper shield, cooled by the incorporated liquid nitrogen carrying lines. The cell is insulated from the flange by the ceramic mount.

minimum of heat transfer between the cell and the cell flange, a glass ceramics mount is used. During the initial tests the 10-25 K temperature gradient along the cell started to raise concerns regarding the possible damage to the cell and the homogeneity of the temperature in the cell region. As a result, an additional cooling element was included. This element is meant to cool the glass ceramics mount in the vicinity of the cell and it is connected to the liquid nitrogen inlet tube. As a consequence, the gradient along the cell decreased below 5 K, but also the temperature reached has slightly increased.

In order to bring the liquid nitrogen into the cell, the only reasonable approach, considering the space, is to feed it in from behind the magnet, through the cell flange and preamplifier. This way, the liquid nitrogen flows through the magnet, pass through the preamplifier, the cell mounting flange and reach the copper shield. This means that the preamplier layout had to be redesigned and new mounts drilled in the cell flange. In order to avoid the ice formation in the region of the preamplifier, special titanium feed-through for the

liquid nitrogen lines were built, extending the UHV region until well out of the preamplifier area. They are coupled to separate vacuum surrounded lines (~10^{-2} mbar) which bring in and out the cooling liquid. The connection point is heated by the means of heater bands whose temperature is measured by a NiCr-Ni (Type K) sensor and actively controlled with a BVT 3300 Digital controller.

The temperature is monitored by two E-type thermocouples. The first one is situated below the lower trapping plate, between the plate and the Shapal ceramic plate cooling it. The second one is above the upper trapping plate, between the plate and the Shapal ceramic which cools it. The thermocouples are connected to a BVT3300 module which has a dedicated auxiliary sensor module. Using a RS232 serial link the BVT unit communicates with a PC computer running LabView.[24] The software records and displays the temperature of the cell, the liquid nitrogen level, the evaporator power and the BVT3300 unit status. To avoid the noise pick-up, by the ICR signal cables, the temperature sensor lines were shielded and the temperature measurement will be switched off during the MS scans.

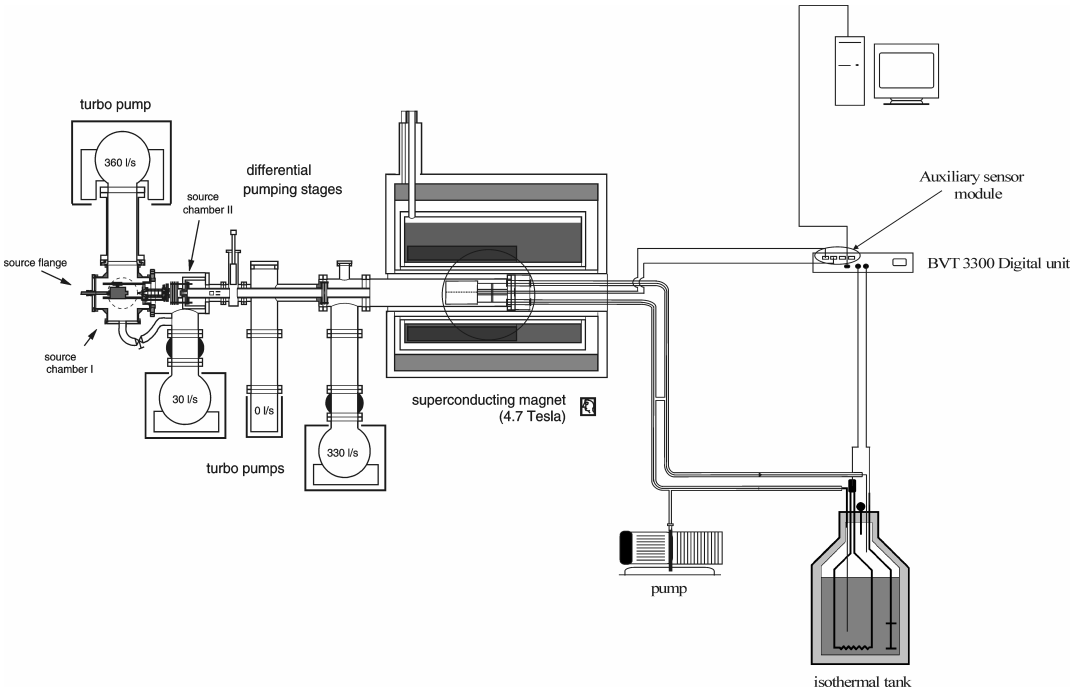

Figure 2. The temperature controlled ICR "infinity" cell experimental setup.

8.3 The characteristics, performance and parameters of the cooled-cell.

A number of tests were done with the temperature-controlled cell in order to evaluate its thermal behavior. The temperature of the cell depends on the liquid nitrogen heater power. In the tests, the liquid nitrogen evaporator power was gradually raised from 0% to 100% and the temperature reached by the cell was recorded. In the tests the temperature was decreased in steps of 10% liquid nitrogen heater power to decrease the risk of structural damage to the cell. Figure 3 shows examples of the cell temperature using different heater powers. As can be seen in Figure 3, there is a sharp initial decrease of the temperature that, within 20 minutes, will reach a steady temperature which can be maintained for a long time. The curves in the panel b) of the figure show that the lowest reached temperature, in the test stand, was 135K, in the at 100% heater power. The temperatures shown in Figure 3 represent both cell thermocouples coupled to the channel 0 and 1 of the BVT 3300 unit. As can be seen there is a difference between the two readings so there is a temperature gradient along the cell. The temperature gradient as a function of heater power, as shown in Figure 4, is not constant, increases with heater power until it reaches a maximum of 5K at 70% and then goes down to ~3K at 100%. While we the temperature measuring points are one above the other, the readings of the lower sensor are affected by the cell ceramic mount which from its vicinity.

The final cell temperature under thermal equilibrium as a function of heater power was measured as can be seen in Figure 5. Using this representation one can easily approximate the needed liquid nitrogen heater power for a desired target temperature. The experimental points were fitted using a quadratic regression resulting in the curve described by:

$$Y = 14.7 \cdot 10^{-3} \cdot X^2 - 29.44 \cdot 10^{-1} \cdot X + 285.88$$

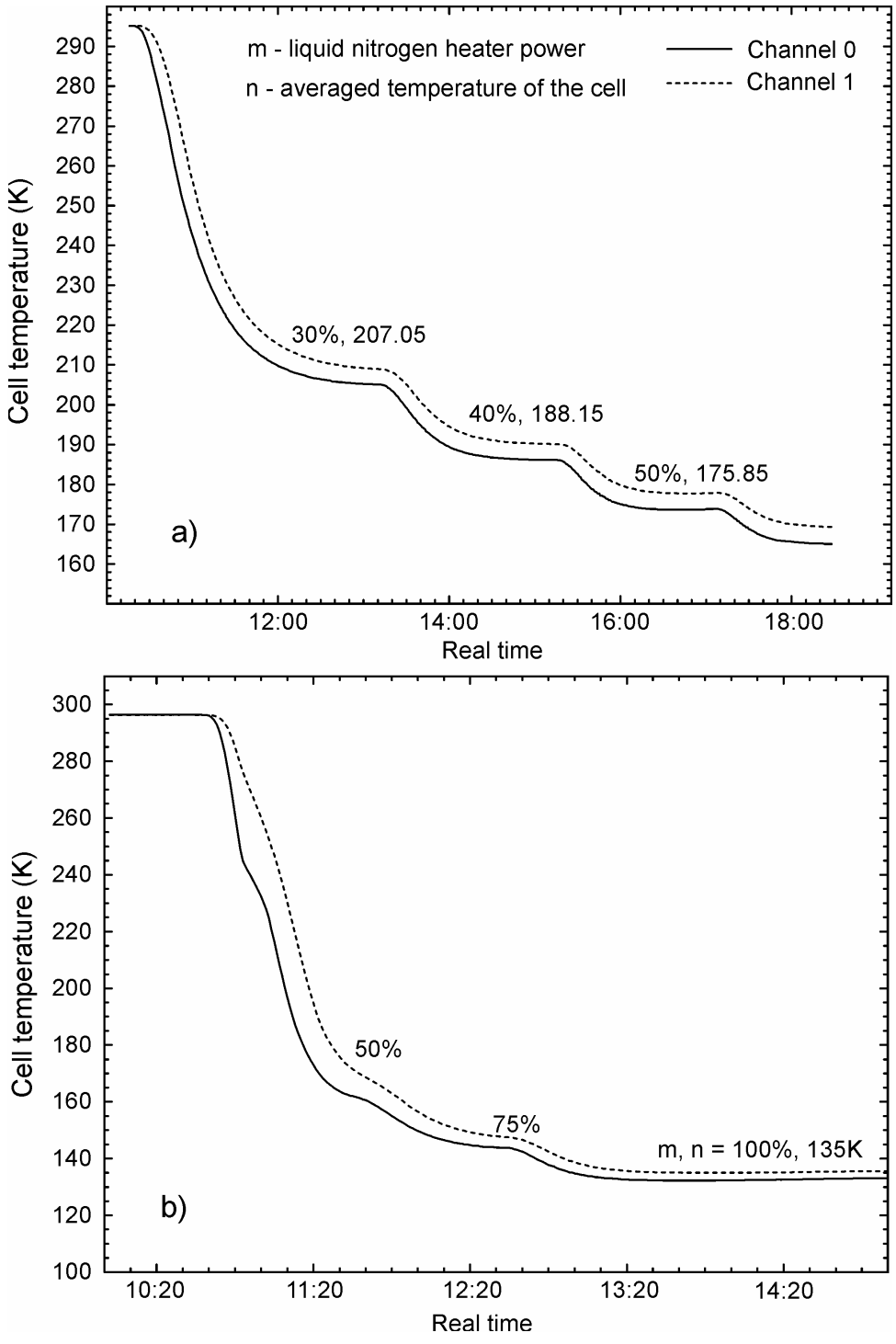

Figure 3. The cooled-cell temperature behavior versus time. The cell temperature depends directly of the liquid nitrogen heater power. In the panel a) the heater was powered initially to 30%, the time needed for the temperature to stabilize and the final temperature were measured. Once the temperature stabilized the power was increased to 40% then 50%. The panel b) shows the lowest temperature that can be obtained for 100% heater power: 135K. To avoid any structural damage in a very fast cooling process the decrease of the temperature was done in steps, first using a 50% and then 75% heater power.

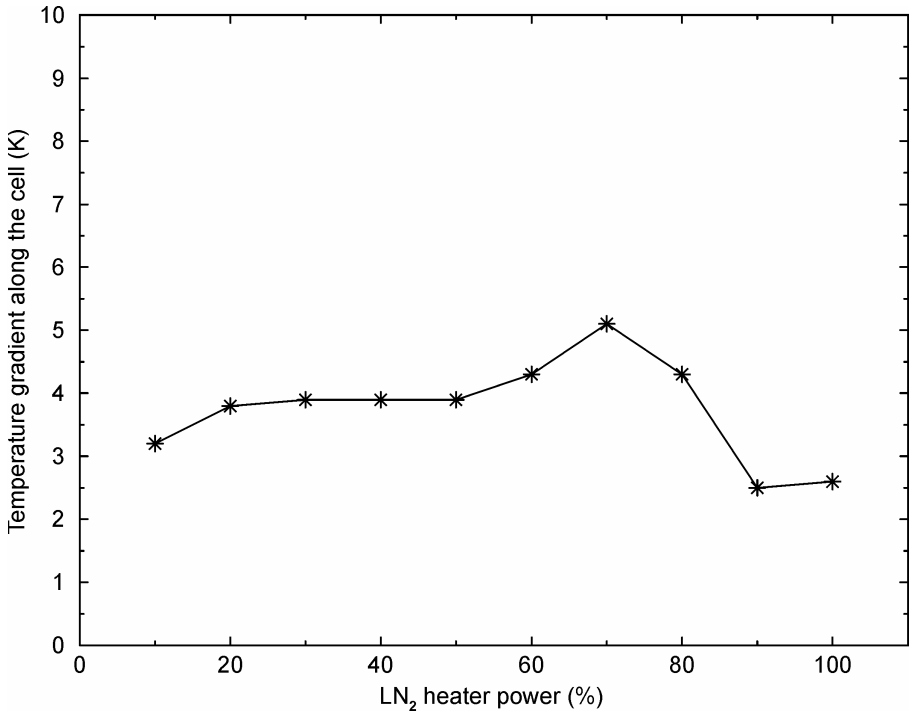

Figure 4. The dependence of the temperature gradient along the cell on the liquid nitrogen heater power.

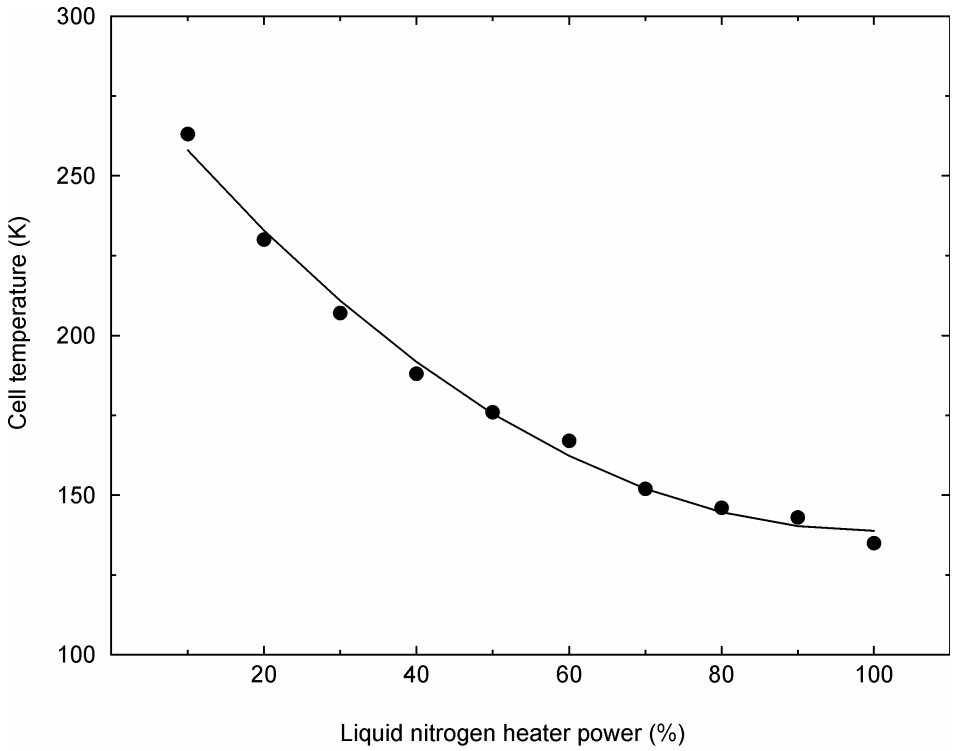

Figure 5. The final cell temperature curve of the lowest temperature for different heater powers during the cooling experiments.

During the cooling a considerable decrease of the pressure in the ICR cell was seen. Due to the cooled surfaces, which acted as cryo-pumps, the pressure has decreased below 10^{-10} mbar for temperatures below 200 K. This, in turn will generate an increase in the resolution and thus higher mass accuracy.

Comparable setup which have, to the best of our knowledge, yielded published results are operated by Ron van Heeren and coworkers[22] at FOM-AMOLF in Amsterdam and Evan R. Williams[11] at University of California. The Amsterdam variable-temperature cell has an open geometry, which facilitates experiments with pulsed collision gas. The strength of our design, with an almost complete enclosure of the cell interior with cooled walls lies in the well-defined radiation temperature near 135 K. With an open cell, room-temperature radiation covers a significant fraction of the steric angle. The case of cell used by Williams and coworkers is completely enclosed, with the exception of 10 holes, by a nitrogen cooled thermal jacket. While this design removes the possibility that any room temperature radiation to "leak" inside the cell, the pumping of cell interior might be not so easy. Also the low temperature is maintained for over 8 hours prior to measurements, which is considerably longer than the ~ 3 hours needed with our setup for the lowest temperature (135K) our cell can reach.

8.4 References

[1] R. C. Dunbar, *J. Phys. Chem*. **1994**, *98*, 8705.

[2] R. C. Dunbar, T. B. McMahon, *Science* **1998**, *279*, 194.

[3] W. D. Price, E. R. Williams, *J. Phys. Chem. A* **1997**, *101*, 8844.

[4] W. D. Price, P. D. Schnier, E. R. Williams, *J. Phys. Chem. B* **1997**, *101*, 664.

[5] W. D. Price, P. D. Schnier, E. R. Williams, *Anal.Chem.* **1996**, *68*, 859.

[6] K. Paech, R. A. Jockusch, E. R. Williams, *J. Phys. Chem. A* **2002**, *106(42)*, 9761.

[7] R. A. Jockusch, A. S. Lemoff, E. R. Williams, *J. Phys. Chem. A* **2001,** *105(48)*, 10929.

[8] R. A. Jockusch, K. Paech, E. R. Williams, *J. Phys. Chem. A* **2000**, *104(14)*, 3188.

[9] S. E. Rodriguez-Cruz, R. A. Jockusch, E. R. Williams, *J. Am. Chem. Soc.* **1999**, *121(38)*, 8898.

[10] J. S. Klassen, P. D. Schnier, E. R. Williams, *J. Am. Soc. Mass Spectrom.* **1998**, *9(11)*, 1117.

[11] R. L. Wong, K. Paech, E. R. Williams, *Int. J. Mass Spectrom.* **2004**, *232(1)*, 59.

[12] P. D. Schnier, J. S. Klassen, E. F. Strittmatter, E. R. Williams, *J. Am. Chem. Soc*, **1998**, *120*, 9605.

[13] M. B. Comisarow, *Adv. Mass Spectrom.* **1980**, *8*, 1698.

[14] S. H. Lee, K.–P. Wanczek, H. Hartmann, *Adv. Mass Spectrom.* **1980**, *8*, 1645.

[15] J. L. Elkind, F. D Weiss, J. M Alford, R. T. Laaksonen, R. E. Smalley, *J. Chem. Phys.* **1988,** *88,* 5215–5224.

[16] P. Caravatti, M. Allemann, *Org. Mass Spectrom.* **1991**, *26*, 514.

[17] S. C. Beu, D. A. Laude Jr., *Int. J. Mass Spectrom. Ion Proc.* **1992**, *112*, 215.

[18] G. Gabrielse, L. Haarsama, S. L. Rolston, *Int. J. Mass Spectrom. Ion proc.* **1989**, *88*, 319.

[19] R. L. Wong, E. W. Robinson, E. R. Williams, *Int. J. Mass Spectrom.* **2004,** *234(1-3)*, 1.

[20] M. Sena, J. M. Riveros, *J. Phys. Chem.* **1997**, *101*, 4384.

[21] M. Sena, J. M. Riveros, *Int. J. Mass Spectrom.* **2003**, *227*, 135.

[22] X. Guo, M. Duursma, A. Al-Khalili, L. A. McDonnell, R. M. A. Heeren, *Int. J. Mass Spectrom.* **2004**, *231*, 37-45.

[23] X. Guo, M. Duursma, A. Al-Khalili, R. M. A. Heeren, *Int. J. Mass Spectrom.* **2003**, *225*, 71-82.

[24] LabView 6.0, National Instruments Corporation, Austin, USA

9. Summary

Besides bulk solutions, ions solvated in small finite clusters produced in experiments with supersonic expansion beams are very convenient medium for the studies of chemical reactions. Since the FT-ICR measurement yields unambiguous information about the chemical composition of the cluster, the effects of impurities which always plague experiments in bulk solutions can be completely eliminated. Taking advantage of the black body radiation, which allows the gentle removal of solvent molecules, one can easily study the ion chemistry as a function of the number of solvent molecules. Additionally one can study the influence of the solvation upon their chemistry by allowing them to interact with one or more reactants.

Using the laser vaporization source developed in our laboratory a range of hydrated ions can be produced. It can easily produce hydrated metal ions, $M^+(H_2O)_n$, but interestingly, solvated monovalent ions regardless of the preferred oxidation state of the element in question and whether the monovalent ions are known in bulk aqueous chemistry or not. In this study the use of a Zn target ensured the formation of clean hydrated electrons $(H_2O)_n^-$ distributions, eliminating the formation of metal anions and anion clusters.

The solvated electron clusters provide an interesting medium for studying reactions of aqueous electrons. These simple reactants exhibit a very multifaceted chemistry with a surprising variety of chemical reactions, which can be crudely classified into at least for categories, that is collisional activation, ligand exchange, core exchange and rearrangement of covalent bonds.

Species like CO, toluene and C_2H_4 do not react at all with the solvated electron. The only process observed is a collision-induced increase of the fragmentation rate of the cluster.

Methanol is, similar to water in that it can form relatively strong hydrogen bonds. However, being less polar than water the bonds are weaker and its ability to from hydrogen bonded networks is reduced because counting that it has only one OH bond. In reaction with the hydrated electron it replaces water molecules from the hydration shell until, at most, 8 methanol molecules were observed in the clusters, that is $(H_2O)_n(CH_3OH)_8^-$. These will, however, most likely remain near the cluster surface, and as the fragmentation becomes dominant, will eventually also preferentially "evaporate" from the cluster. Methanol does not provide additional stabilization of the electron, compared with the purely water hydrated ones, so that the electron detachment process start to compete again when the number of sovent molecules drops below 30.

Species which exhibit an appreciable electron affinity in solution, can simply attach the electron, forming a negative ion, and replacing thus the ionic core of the cluster. The CO_2 and O_2 react efficiently with $(H_2O)_n^-$ because of the presence of low-lying empty π^* orbitals in both CO_2 and O_2. The molecular CO_2^- and O_2^- anions formed are concurrently solvated and stabilized by the water ligands to form $CO_2^-(H_2O)_n$ and $O_2^-(H_2O)_n$. Core exchange reactions are also observed, transforming $CO_2^-(H_2O)_n$ into $O_2^-(H_2O)_n$ upon collisions with O_2. This is in agreement with predictions by density functional theory calculations, that $O_2^-(H_2O)_n$ clusters are thermodynamically more favorable than the $CO_2^-(H_2O)_n$. Electron detachment from the product species is only observed for $CO_2^-(H_2O)_2$, in agreement with the calculated electron affinities and solvation energies. Since the electron is intimately involved in the course of the reaction and binding of the oxygen molecule, we have never observed a second O_2 or CO_2 to be taken up by the cluster, regardless of its size.

Acetone and acetaldehyde behave similarly to carbon dioxide and no H/D exchange was observed in the case of deuterated acetaldehyde. Both detach the electron, but not earlier as final products containing 2 and 3 water molecules are formed. Benzonitrile can also realize an ionic core exchange followed by a ligand exchange process so that up to 7 of its molecules

can go into the clusters and eventually due to the fragmentation all the water is lost forming $(C_6H_5CN)_{2,3,4}^-$ as final products. At longer time they also detach the electron.

The strong acid hydrogen chloride, HCl, is taken up by the clusters, presumably ionically dissolved. The proton is reduced, through an electron transfer, to atomic hydrogen evaporating from the cluster. This process is accompanied by black-body radiation and collision induced loss of water molecules. The mass spectrometrically observed reaction products are $Cl^-(H_2O)_{n-3}$ clusters, whose further fragmentation and ligand exchange ultimately lead to saturation of the cluster with hydrogen chloride. The process involves the reaction between a proton and an electron thus the most fundamental electrochemical reaction is clearly observed in finite clusters.

The reaction with acetonitrile involves a rearrangement of the covalent bonds. The reaction mechanism involves a solvent stabilized covalent radical anion as an intermediate. A proton can be transferred from a water molecule, CH_3CHN evaporates and $OH^-(H_2O)_n$ remains. An H/D-exchange reaction involving the methyl group of acetonitrile is observed in the small anionic water cluster $OH^-(CD_3CN)(H_2O)_2$. In this cluster, a randomization of H and D atoms takes place, and in subsequent collisions with CD_3CN, the potentially partially deuterated acetonitrile is replaced by the fully deuterated species. In sequential collisions, fully deuterated clusters $OD^-(CD_3CN)(D_2O)_2$ are obtained as final products. The H/D-exchange does not occur in $OH^-(CD_3CN)(H_2O)_3$ or larger clusters. Density functional calculations show that in these larger species, the OH^- does no longer directly attack the methyl group, and the barriers for H/D-exchange become higher than those for ligand loss reaction channels. This is a very subtle influence of solvation on an H/D-exchange reaction in the gas phase, where a relatively acidic methyl group encounters a strongly basic reaction partner.

To get insight into the validity of the previously proposed proton transfer mechanism the reactions of hydrated aluminum ions $Al(H_2O)_n^+$, $20 < n < 60$, with methanol and formic

acid were carried out. Besides black body radiation and collisionally induced fragmentation, also efficient ligand transfer processes as well as an intracluster oxidation of the aluminium take place. While in pure $Al(H_2O)_n^+$ ions this reaction, where the Al^+ is oxidized to Al^{3+} and water reduced to yield molecular H_2 proceeds only in a limited size range of $11 < n < 24$, addition of formic acid, similar to the previously studied addition of HCl, removes the upper limit, but the reactions proceed more slowly. With methanol, the upper limit remains, but it is shifted to higher values of n. These observations are consistent with our previously proposed "acid catalyzed", concerted proton transfer mechanism, with the efficiency of the reaction being highest in the presence of HCl, and decreasing with the decreasing acidities of formic acid and methanol.

In order to move from a qualitative to a quantitative approach in the description of the stability of molecular clusters a temperature controlled cell is under development. The temperature equilibrates within 20 minutes and the lowest temperature reached in the test was 135 K. The cell has a wide range of potential application among which one can mention extracting activation energies from BIRD experiments through master equation modeling, increase of resolution by decreasing the pressure inside the cell whose surfaces act as cryo-pumps, extraction of binding energies from temperature resolved radiative association kinetics and increase of the life-time for non covalent complexes and molecules which may undergo lifetime broadening in long detection cycles.

A List of Publications

1. **Single Molecule Precipitation of Transition Metal(I) Chlorides in Water Clusters**
   B. S. Fox, O. P. Balaj, I. Balteanu, M. K. Beyer, and V. E. Bondybey
   J. Am. Chem. Soc. **2002**, *124*, 172-173.

2. **Black Body Radiation Induced Hydrogen Formation in Hydrated Vanadium Cations $V^+(H_2O)_n$**
   B. S. Fox, I. Balteanu, O. P. Balaj, H. C. Liu, M. K. Beyer, and V. E. Bondybey
   Phys. Chem. Chem. Phys. **2002,** *4*, 2224-2228.

3. **Reactions of Hydrated Aluminum Ions with Methanol and Formic Acid**
   O. P. Balaj, E. P.F. Lee, I. Balteanu, B. S. Fox, M. K. Beyer, J. M. Dyke, and V. E. Bondybey
   Int. J. Mass Spectrom. **2002,** *220*, 331-341.

4. **Aqueous Chemistry of Transition Metals in Oxidation State (I) in Nanodroplets**
   B. S. Fox, O. P. Balaj, I. Balteanu, M. K. Beyer, and V. E. Bondybey
   Chem. Eur. J. **2002,** *8*, 5534-5540.

5. **Very Low Rate Constants of Bimolecular CO Adsorbtion on Anionic Gold Clusters: Implications for Catalytic Activity**
   I. Balteanu, O. P. Balaj, B. S. Fox, M. K. Beyer, Z. Bastl, and V. E. Bondybey
   Phys. Chem. Chem. Phys. **2003,** *5*, 1213-1218.

6. **Addition of a Hydrogen Atom to Acetonitrile by Hydrated Electrons in Nanodroplets**
   O. P. Balaj, I. Balteanu, B. S. Fox-Beyer, M. K. Beyer and V. E. Bondybey
   Angew. Chem. Int. Ed. **2003**, *42*, 5516-5518.

7. **The effect of charge upon CO-adsorbtion by ionic group 5 and group 9 transition metal clusters**
   I. Balteanu, U. Achatz, O. P. Balaj, B. S. Fox, M. K. Beyer and V. E. Bondybey
   Int. J. Mass Spectrom. **2003,** *229*, 61-65.

8. **Size- and Charge-state-dependent Reactivity of Azidoacetonitrile with Anionic and Cationic Rhodium Clusters $Rh_n^{\pm}$**
   I. Balteanu, O. P. Balaj, B. S. Fox-Beyer, P. Rodrigues, M. T. Barros, A. M. C. Moutinho, M. L. Costa, M. K. Beyer and V. E. Bondybey,
   Organometallics **2004**, *23*, 1978-1985.

9. **Base-Catalized Hydrogen/Deuterium Exchange between Water and Acetonitrile in AnionicWater Clusters**
   O. P. Balaj, C.-K. Siu, Iulia Balteanu, B. S. Fox-Beyer, M. K. Beyer and V. E. Bondybey
   J. Phys. Chem. **2004**, *108*, 7506-7512.

10. **Reactions of platinum clusters $^{195}Pt_n^{\pm}$, n=1-24, with N_2O studied with isotopically enriched platinum**
    I. Balteanu, O. P. Balaj, M. K. Beyer and V. E. Bondybey
    Phys. Chem. Chem. Phys. **2004**, *6*, 2910-2913.

11. **Free electrons, the simplest radicals of them all: chemistry of aqueous electrons as studied by mass spectrometry**
    O. P. Balaj, C.-K. Siu, I. Balteanu, M. K. Beyer and V. E. Bondybey
    Int. J. Mass Spectrom. **2004**, *238*, 65-74.

12. **Reactions of Hydrated Electrons $(H_2O)_n^-$ with Carbon Dioxide and Molecular Oxygen: Hydration of the CO_2^- and O_2^- Ions**
    O. P. Balaj, C.-K. Siu, I. Balteanu, M. K. Beyer and V. E. Bondybey
    Chem. Eur. J. **2004**, *10*, 4822-4830.

13. **Catalytic Oxydation of CO with N_2O on Gas-Phase Platinum Clusters**
O. P. Balaj, I. Balteanu, T. T. J. Roßteuscher, M. K. Beyer and V. E. Bondybey
Angew. Chem. Int. Ed. **2004**, *43*, 6519-6522.

14. **Reactions of Rhodium Cationic Clusters with Ethane**
I. Balteanu, O. P. Balaj, M. K. Beyer and V. E. Bondybey
In preparation.

15. **Saturation Reactions of Platinum Clusters $^{195}Pt_n^{\pm}$, n=1-23, with CO studied with isotopically enriched platinum**
I. Balteanu, Z. Sun, O. P. Balaj, M. K. Beyer and V. E. Bondybey
In preparation.

16. **Reactions of Hydrated Electrons with Hydrogen Chloride: Formation of Atomic Hydrogen**
C.-K. Siu, O. P. Balaj, I. Balteanu, M. K. Beyer and V. E. Bondybey
In preparation.

B. List of Presentations at Scientific Workshops and Conferences

1. **Reactions of hydrated aluminium ions with methanol and formic acid**
   O. P. Balaj, I. Balteanu, M. K. Beyer and V. E. Bondybey
   3rd Meeting of the RTN Network on "Reactive Intermediates Relevant in Atmospheric Chemistry and Combustion", 11-14 October 2001, Garching b. München, Germany
   Talk

2. **Reactions of hydrated aluminium ions with methanol and formic acid**
   O. P. Balaj, I. Balteanu, M. K. Beyer and V. E. Bondybey
   6th European workshop on Fourier Transform Ion Cyclotron Resonance Mass Spectrometry, 16-19 October 2001, Rolduc Monastery, Kerkrade, The Netherlands
   Talk

3. **The Garching ICR cooled cell development**
   O. P. Balaj, B. S. Fox, I. Balteanu, M. K. Beyer, V. E. Bondybey
   35. DGMS-Diskussionstagung, 3-6 March 2002, Heidelberg, Germany
   Poster

4. **Black Body Radiation Induced Hydrogen Formation in Hydrated Vanadium Cations**
   O. P. Balaj, B. S. Fox, I. Balteanu, M. K. Beyer and V. E. Bondybey
   66. Frühjahrstagung der Deutschen Physikalischen Gesellschaft, 4-8 March 2002, Osnabrück, Germany
   Talk

5. **Development of a variable temperature ICR cell**
   O. P. Balaj, B. S. Fox, I. Balteanu, M. K. Beyer, V. E. Bondybey
   4th Meeting of the RTN Network on "Reactive Intermediates Relevant in Atmospheric Chemistry and Combustion", 18-23 April 2002, Heraklion, Crete
   Talk and Poster

6. **Temperature behaviour of the liquid-nitrogen ICR-cell**
   O. P. Balaj, B. S. Fox, I. Balteanu, M. K. Beyer, V. E. Bondybey
   5th Meeting of the RTN Network on "Reactive Intermediates Relevant in Atmospheric Chemistry and Combustion", 8-11 September 2002, Southampton, UK
   Poster

7. **The Garching ICR cooled cell**
   O. P. Balaj, B. S. Fox, I. Balteanu, M. K. Beyer, V. E. Bondybey
   4th International Conference on Cryocrystals and Quantum Crystals, 27-31 October 2002, Freising, Germany
   Poster

8. **Wet electrons and their reactions**
   O. P. Balaj, B. S. Fox, I. Balteanu, M. K. Beyer, V. E. Bondybey
   6th Meeting of the RTN Network on "Reactive Intermediates Relevant in Atmospheric Chemistry and Combustion", 26-30 March 2003, Bremen, Germany
   Talk and Poster

9. **H/D exchange at methyl groups in anionic water clusters**
   O. P. Balaj, B. S. Fox, I. Balteanu, M. K. Beyer, V. E. Bondybey
   7th Meeting of the RTN Network on "Reactive Intermediates Relevant in Atmospheric Chemistry and Combustion", 3-7 September 2003, Saint Lambert des Bois, France
   Poster

10. **The development of a temperature controlled ICR-infinity cell**
    O. P. Balaj, B. S. Fox, I. Balteanu, M. K. Beyer, V. E. Bondybey
    7th European workshop on Fourier Transform Ion Cyclotron Resonance Mass Spectrometry, 28 March -1 April 2004, Konstanz, Germany
    Poster

11. **Addition of an H atom to acetonitrile by hydrated electrons in nanodroplets**
O. P. Balaj, B. S. Fox, I. Balteanu, M. K. Beyer, V. E. Bondybey
8th Meeting of the RTN Network on "Reactive Intermediates Relevant in Atmospheric Chemistry and Combustion", 6-9 April 2004, Lyndhurst, UK
Talk

12. **Addition of an H atom to acetonitrile by hydrated electrons in nanodroplets**
O. P. Balaj, B. S. Fox, I. Balteanu, M. K. Beyer, V. E. Bondybey
68. Frühjahrstagung der Deutschen Physikalischen Gesellschaft, 22-26 March 2002, München, Germany
Talk

13. **Chemistry of Aqueous Electrons Studied by Mass Spectrometry**
O. P. Balaj, B. S. Fox, I. Balteanu, M. K. Beyer, V. E. Bondybey
Gordon Research Conference "Molecular & Ionic Clusters", 5-10 September 2004, Aussois, France
Poster

Acknowledgements

I would like to thank my supervisor, Prof. Dr. Vladimir E. Bondybey for the great ideas, overwhelming experience and very useful advice which shaped my work. He was always open to discussion and happy to share his knowledge with me.

Without the critical advices of Dr. Martin Beyer, the "şef" of the ICR group, everything in the laboratory would have been much more difficult. His support and his enthusiasm have kept me going at full speed most of the time. Thank you!

Special thanks to all the members of the ICR group, Brigitte S. Fox-Beyer, Iulia Balteanu and more recently Chi-Kit Siu, Sun Zeng and again Martin Beyer. Most of the theoretical calculations presented in this work were done by Dr. Siu but the contributions of Dr. Martin Beyer and, in the case of aluminum, Dr. Edmond P.F. Lee have greatly helped and all are gratefully acknowledged. In this group I have found an extremely creative environment and the freedom to discussions almost everything. It is a pleasure to work with you and it was fun. I have enjoyed to share with you bits of Romanian culture and to see you surprised and amused when, suddenly, pieces of "popular" philosophy would leak out.

A special place in this is granted to Matthias Stecher, an absolutely out of ordinarily fellow. His work, help and technical advice are invaluable. I also thank Peter Kämmerer for getting me out of the not rare troubles with the computer systems.

Sabine Kullick, our secretary has won some great battles with the paperwork, and not only, for me.

I want to thank also to the other members of the Bondybey group, Dr. Marcin Frankowski, Dr. Alice Smith-Gicklhorn, Dr. Elena Savchenko for their friendly and unconditioned help. The same goes for the ex-members Dr. Bernhard Urban and Dr. Dieter Kraus.

During my time here I was also one of the Young Researcher in the European Union's "Reactive Intermediates Relevant in the Atmospheric Chemistry and Combustion". My presentation, language and scientific skills have been honed by a series of meetings and talks. I had thus the possibility to meet other YR, discuss and share ideas. I would also like to thank to all people involved and especially to Prof. Dr. John Dyke from Southampton University, the network scientific coordinator, and Prof. Dr. C.A. de Lange from Vrije Univeriteit from Amsterdam, the network manager. The network's financial support is gratefully acknowledged.

I am here because one man has fought hard to get me the German visa even when there was little hope left. Thank you very much Dr. Horia Porteanu.

The electronics and machine workshop provided us with excellent work and continuous troubleshooting support.

Financial support by the Deutsche Forschungsgemeinschaft and the Fonds der Chemischen Industrie is gratefully acknowledged.

To the end the deepest thank you is reserved to my parents.

Multumesc mama, multumesc tata, pentru ca m-ati sustinut si ati fost intotdeauna alaturi de mine. Ati crezut in mine si ati luptat alaturi de mine. Mi-ati fost model in viata si iata ca baiatul vostru este capabil sa stea pe picioarele lui si sa reuseasca. Multumesc!